Investigating the Energetics and Functional Properties of Quinones and Chlorophyll in Photosynthetic Reaction Centers

by

Jennifer Madeo

☐

☐

☐

☐

☐

☐

A dissertation submitted to the Graduate Faculty in Engineering in partial fulfillment of the requirements for the degree of Doctor of Philosophy, The City University of New York

2005

UMI Number: 3187384

ProQuest Information and Learning Company
300 North Zeeb Road
P.O. Box 1346
Ann Arbor, MI 48106-1346

This manuscript has been read and accepted for the

Graduate Faculty in Engineering in satisfaction of the

dissertation requirement for the degree of Doctor of Philosophy.

8/22/05	Professor Marilyn Gunner
Date	Chair of Examining Committee
8/22/05	Mumtaz Kassir
Date	Executive Officer

Professor Maribel Vazquez (BME)

Professor Carol Steiner (ChemE)

Professor Alexander Couzis (ChemE)

Supervision Committee

THE CITY UNIVERSITY OF NEW YORK

Abstract

Investigating the Energetics and Functional Properties of Quinones and Chlorophyll in Photosynthetic Reaction Centers

by

Jennifer Madeo

□

Adviser: Professor Marilyn Gunner

The first steps for the process of converting light into chemical energy in photosynthesis occur within membrane-bound proteins called the reaction centers (RCs). When the RC is excited by light a series of electron transfer reactions take place. The RC has bound co-factor compounds that are specifically tuned to accept and donate the electron in the reaction series. The protein is responsible for creating the right micro-environment for the proper co-factor orientations and tune the energy levels to drive the electron transfer reactions.

Three RCs are the focus of this work. The first RC is from the purple bacteria *Rhodobacter sphaeroides*. These RCs contain two chemically identical quinones (ubiquinone-10). Electron transfer between these two quinones is favorable because the protein modifies their environment such that Q_A is lower potential than Q_B. The negatively charged semi-quinone binds more tightly and dissociates more slowly than the neutral quinone. The binding affinities and rate constants for thirteen quinones (eight

neutral and five negatively charged) at the Q_A site were measured. It is shown that a negative charge leads to a different binding mechanism as well as slower binding rate.

The shift in pK_a of hydroxyl containing quinones and the relative affinities of anionic quinones was determined and compared both experimentally and computationally. The computational method is Mulpti-Conformational Continuum Electrostatics (MCCE). The good agreement between experimental and computational results confirms that electrostatics is the dominant way that the Q_A site modifies quinone chemistry.

The second two RCs come from cyanobacteria, which contain two RCs (PSI and PSII). The primary electron donor, a chlorophyll a dimer, is the same for both PSI and PSII. Despite this the redox potentials of the co-factors bound to these RCs are very different (about 600mV). Only PSII has a high enough potential to oxidize water. MCCE was used to calculate the redox midpoint potentials of the co-factors bound to PSI and PSII in effort to understand the role that electrostatics plays in fine-tuning these midpoint potentials. These results are compared with experimental results in an effort to understand how the protein modifies the co-factor environment.

□

Acknowledgements

I would like to thank my thesis advisor, Dr. Marilyn Gunner, for all her support and education, for giving me the opportunity to work in the field of Biophysics both experimentally and computationally.

I am grateful to Dr. Harold Falk for his help with the Mathematica software and insights into mathematical modeling, to Dr. Mark Paddock for his helpful discussions about pK_a shifts in the Q_A site, to Xinyu Zhang for great experimental advise and guidance, to Yifan Song, Junjun Mao, Jun Zhang and Rajesh Satyamurti for all their help with MCCE.

I would like to thank my committee members for their time and advice.

I would like to thank my parents, Gary and Robyn Madeo and brother Russell Madeo, for all their support during my long education.

Lastly, I would like to thank my husband, Mohamad Zoghi Moghadam, for all his patience, support and guidance, without which I would not have come this far.

TABLE OF CONTENTS

□

LIST OF TABLES

LIST OF FIGURES

Chapter 1: Introduction and Background

I) Introduction

1-A) *Significance and Applications*

In the process of photosynthesis light energy from the sun is converted into chemical potential energy. Complex protein structures optimize this energy flow leading to efficient solar energy conversion and storage. Sunlight is the largest source of power on Earth, providing $1.2x10^{17}$ Watts (Lewis and Crabtree 2005). This solar resource can be exploited through solar electricity. This is a process in which sunlight is converted into electricity via photovoltaic cells and solar fuels, the conversion of solar energy into chemically useful energies. To date, no artificial system can match the efficiency and complexity of biological organisms. Elucidation of the molecular mechanism of photosynthesis is essential for optimizing and designing high efficiency natural, artificial or synthetic photosynthetic components. Some current areas of research addressing the challenges for harvesting the energy from the sun and converting it into useful energy are genetically engineering plants and bacteria to be more efficient so that less land area is needed to produce the energy, designing low-cost artificial photosynthetic systems with high efficiency and chemically synthesizing components that can mimic photosynthesis by absorbing sunlight and converting it to useful fuels such as CH_4 and H_2 (Janouskova and others 2005; Tani and Barrington 2005; Trommer and others 2005). Efficient solar fuel generation requires efficient light absorption, charge separation and use of the separated charges in fuel-forming reactions. A major challenge for all this research is to increase the efficiency of light harvesting and converting light energy into chemical

energy. Light harvesting systems are currently being designed and there is continuing research to optimize these designs (Lidell 2004; Seth 1996; van der Boom 2002).

Reaction centers (RCs) are the proteins in which the first photoeletrochemical step of photosynthesis occurs (Okamura and others 1982). A special pair of chlorophyll molecules, bound to the RCs, are excited by light to begin the process of electron transfer, which stores the photon's energy in the form of charge separation. A donor-acceptor triad contained within a spherical nanoscale lipid compartment has been used to pump protons and drive the synthesis of ATP (Steinburg-Yfrach 1998). Thus this energy transfer has been measured. Also a multi-step electron transfer cascade with a potential high enough to oxidize an Mn complex has been designed (Sun 2001). Basic research focusing on the electron transfer reactions that take place in proteins is a necessary contribution to the future of these designs. Any research focused on discovering how the protein fine-tunes the energy levels of its bound redox-active co-factors is useful for increasing the efficiencies of these designs.

The most successful designs will be those that most closely mimic biological supramolecular structures. For example, it has been shown that generating multiple charge carriers from the absorption of one photon (similar to RCs) leads to more efficient solar cells (Nozik 2002; Schaller 2004). To further meet this criteria there must be an understanding of the intermolecular forces that hold biological structures together, and an understanding of the interactions between proteins and their bound co-factors. To design a nano-material with high efficiency, control of the nano-architecture is needed. The efficiency of photoelectrochemical cells increases when they are nano-structured, thus understanding interactions on this scale are important (Gratzel 2001; Hagfeldt and

Gratzel 2000; O'Regan 1991). Understanding electron transfer at the molecular level, on natural systems, plays an important role for designing these photoelectrochemical cells (Nelson 1999).

Proteins are not just inert scaffolds for their redox active co-factors because they actively promote, enhance and control the electron transfer reactions that take place in them. Biology has reached the ideal photochemical design due to the active environment created by the protein. For a successful design the redox active co-factors must be in matrix that can alter their electronic properties, just as they are in natural proteins. Thus biophysical research on photosynthetic systems may show how to apply these concepts in artificial systems. In RCs the environment is dynamic and is constantly adjusting to minimize the energy penalty of charge separation. Specific motions of individual amino acids are important for controlling electron flow (Jeuken 2003; Nonella and Schulten 1991). In addition the electrostatic environment of the RCs provides site-specific redox potentials for bound co-factors, which controls the direction of electron flow (Alexov 2003; Rabenstein and others 2000). The big challenge in the design of artificial photosynthetic systems are to mimic the structural dynamics and electrostatics of RCs in order to more efficiently convert the captured the light energy. Current research will focus on the interplay between charge separation and the protein environment (Baxter and others 2004a; Baxter and others 2004b). Biophysical methods are important to advance these areas. A state-of-the-art example of this is the temporal and spatial imaging of electron density disturbances associated with charge and electrical-field disturbances in water (Abbamonte and others 2004). This method monitors changes due to oscillating molecular dipoles. Advances in this technique could provide opportunities to map

electronic responses in solar fuel cells in the future (Brixner and others 2005) (Schotte and others 2004).

Since photosynthesis is the primary source of food on the earth, research concerning its molecular mechanism can impact agriculture and the food industry. Herbicides are chemicals used to reduce the growth of unwanted crops thus enhancing food production. Inhibitors that block quinone electron transfers in reaction centers are good herbicide candidates (Ginet and Lavergne 2001). Without this electron transfer step, photosynthesis in the unwanted crop ceases. These inhibitors must bind tightly in the quinone pocket in order to displace the native quinone. Understanding the interactions between the protein and the quinone will help to develop more effective herbicides (Draber and others 1991; Stein and others 1984).

1-B) Non-cyclic Photosynthesis in Plants

Photosynthesis is responsible for all life on earth. During this process plants trap solar energy and use it to synthesize carbohydrate. The basic reaction for green plants is deceptively simple as follows:

$$H_2O + CO_2 \rightarrow (CH_2O)_n + O_2$$

In this redox reaction water is oxidized to molecular oxygen and carbon dioxide is reduced to carbohydrate (Xiong and Bauer 2002). The oxygen byproduct diffuses into the atmosphere and hence permits aerobic metabolism on earth (Blankenship and Prince 1985). The energy for this highly endothermic reaction is provided by light. The mechanism of photosynthesis is complicated and requires the interplay of many proteins and co-factors.

Harvesting the energy of light and converting it to a chemically useful form makes photosynthesis the most intriguing process on earth. The amount of solar free energy captured by photosynthetic organisms per year is more than the amount of fossil-fuel energy consumed world-wide (Peter Raven. 1999). Furthermore, the process of photosynthesis involves coupled electron and proton transfers across biological membranes (Cramer and Crofts 1982; Feher and others 1989; Govidnjee 1982). This mechanism is also used in oxidative respiration hence discovering the mechanism of photosynthesis is a central goal of biochemical research.

Photosynthesis takes place in chloroplasts, a membrane-enclosed organelle found in plant cells (Peter Raven. 1999). Although the reaction above is shown as a single redox equation, the processes of water oxidation and carbon dioxide reduction are separate. The separation is based on the dependence of light. The light dependent process is water oxidation (Barber 2002; Barter and others 2003). This process takes place in the chloroplast inner membrane. Pigment molecules, mainly chlorophyll, absorb the light and become excited to a higher energy state. This drives a series of electron transfer reactions that result in storing the light energy in chemical bonds. The light independent process is where the energy stored by the light dependent reactions is used to reduce CO_2 to carbohydrate. This process takes place outside the membrane. I will only elaborate on the light dependent reactions because they are relevant to my research.

The steps of the light dependent process in plants are illustrated in Figure 1-1. The process requires the cooperation of two highly organized protein-pigment complexes known as photosystems (PSI and PSII) (Nelson and Ben-Shem 2004; Nugent 1996; Youvan and Marrs 1987). Each photosystem can be independently excited by light. The

photosystems are subdivided into two main components; a large antenna complex and a central reaction center (RC). The chloropyll pigments of the antenna complex gather the light energy and direct it to the RC. These pigments become excited by the light and transfer the energy among themselves by a process called resonance energy transfer. There is no redox chemistry in this light gathering step. The RC contains a special pair of chlorophyll molecules (P). P is special because it is the only pigment that becomes oxidized after being excited by light energy.

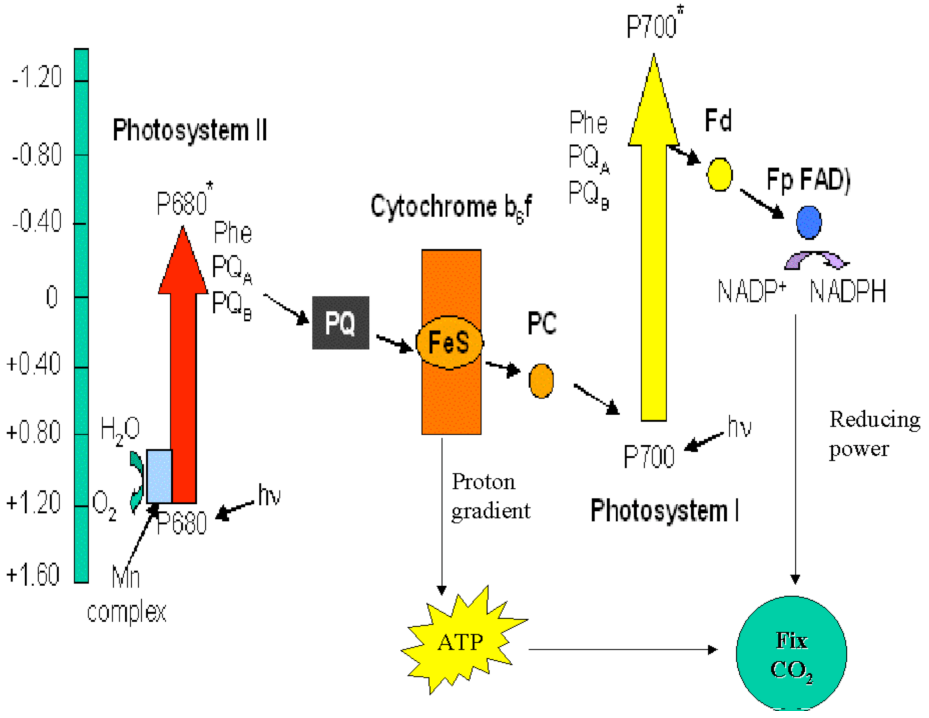

Figure 1-1: The light dependent reactions in plant photosynthesis.

1) Light excites chlorophyll molecules of antenna proteins in PSII.; 2) Energy is directed to the reaction center where P680 gets excited and then oxidized.; 3) An electron transport chain eventually reduces the cytochrome b/f complex.; 4) The cytochrome b/f complex pumps protons to generate the electrochemical gradient needed for the synthesis of ATP.; 4) Light excites antenna of PSI and energy is funneled to its reaction center.; 5)

P700 gets oxidized and starts another electron transport chain.; 6) The result of this chain is that NADP gets reduced to NADPH. Both the ATP and NADPH are used to fix CO_2 into carbohydrate in the Calvin cycle. For plants, water splitting into O_2 extracts the electrons to re-reduce P680 and a mobile electron carrier, plastocyanin, re-reduces P700 (Peter Raven. 1999).

Figure 1-1 shows how the two photosystems work together. Oxidation of P680, the special chlorophyll pair of the PSII RC, leads to a series of electron transfer reactions (Nelson and Ben-Shem 2004). The final electron acceptor in this series is a plastoquinone (Q_B), a compound containing two carbonyl groups (Feher and others 1989). This quinone is reduced to a quinol by two electron transfers and the addition of two protons. The quinol dissociates from the reaction center and is replaced by another quinone from an outside pool (Feher and others 1989). The reduced quinol carries these electrons through the membrane and delivers them to the cytochrome b/f complex. Electron transfers in the cytochrome b/f complex provide the energy for pumping protons (H^+) against their concentration gradient (Cramer and others 2004). This achieves an electrochemical potential across the membrane. Dissipation of this gradient provides the energy to drive the synthesis of ATP in the process of photophosphorylation (Bianchet and others 2000) (Abrahams and others 1994).

Oxidation of P700, the special pair of the PSI RC, leads to another series of electron transfer reactions (Fromme and others 2001). The final electron acceptor is the coenzyme NADP. NADP is reduced to NADPH by two electron transfers and a proton. The NADPH and ATP are used later, in the light independent reactions (the Calvin cycle) of

photosynthesis, to reduce CO_2 to carbohydrate (Moller 2001). P700 is re-reduced by plastocyanin, the final electron acceptor of the cytochrome b/f complex. Plastosyanin is a mobile carrier that transports electrons from the cytochrome b/f complex to PSI (Fromme and others 2001).

The process described above for plants is known as non-cyclic photosynthesis because the re-reduction of P680 requires extracting electrons from water molecules. As soon as four electrons have been removed from two water molecules, oxygen gas is generated as a byproduct. Therefore, in order to keep the process going water must be consumed.

1-C) Cyclic Photosynthesis in Purple Bacteria

RCs from the purple bacteria species, *Rhodobacter sphaeroides* undergo cyclic photosynthesis. In contrast to plants, photosynthesis in this species requires only one RC, bacteriochlorophyll as the special pair and no oxygen byproduct is evolved. Also this process takes place in the cell membrane, rather than the chloroplasts in higher plants (Peter Raven. 1999). Instead of extracting electrons from water, the special pair, P870, is re-reduced by a mobile protein called cytochrome c2 (Adir and others 1996).

Antenna complexes, LHI and LHII, collect the light energy and funnel it to the RC. P870 is excited and loses an electron (Fleming and van Grondelle 1997). This oxidation leads to a series of electron transfer reactions. The final electron acceptor is a bound quinone (Q_B). As in PSII this quinone is reduced to quinol (QH_2) by two electron transfers and two protons. QH_2 dissociates and carries the electrons to the integral membrane bc1 complex (Fyfe and others 2002). Electron transfer reactions in the bc1

complex are coupled to proton pumping, generating an electrochemical gradient similar to the cytochrome b/f complex in plants. The electrochemical gradient is dissipated to form ATP.

The final electron acceptor for the bc1 complex is cytochrome c2 (Adir and others 1996). Cytochrome c2 carries electrons from the bc1 complex and donates them back to the P870 in the RC. Two cytochrome c2 molecules are needed to make one doubly reduced quinol. This is the opposite redox chemistry of the mobile quinol. The quinol carries two electrons from RC to the bc1 complex. This whole process is called cyclic photosynthesis because all of the reactants and products are recycled hence there is no evolving byproduct (Cramer and others 2004).

1-D) Crystal Structure of Bacterial Reaction Centers, Photosystem I and Photosystem II

The bacterial reaction center is the first integral membrane protein whose three dimensional structure was solved at the atomic level via X-ray crystallography (Stowell and others 1997). RCs isolated from Rhodobacter sphaeroides contain three membrane-spanning protein chains (L,M and H) and ten co-factor molecules. Figure 1-2-A shows the three-dimensional structure obtained from X-ray crystallography (pdb file 1AIG). The L chain contains 266 residues, 15 alpha helices and 11 beta turns. Five L chain helices span the membrane. The M chain contains 296 residues, 16 helices and 22 beta turns. Five helices of this chain also span the membrane. The L and M chains appear to be derived from a single ancestral gene that underwent duplication. They have 33% sequence similarity (Abresch and others 1997). The L and M chains are evolutionarily related to PSII in green plants. The L and M chains are structurally related to each other

by a 180-degree rotation about a twofold axis (c_2) normal to the plane of the membrane. Lastly, the chain H contains 237 residues, 7 helices and 9 beta strands. The bulk of the H chain is located on the cytoplasmic side of the membrane and it contains only one transmembrane alpha helix.

The co-factor molecules bound to the RC span the membrane and are the active players in the electron transfer reactions. The protein plays an important but passive role. The protein is responsible for creating the right micro-environment for the proper co-factor orientations and tune the energy levels to drive the electron transfer reactions. These co-factors form two branches (A and B) that are symmetrical about the c_2 axis. This is shown in Figure 1-2. The A branch is associated with the L chain and the B with the M chain.

The co-factors are four bacteriochlorophylls, two bacteriopheophytins, two quinones and a non-heme Fe^{2+} ion. Two of the bacteriochlorophylls form the special pair, P. From the periplasmic to the cytoplasmic sides of the membrane each branch consists of a bacteriochlorophyll monomer (B_A and B_B), a bacteriopheophytin (H_A and H_B) and a ubiquinone-10 (Q_A and Q_B). The iron is found between the two ubiquinones (Fig. 1-2).

Crystal structures of PS I (2.5 A) (Jordan and others 2001) and PS II (3.5 A) (Ferreira and others 2004) from cyanobacteria *Synechoccus elongatus* have been resolved and deposited in the protein data bank. PSI and PSII are much larger than the RC from purple bacteria each containing more than 10 protein subunits. Similar to RCs from purple bacteria, there are two main subunits that bind each branch of the redox-active co-factors: PsaA and PsaB in PS I and D_1 and D_2 in PS II. Also similar to RCs from purple bacteria, the crystal structures reveal that the redox-active co-factors in both

photosystems are arranged in two symmetric branches related by a pseudo-axis perpendicular to the membrane (Fig. 1-2).

Electron transfer in PSI starts with primary donor (P_{700}), which is a heterodimer containing chlorophyll a (Chla) and its $C13^2$-epimer chlorophyll a' (Fromme 1996; Fromme and others 2001; Webber and Lubitz 2001). Upon excitation P_{700} gives its electron to either of the two adjacent chlorophyll a monomers. Electron transfer can occur either down the A or B co-factor branch (Brettel and Leibl 2001; Guergova-Kuras and others 2001). The monomeric chlorophyll gives its electron to phylloquinone. Both the A and B branch contain a phylloquinone. From the phylloquinone the electron reaches the first iron sulfur cluster F_x located on the pseudo-symmetry axis (Fig. 1-2). Two more iron sulfur clusters follow F_x (F_A and F_B, which are not shown in Figure 1-2). At F_B the electron is transferred to the water soluble electron carrier ferrodxin which use it to get reducing power.

In PS II ET always occurs along the co-factor chain bound to D_1 (Barter and others 2003; Rutherford and Faller 2002). The primary donor is a chlorophyll a homodimer, P_{680} which gets excited and gives its electron to pheophytin. Pheophytin donates to the first plastoquinone (Q_A) and then $Q_A^{\bullet -}$ passes the electron to Q_B, bound to D_2. Similar to RCs from purple bacteria, both Q_A and Q_B are the same chemical species, plastoquinone. Between the two quinones, there is a non-heme iron atom. For both PSI and PSII, the Chla monomers that make up the special pairs are named according to the branch they are closest to; P_A and P_B for P_{700} and P_{D1} and P_{D2} for P_{680}.

Despite their similar geometry, the redox active co-factors of PS I and PS II have very different potentials (Li and others 2004; Rappaport and others 2002). PS II, with its

ability to extract electrons from water (E_m = 820mV), is the most powerful oxidizing agent known in biology, while the role of PS I is to generate strong reducing equivalents, thus its co-factors are much lower potential. The redox potential of P_{700} is 470mV (Webber and others 1996) while P_{680} is on the order of 1150 to 1260 mV (Nugent 1996; Rappaport and others 2002). Thus these photosystems provide very different environments for their co-factors. The electronic structure of the oxidized primary donor and interactions with the protein environment determine the redox potential in both photosystems (Rutherford and Faller 2002; Webber and Lubitz 2001). The crystal structures have shown that the major organizational difference between P_{700} and P_{680} is the distance between the chlorophylls (6.34A for P_{700} and 8.15A for P_{680}). Thus P_{680} is less coupled and may be monomeric (Mulkidjanian 1999; Rutherford and Faller 2002; Rutherford and Nitschke 1996) while P_{700} behaves more like a dimer. Furthermore P_{700} is a heterodimer where P_A is Chla', the C-13^2 epimer of P_B (Chla) (Jordan and others 2001). No chlorophyll isomers are found in PS II.

The reasons why P_{680} is about 600mV higher potential than P_{700} and plastoquinones in PS II are about 500mV higher potential that the phylloquinones bound to PS I are a mystery. Factors that could play a role include electrostatic interactions with the surrounding protein, ring torsion, hydrogen bonding and the dimeric quality of the primary donors. The work presented here uses multi-conformational continuum electrostatics (MCCE) to investigate the role of electrostatics in tuning the redox potential of P_{700}, A_{1A} and A_{1B} in PS I and P_{680}, Q_A and Q_B in PS II. The differential interactions between these co-factors and their protein environment have a significant effect on their electrochemistry.

Figure 1-2: Crystal structures of the three RCs focused on in this research. Left: the crystal structure revealing the protein subunits and highlighting the embedded co-factors. Right: shows the co-factors without the surrounding protein.

A) Bacterial RCs from the purple bacteria *Rhodobacter sphaeroides* (PDB 1AIG)

B) Photosystem I (PSI) from cyanobacteria *Synechoccus elongatus* (PDB 1JB0)

C) Photosystem II (PSII) from cyanobacteria *Synechoccus elongatus* (PDB 1S5L)

A

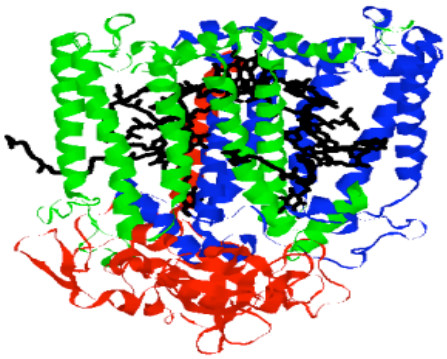

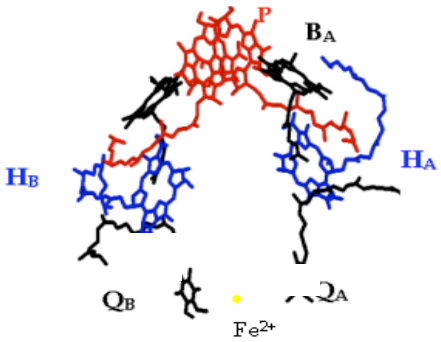

B

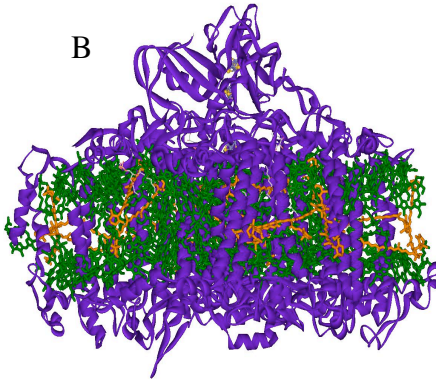

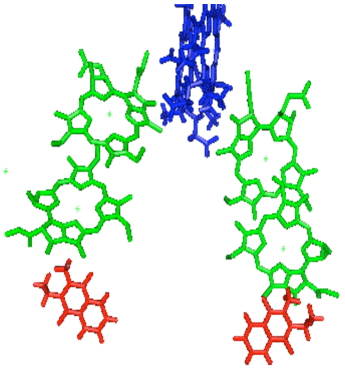

C

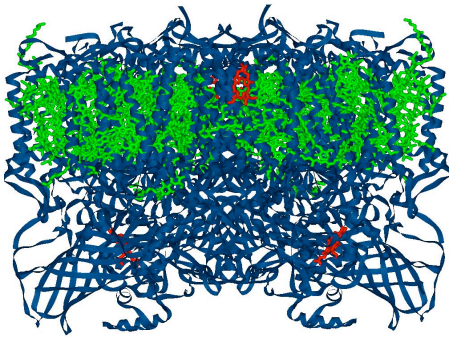

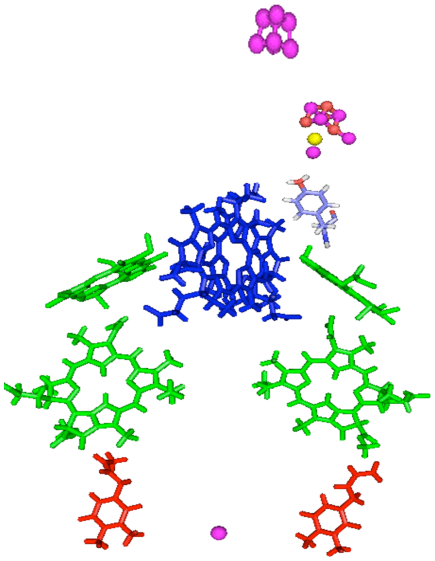

II) Methods

II-A) *Measuring Light Induced Absorbance Changes in Real Time:*

Flash photolysis is a technique where samples are irradiated with short, high intensity light and then short-lived intermediates are followed in real time (van Mourik and others 2001). Fast optical absorption measurements are used to follow the changes with time (Boxer and others 1989). Light induced absorbance changes are measured in our laboratory using a flash spectrophotometer designed by the University of Pennsylvania Biomedical Instrumentation Group (Xu and others 2002; Xu and Gunner 2001). A 10us flash actinic light from a xenon flash lamp excites the reaction centers. The measuring light reaches the sample perpendicular to the actinic light. A continuous quartz-halogen tungsten lamp (QHT) provides the measuring light. The measuring light is sent through a monochromator. The monochramtor can be set to illuminate the sample with a chosen wavelength. This wavelength is set depending on which electron transfer reaction you want to follow in time (Baciou and others 1990).

For the work presented here, the monochromator is set to 430nm to follow the change from oxidized to reduced P (Xu and others 2002). The light induced absorbance changes due to this electron transfer event give the largest amplitude at this wavelength. It is therefore the easiest signal to follow (Xu and Gunner 2000). A photomultiplier tube (PMT) detects the transmitted light. The data is then sent to a digital oscilloscope for recording and storing. The oscilloscope also receives input from the flasher to synchronize the flash with the measurement. Synchronized, single turnover measurements are made (Li and others 1998; Li and others 2000). This allows for signal averaging hence maximizing the signal to noise ratio. As shown in Figure 1-3, the output

of the oscilloscope is a kinetic trace of voltage versus time. The amplitude is directly proportional to the number of reaction centers excited by the flash (or in other words, the amount of oxidized P that was formed) (Xu and others 2002).

The software IGOR Pro (WaveMetrices) is used to further analyze the kinetic data from the oscilloscope. The kinetic traces are fit with exponential functions (Figure 1-2). A_0 is usually only about 5% of the total amplitude and hence is ignored in the analysis (Xu and others 2002). The cause of this residual amplitude is probably some decay that cannot be detected on this timescale (Xu and Gunner 2001). The number of exponentials needed to fit the data reflects the number of kinetic phases in the reduction reaction. The amplitude of each phase is also obtained from the fit.

For the work presented in these studies, Q_B is removed and charge recombination from Q_A back to P is observed (Gao and others 1990; Okamura and others 1974). This is because charge recombination is about 1000-times slower than the forward electron transfer reactions, thus removing Q_B eliminates the fast reaction and allows the charge recombination from Q_A to be observed (Allen and others 1998; Baciou and others 1990; Feher and others 1985).

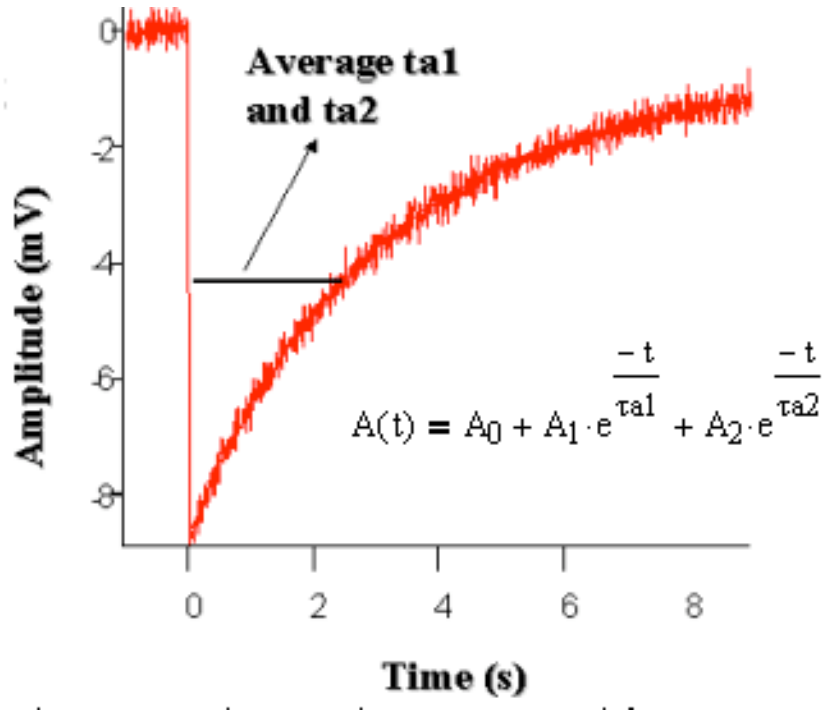

Figure 1-3: Kinetic Trace Output From Oscilloscope

The re-reduction of P is watched in real time at 430nm. The amplitude is proportional to the amount of P that was oxidized by the flash of light. The trace is fit with the shown exponential equation. The number of exponential terms needed to best fit the trace indicates the number of electron transfer reactions that are re-reducing P.

II-B) Multi-Conformational Continuum Electrostatics (MCCE)

MCCE is a computational method that combines continuum electrostatics and molecular mechanics to uncover protein structure/function relationships (Georgescu and others 2002; Mao and others 2003; Zhu and Gunner 2005). This method starts with the

atomic coordinates of a protein from the protein data bank (PBD) (Berman and others 2000) and calculates the electrostatic pairwise interactions between residue side chains and the residues with the backbone. PARSE charges and radii are used to get the atomic partial charges of the side chain and backbone (Sitkoff and others 1994). Each specified side chain and ligand position and charge is called a conformer (Alexov and others 2000). The method differs from ordinary electrostatic calculations in that multiple side chain positions are generated to better simulate the conformational freedom of the side chains in the protein structure. The assumption that the protein is a static structure identical to the x-ray crystal structure is a serious limitation (Gordon and others 1999). This also allows for the analysis of changes in protein conformation that accompany changes in ionization state (Song and Gunner 2004). The dielectric relaxation that accompanies a change in charge is very important for understanding the atomic level function of RCs because the bound redox-active co-factors can be neutral or ionized during electron transfer (Bashford and Case 2000). With MCCE there can be several conformers for any given residue or group (Georgescu and others 2002).

Classical electrostatics is used to get the interaction energy between all the conformers. The finite difference method, DelPhi (Nicholls and Honig 1991), is used to solve the Poisson-Boltzmann equation (Das and others 1995) to give the potential field of the protein due to each conformer.

$$\nabla \bullet \varepsilon(r) \cdot \nabla \bullet \phi(r) - \kappa^2(r) \cdot \varepsilon(r) \cdot \phi(r) = -4\pi\rho(r)$$

ε(r) is the position dependent dielectric constant. In MCCE the dielectric constant of the protein material is 4 and the surrounding aqueous material is 80 (Elcock and McCammon 1997). If there are any cavities in the protein structure (space that are not occupied by a

side chain, backbone or bound co-factor) MCCE treats that space as dielectric 80. $\phi(r)$ is the potential field (the position dependent potential (voltage)). $\rho(r)$ is the charge density. The κ^2 term accounts for the effect of electrolytes on the potential field. In regions of ion accessibility, $\kappa^2 = 8\pi e^2 I/\varepsilon(r)kT$, where I is the ionic strength, e is the charge, k is Boltzmann's constant and T is the temperature. This term accounts for the exponential decay of the potential due to the electrolyte (Bashford and Case 2000; Murphy 2000). MCCE calculations are done with an ionic strength of 150mM salt and at a temperature of 27°C.

One DelPhi calculation is done for each conformer in the protein structure (Georgescu and others 2002). Each DelPhi has atomic partial charges only on one conformer (the atomic charges for all other atoms are set to zero). This gives a charge distribution that generates a potential at the positions of all the other atoms in the structure (Nicholls and Honig 1991). Thus the potential is collected at the atoms for all the other conformers. Pairwise interactions are obtained by multiplying this potential with the partial charges of the atoms at their respective positions (Mao and others 2004).

In addition to pairwise interactions MCCE calculates the reaction field energy of every conformer. This is free energy of transferring the conformer out of the high dielectric aqueous surroundings ($\varepsilon = 80$) to the low dielectric protein environment ($\varepsilon = 4$). Charged groups and dipoles tend to be better solvated in the high dielectric medium, thus the reaction field energy is unfavorable (a positive number) (Bader and others 1997). This energy is determined by a second set of DelPhi calculations with all the residues in their original positions (uncharged) except for the conformer of interest (charged). All of these electrostatic energies are stored as look-up tables in the program. The non-electrostatic

energy components include torsion ($\Delta G_{torsion}$) and Lennard-Jones interactions (ΔG_{nonel}). Torsion is the energetic cost of rotating atoms around covalent bonds. Lennard-Jones interactions are the distance dependent attractions and repulsions between non-bonded atoms due to induced dipolar effects (Freindorf and Gao 1996).

Once the electrostatic calculations are finished Monte-Carlo (MC) sampling (Colominas and others 1999) is used to determine the equilibrium distribution of ionization and conformational states. Monte Carlo samples microstates, where a microstate is defined as having one conformer for every side chain, co-factor and water (Ahlström and others 1988). MC sampling is done over a defined range pH or E_h values. The occupancy of each conformer is determined for each pH or E_h value. For a particular redox active group or acidic or basic group MC gives rise to a titration curve. The midpoint of the curve gives the pK_a or E_m of the group. Figure 1-4 gives an overview of the MCCE method

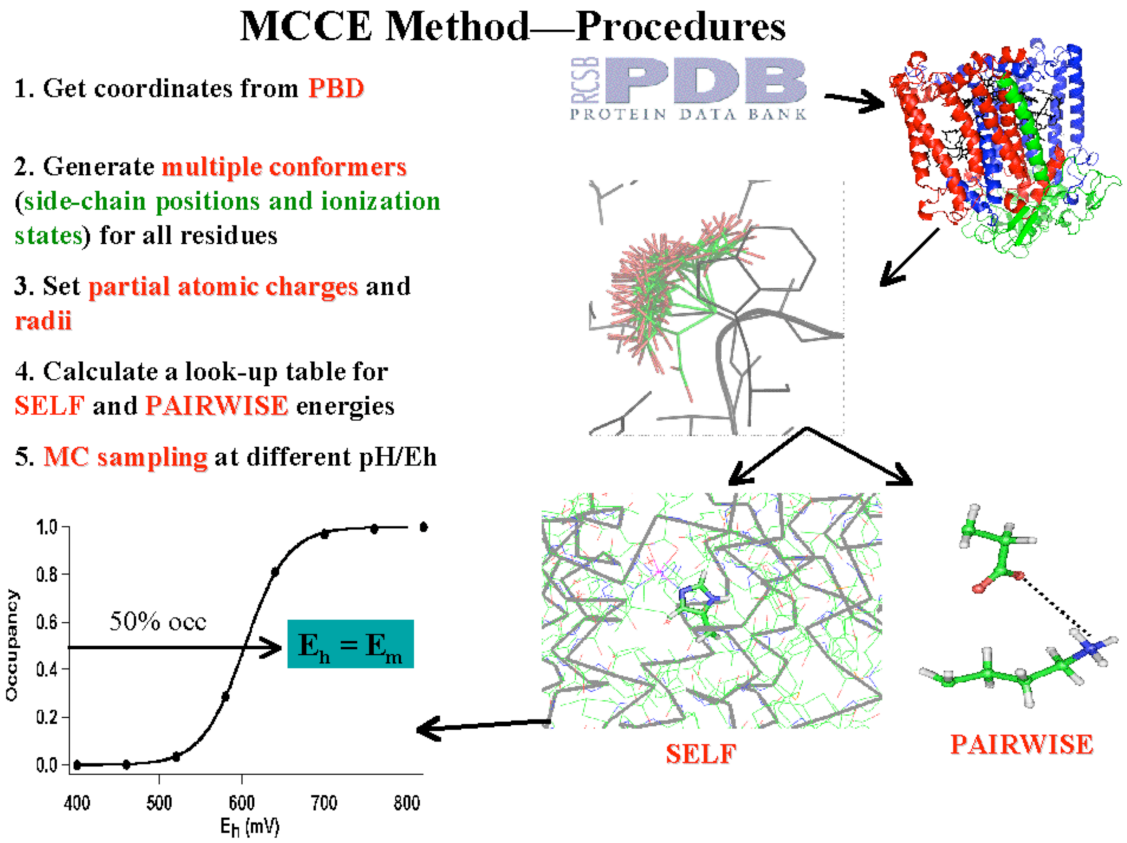

Figure 1-4: Overview of the MCCE method.

The atomic coordinates are obtained from the protein data bank. Multiple conformers are generated in order to better simulate protein dynamics. Partial charges and atomic radii are set according to pre-defined values. DelPhi calculations are run to generate energy look-up tables. Self-energies include the reaction field energy, torsion, Lennard-Jones and the intrinsic affinity of the group for its proton or electron (if the group is redox active, acidic or basic). MC sampling is used at different E_h (or pH) values to generate a titration curve yielding the E_m (or pK_a) of a group of interest.

The free energy of microstate x (ΔG_x), at a given pH and E_h, is the sum of the electrostatic and non-electrostatic energy terms (Mao and others 2003).

$$\Delta G_x = \sum_{i=1}^{M} \delta_x(i)\{\gamma(i)[2.3k_bT(pH - pK_{sol,i}) - nF(Eh - Em_{sol,i})]$$

$$+(\Delta\Delta G_{rxn,i} + \Delta G_{torsion,i} + \Delta G_{pol,i} + \Delta G_{nonel,i})\}$$

$$+\sum_{i=1}^{M} \delta_x(i) \sum_{j=i+1}^{M} \delta_x(j)[\Delta G_{ij}^{el} + \Delta G_{ij}^{nonel}]$$

where k_bT is 0.59 kcal/mol (25.8 meV), *M* is the number of conformers, $\delta_x(i)$, is 1 for conformers that are present in the state and 0 for all others, $\gamma(i)$ is 1 for base and –1 for acids, and 0 for polar groups and waters, *n* is the number of electrons gained or lost in redox reactions, *F* is the Faraday's constant, $pK_{sol,i}$ is the pK_a of the ith group in solution. $E_{m,sol,i}$ is the midpoint potential of the ith cofactor in solution (Alexov and others 2000; Mao and others 2004; Song and Gunner 2004). $\Delta\Delta G_{rxn,i}$ is the difference between the conformer reaction field energy (desolvation energy) in solution and protein, which was influenced by the protein structure, size and the position of the amino acids. $\Delta G_{torsion,i}$ is the conformer torsion energy. Each conformer has a pair-wise electrostatic interaction with the backbone and with side chains that have no conformational degrees of freedom, this polar energy is summed for each conformer as $\Delta G_{pol,i}$. For each conformer, Lennard-Jones interactions with the backbone and with all side chains with no degrees of freedom were summed and added to the torsion angle energy as $\Delta G_{nonel,i}$. ΔG_{ij} is the sum of the electrostatic and non-electrostatic pair-wise interaction between all possible conformers.

Chapter 2: Modeling Binding Kinetics at the Q_A site in Bacterial Reaction Centers

2-A) Introduction: Bacterial reaction centers (RCs) catalyze a series of electron transfer reactions reducing a neutral quinone to a bound, anionic semiquinone. The association rates of thirteen tailless neutral and anionic benzo- and naphthoquinones for the Q_A site were measured and compared. The K_ds for these quinones range from 0.08-90 M. For the eight neutral quinones, including duroquinone (DQ) and 2,3-dimethoxy-5-methyl-1,4-benzoquinone (UQ_0), the quinone concentration and solvent viscosity dependence of the association rate indicate a second order rate-determining step. The association rate constants (k_{on}) range from 10^5-10^7 $M^{-1}s^{-1}$. Association and dissociation rate constants were determined at pHs above the hydroxyl pK_a for five hydroxyl naphthoquinones. These negatively charged compounds are competitive inhibitors for the Q_A site. While the neutral quinones reach equilibrium in milliseconds, anionic hydroxyl quinones with similar K_ds take minutes to bind or dissociate. These slow rates are independent of ionic strength, solvent viscosity and quinone concentration indicating a first order rate-limiting step. The anionic semiquinone, formed by forward electron transfer at the Q_A site, also dissociates slowly. It is not possible to measure the association rate of the unstable semiquinone. However, since the protein creates kinetic barriers for binding and releasing anionic hydroxyl quinones without greatly increasing the affinity relative to neutral quinones, it is suggested that the Q_A site may do the same for anionic semi-quinone. Thus, the slow semi-quinone dissociation may not indicate significant thermodynamic stabilization of the reduced species in the Q_A site.

Photosynthetic reaction centers (RCs) are integral membrane proteins that catalyze light initiated electron transfer reactions across the membrane. In the bacteria *Rhodobacter sphaeroides,* RCs have nine bound co-factors embedded in three polypeptide chains (L, M and H). These cofactors are arranged in two symmetric branches spanning the membrane (Stowell and others 1997). The primary electron donor P, a bacteriochlorophyll dimer, absorbs a photon obtaining the energy to reduce the active branch bacteriopheophytin (H_A). The reduced $H_A^{\bullet-}$ in turn reduces the primary quinone, Q_A, resulting in the $P^{\bullet+}Q_A^{\bullet-}$ state, separating charge 25Å across the cell membrane. $Q_A^{\bullet-}$ reduces the secondary quinone, Q_B, yielding $P^{\bullet+}Q_B^{\bullet-}$. In isolated RCs, charge recombination, reducing $P^{\bullet+}$, competes with forward electron transfer. This can occur from $Q_B^{\bullet-}$, from $Q_A^{\bullet-}$ when the Q_B binding site is empty, or from $H_A^{\bullet-}$ if the Q_A site is empty (Gunner 1991; Kirmaier and Holten 1993).

In *Rb. sphaeroides* RCs the quinone in the Q_A and Q_B sites are both ubiquinone-10 (UQ_{10}). The Q_A and Q_B binding sites have different affinities for the various UQ_{10} redox states, allowing them to play different functional roles. Thus, electron transfer from $Q_A^{\bullet-}$ to Q_B is favorable despite their chemical identity (Zhu and Gunner 2005). Q_A accepts only one electron, forming the semiquinone, while two cycles of electron transfer forms the doubly reduced quinol at the Q_B site (Okamura and Feher 1995; Wraight 2004). The quinol dissociates rapidly allowing another free quinone to bind the Q_B site and restart the cycle (Graige and others 1996; McPherson and others 1990).

The redox midpoint potentials (E_m) for semi-quinone formation are difficult to measure in water because quinones are reduced directly to the dihydroquinone, without formation of a stable semi-quinone intermediate (Rich and Bendall 1979; Zhu and

Gunner 2005). However, a variety of studies place the E_ms for UQs higher in the Q_A and Q_B sites relative to aqueous solution (Ishikita and others 2003; Warncke and Dutton 1993b; Woodbury and others 1986; Zhu and Gunner 2005). A shift in E_m requires that the product semi-quinone bind more tightly than the neutral reactant quinone (Zhu and Gunner 2005). However, since semi-quinones are not stable in solution, their affinity cannot be measured directly by titration. Previous studies measuring the semi-quinone lifetime in the binding site have shown that the anionic semi-quinone dissociates more slowly than the neutral quinone (Diner and others 1984; Kalman and Maroti 1994). As long as k_{on} slows less than k_{off}, the semiquinone K_d would be tighter than the neutral, in agreement with the E_m being higher in the protein.

Hydroxyl quinones at pHs above their pK_as are stable anionic inhibitors at the Q_A site whose association and dissociation rates can be directly measured. The work presented here measures the association rate constants for functional neutral and anionic hydroxyl quinones at the Q_A site of RCs from *Rb. sphaeroides*. The binding mechanism is determined and the correlation of affinity with dissociation rate is compared. Parallels between binding the anionic hydroxyl quinones and the semi-quinone formed in the Q_A site by the electron transfer reaction are explored.

2-B) Methods and Materials

Reaction Center Isolation and Activity: Rb. sphaeroides poly-histidine-tagged RCs were isolated as described previously (Goldsmith and Boxer 1996). The RCs were purified on Ni-NTA (nitrilotriacetic acid) resin. The Ni-NTA column was washed with 0.05% LDAO in 10mM Tris buffer and the RCs were eluted with 40mM imidazole in 0.05% LDAO at pH 8. Q_A removal (Okamura and others 1975; Woodbury and others 1986) yielded RCs with less than 10% of the native ubiquinone left in the Q_A site and empty Q_B sites. The RC concentration was determined given $\varepsilon_{802} = 0.288\ \mu M^{-1}cm^{-1}$. A 10$\mu$s xenon flash excited the ground state RCs and formed the charge separated state, $P^{\bullet+}Q_A^{\bullet-}$ ($RCQ^{\pm}$). A photomultiplier tube monitored the $P^{\bullet+}$ signal at 430nm. The concentration of $RCQ^{\pm}$ was obtained from the initial amplitude change ≈100 μs after the flash obtained given $\varepsilon_{430} = 8.69*10^3\ \Delta OD/M$.

Determining Q_A Binding Affinity: The amplitude of the ΔA_{430} is directly proportional to the RCQ concentration.

$$RCQ = \left(\frac{\Delta A - \Delta A_{\min}}{\Delta A_{\max} - \Delta A_{\min}} \right) \cdot RC_T$$

where RC_T is the total RC concentration. ΔA_{min} the flash induced amplitude change found before quinone addition due to the 5-10% residual ubiquinone-10 left in the Q_A site. ΔA_{max} is the amplitude when all RCs have bound a functional quinone. The best-fit for the dissociation constant (K_d) was determined from equation 2 using the dependence of ΔA_{430} on the total quinone concentration (Q_T) using the Levenberg-Marquardt fitting program in IGOR Pro (WaveMetrics).

$$\Delta A(Q_T) = \left(\frac{\Delta A_{\max} - \Delta A_{\min}}{2 \cdot RC_T} \right) \cdot [K_d + Q_T + RC_T - \sqrt{-4 \cdot Q_T \cdot RC_T + (K_d + Q_T + RC_T)^2}]$$

Eight neutral, active quinones (2-bromo naphthoquinone (2-Br-NQ), 2,3-dimethyl naphthoquinone (2,3-diMe-NQ), 2-methoxy naphthoquinone (2-MeOx-NQ), 2-methyl naphthoquinone (2-Me-NQ), tetramethyl-benzoquinone (duroquinone, DQ), 1,2 naphthoquinone (1,2-NQ), 1,4 naphthoquinone (1,4-NQ) and 2,3-dimethoxy-5-methyl-1,4-benzoquinone (UQ_0)) and five hydroxyl quinones (5-hydroxy-3-methyl-naphthoquinone (5-OH-3-Me-NQ), 5-hydroxy-naphthoquinone (5-OH-NQ), 2-hydroxy-3-isopropyl-naphthoquinone (2-OH-3-Iso-NQ), 2-hydroxy-3-methyl-naphthoquinone (2-OH-3-Me-NQ) and 2-hydroxy-naphthoquinone (2-OH-NQ)) purchased from Sigma were studied.

Hydroxyl quinones at pH's above their pK_a are anionic competitive inhibitors of the Q_A site. K_Is were determined by the ability of the inhibitors to displace the functional duroquinone (DQ) from the Q_A site, diminishing ΔA_{430}. The equilibrium amplitude of active RCs was determined as a function of the inhibitor concentration with 30 μM DQ (K_d = 0.4 μM), 1 μM RCs and 0.005% LDAO, 10 mM buffer. Tris was used at pH 7.8 and Caps for measurements at pH 10.2. The K_I was obtained fitting equations 3 and 4 with Mathematica 4.2. Here RCQ is the concentration of duroquinone-bound RCs and RCI is the concentration of hydroxyl quinone-bound RCs.

$$K_d = \frac{(RC_T - RCQ - RCI) \cdot (Q_T - RCQ)}{RCQ}$$

$$K_I = \frac{(RC_T - RCQ - RCI) \cdot (I_T - RCI)}{RCI}$$

Determining Hydroxyl Quinone pK_as in solution: The pK_as for the five hydroxyl quinones were determined using the difference absorbance spectra of the ionized species relative to the neutral measured between 450nm and 530nm. Succinic acid (pH 3-5), Mes (pH 5.5-6.5), Tris (pH 7.5-8.5), Ches (pH 9-10) and Caps (pH 10.5-11.5) were used as buffers. The data was fit to equation 5 where ΔA is the absorbance relative to that found at pH 3 and ΔA_{max} is the absorbance at pH 11 minus that at pH 3. The pK_a values and wavelengths monitored for each quinone are listed in table 2-2.

$$pH = pK_a + \log\left(\frac{QO^-}{QOH}\right) = pK_a + \log\left(\frac{\Delta A}{\Delta A_{max} - \Delta A}\right)$$

Quinone Association Rate Constants: The change in $RCQ^{\pm}$ monitored by ΔA_{430} following a second flash was used to derive the second order association rate constant (k_{on}) for the active, neutral quinones (See legend to Fig. 1 and appendix for a more complete description of the model). The sample has 0.9-1.1 μM RC, 10mM Tris, 0.005% LDAO at pH 8 and the Q_B site is empty. The small concentration of RCs with ubiquinone-10 was subtracted from the total RC concentration to accurately reflect the number of available Q_A sites. The additional $RCQ^{\pm}$ found on the second flash was determined at flash intervals of 50ms, 100ms and 200ms. The rate of reforming the ground state from $RCQ^{\pm}$ (k_{AP}) was determined from an exponential fit to the charge recombination kinetics in RCs saturated with added quinone after subtraction of the contribution of the UQ-10 containing RCs. The signal was averaged 10 times. The data was fit with model A in the appendix.

The association rate of the slower binding hydroxyl quinones was measured from the loss of DQ activity with time. The RC concentration was 1μM with 30 μM DQ. The hydroxyl concentration was varied from 7 to 300 μM. The time dependent DQ activity

was measured at 0.5 to 1.0 minute intervals until equilibrium was reached and there was no change in the $RCQ^{\pm}$ formed by a flash.

The Viscosity Dependence of k_{on}: The second order association rate constant (k_{on}) is predicted to be inversely proportional to the solvent viscosity (see equation below) (Xavier and Willson 1998).

$$\frac{k_{on}^{0}}{k_{on}^{v}} = A + B \cdot \frac{\eta}{\eta_0}$$

k_{on}^{0} and k_{on}^{v} are the association rate constants and η_0 and η are the solvent viscosity in the absence and presence of the viscosity modifier, respectively. A and B are fitting parameters where A = 0 and B = 1 in the case for an ideal diffusion-limited interaction. The solvent was modified by adding 10-60% (w/w) glycerol. The values η_0 and η were taken from the CRC Handbook of Chemistry and Physics (David 1995)

2-C) Results

Measuring binding kinetics of active, neutral benzo- and napthoquinones. The association rate constants (k_{on}) were measured by a double flash method (Fig. 2-1). Quinone concentrations were chosen so there is a mixture of RCs with occupied (RCQ) and empty (RC_F) Q_A binding sites. Since there was no indication of Q_B activity, the Q_B site is assumed to be empty. The sample starts off at equilibrium with the quinone freely associating and dissociating from the protein with rates k_{on} and k_{off} (Fig. 2-1a). The first flash forms the charge separated $P^{\bullet+}Q_A^{\bullet-}$ state ($RCQ^{\pm}$) from RCQ, depleting RCQ and leaving RC_F unchanged. Since $Q_A^{\bullet-}$ dissociates much more slowly than Q_A (Kalman and Maroti 1994), the system is no longer at equilibrium. This depletion of RCQ causes association to be much faster than dissociation (k_{on} $[RC_F] >> k_{off}$*[RCQ]), thus additional RCQ is formed, denoted RCQ_{bind}, which can be detected by a second actinic flash. Simultaneously, charge recombination within the $RCQ^{\pm}$ state reforms RCQ at k_{AP}, moving the system back towards equilibrium (see appendixfor a detailed description). Once charge recombination is complete the equilibrium concentrations are restored.

The double flash measurements were carried out at increasing quinone concentration (Fig. 2-2). The second flash, delivered 50, 100 and 200ms after the first generates additional RCQ (RCQ_{bind}). The extra amplitude depends on the time delay, the quinone concentration, light saturation, and k_{AP} all of which can be determined independently and on the association rate constant (k_{on}). The amplitude of the second flash initially increases (when association is the dominant process) and then goes back to the value of the first flash as the delay time becomes longer (Fig. 1). RCQ_{bind} is always small. When K_d is smaller then the RC concentration at sub-saturating quinone there is

little Q_F left to bind. The decay back to the ground state at k_{AP} provides a short window for observation. In addition, the sub-saturating flash means that RCQ is not completely depleted on the first flash. Under conditions used here RCQ_{bind} is less then 10% of the total RCs. However qualitatively, formation of RCQ by association between flashes can be seen in the tighter apparent affinity of RC for quinone on the second flash (Fig. 2). The k_{on} yielding the set of curves that best overall fit to the concentration dependence at the 3 delay times is determined. For duroquinone (DQ) with a K_d of 0.40 M and k_{AP} of 3.4 s^{-1} has a k_{on} of 5.5± 1.5*10^7 $M^{-1}s^{-1}$ and a k_{off} of 3.3s^{-1} (given $k_{off} = k_{on}*K_d$). The k_{on}s for 2,3 dimethoxy-5-methyl BQ (UQ_0) and the other seven tailless 1,4-napthoquinones range from 10^5-10^7 $M^{-1}s^{-1}$ while k_{off} varies from 0.2s^{-1} to 6s^{-1} (Table 2-1).

Figure 2-1: Double flash assay to measure the binding kinetics of the neutral quinones. (a) *(1)* Initially the sample is at equilibrium with $k_{on}[RC_F][Q_F] = k_{off}[RCQ_{eq}]$. $[RCQ_{eq}]$ is the equilibrium concentration of RCs with bound quinone given $[RC_T]$ and $[Q_T]$. *(2)* The first flash initiates electron transfer forming the charge separated state ($RCQ^{\pm}$) with semiquinone bound at the Q_A site, depleting RCQ to (1-)*$[RCQ_{eq}]$ where is the fraction of RCs that absorb a photon on a flash (see supporting information). Now the association rate is faster than dissociation, $k_{on}[RC_F][Q_F] >> k_{off}[RCQ_{eq}]$. *(3)* RCQ is re-formed by association of RC_F and Q_F and by charge recombination from $RCQ^{\pm}$ at k_{AP}. As these two processes take place, a second flash measures the additional RCQ formed due to binding. When charge recombination is complete the initial equilibrium concentrations are re-formed (*1*) so a second flash now generates as much $RCQ^{\pm}$ as the first. (b) Concentration of RC populations as a function of time given =1. At the time of the first

flash (t=0), all RCQ_{eq} is transformed into the charge separated state ($RCQ^{\pm}$), thus [RCQ] = 0 and $[RCQ^{\pm}] = [RCQ_{eq}]$. Net association of RC_F and Q_F yields RCQ_{bind} depleting RC_F. Simultaneously, charge recombination reforms RCQ from $RCQ^{\pm}$ at $k_{AP.}$ When charge recombination is complete $[RCQ] = [RCQ_{eq}]$, $[RCQ^{\pm}]$ and $[RCQ_{bind}] = 0$. A second flash monitors how $[RCQ_{bind}]$ changes with time. For this simulation the Q_A sites are 50% saturated, $[RCQ_{eq}] = [RC_F] = \frac{1}{2}[RC_T]$ and $[Q_T] = \frac{1}{2}[RC_T] + [K_d]$;. K_d=0.6 M, RC_T=1.0 M, k_{on} is $8*10^6 M^{-1}s^{-1}$, and k_{AP} is $3.5s^{-1}$.

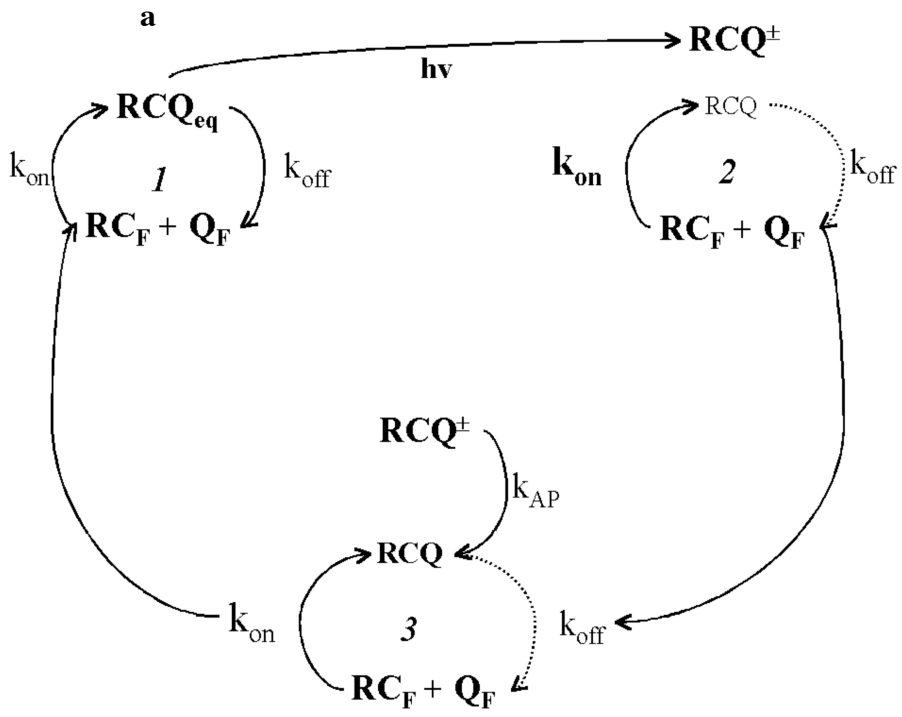

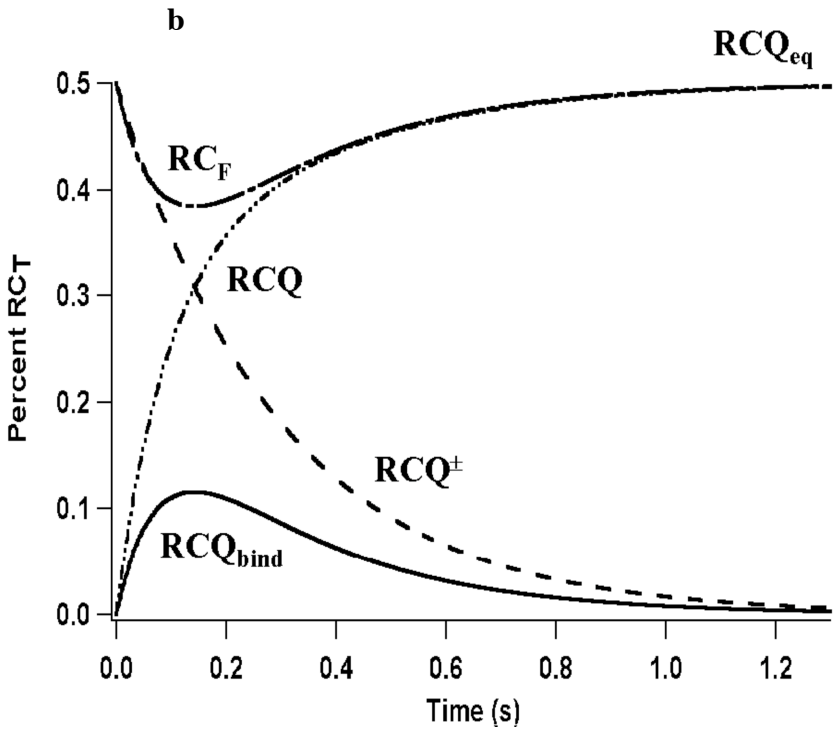

Figure 2-2: The concentration of quinone bound RCs ($RCQ = RC_{eq} + RCQ_{bind}$) as a function of DQ concentration (Q_T) is plotted for the first flash (black), and at delay times for the second flash of t=50ms (red), t=100ms (green) and t=200ms (blue). For time t=0, RCQ_{bind} is zero ($RCQ=RCQ_{eq}$). The data is corrected for 10% residual ubiquinone-10 at Q_A and for light saturation, l, of 85%. The solid lines are solutions to model A (see supporting information) with k_{on} of $5.5*10^6$ $M^{-1}s^{-1}$, K_d of 0.4 μM and k_{AP} of 3.4 s^{-1}. Conditions: 0.93 μM RCs in 10mM Tris at pH 7.8, LDAO=0.005% at room temperature.

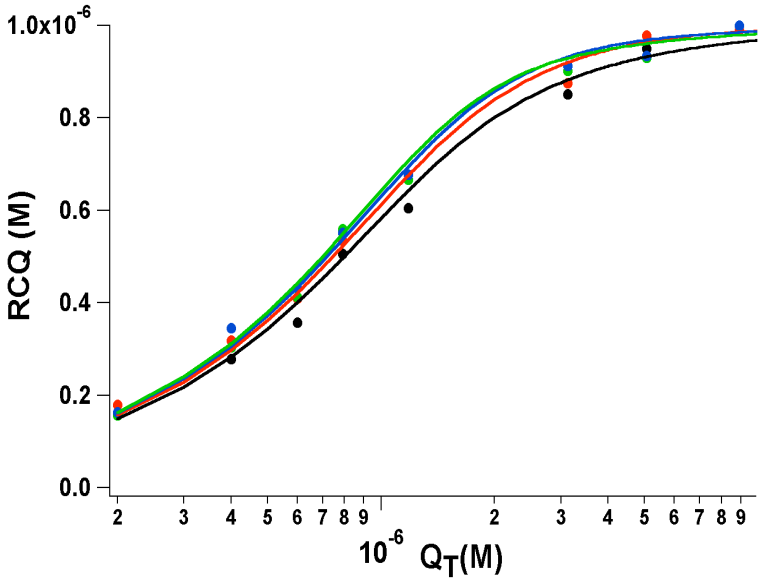

Table 2-1: Binding Rates and Affinities for Neutral Quinones at the Q_A Site of RCs

	Quinone	K_d (□M)	k_{on} x 10^{-6} ($M^{-1}s^{-1}$)	k_{off} (s^{-1})	k_{AP} (s^{-1})
1	UQ_0	86 ± 16	0.07 ± 0.01	6.0	10
2	1,2-NQ	13 ± 3.0	0.07 ± 0.06	0.9	8.3
3	1,4-NQ	7.4 ± 1.2	0.6 ± 0.03	0.6	7.1
4	2-MeOx-NQ	0.5 ± 0.1	0.3 ± 0.1	0.2	12
5	2-Me-NQ	0.6 ± 0.1	2.6 ± 1.0	1.6	7.4

6	DQ	0.4 ± 0.1	5.5 ± 1.5	3.3	3.4
7	2,3-dMe-NQ	0.1 ± 0.02	9.4 ± 3.0	1.3	6.7

Numbers are used as labels in figure 8. K_d was obtained from the amount of $RCQ^{\pm}$ formed after a single flash as a function of the concentration of added quinone (equation 1), k_{on} was measured with the double flash assay (as shown for DQ, Fig.2), k_{off} is derived from $K_d = k_{off}/k_{on}$ and k_{AP} is the $Q_A^{\bullet -}$ to $P^{\bullet +}$ charge recombination rate constant.

Measuring binding kinetics for inactive, anionic hydroxyl naphthoquinones: The pK_as for the hydroxyl quinones range from 4.0 to 9.4 (Table 2-2). Above their pK_a none of these quinones reconstitute Q_A function. Their binding is measured by their competition with the active DQ. The K_Is, at pHs above their pK_as, vary from 0.04 to 5 □M. The neutral 5-OH-2-Me-NQ does bind rapidly and will reconstitute Q_A activity (manuscript in preparation). Measurement of the association of neutral 5-OH-2-Me-NQ is complicated because the Q_A site downshifts the pK_a so the bound quinone is not fully protonated even at pH 7.2.

The pK_a of 5-OH-2-Me-NQ is 9.4. At pH 10.2 the ionized species is a competitive inhibitor at the Q_A site. Its slow association rate was determined from the time dependent loss of DQ activity (Fig. 2-3a). In a sample with 70-80% of the Q_A sites occupied by DQ, 90-300 □M 5-OH-2-Me-NQ was added. Activity is lost as DQ is displaced from the Q_A site with the system reaching equilibrium in 6-10 minutes (Fig. 2-3a). The dependence of the equilibrium DQ activity on the inhibitor concentration

provides a K_I of 5 ±3 M (Table 2-2). To determine the reversibility of binding, the dissociation rate constant, k_{off}, was measured directly from the time dependent increase of activity when DQ is added to a sample is pre-equilibrated with the hydroxyl quinone. Ionized 5-OH-2-Me NQ displays completely reversible binding with a k_{off} of $1.7*10^{-4}$ s^{-1} (Fig. 2-3b).

Figure 2-3: Time dependence of DQ dependent activity in the presence of 5-OH-2-Me NQ at pH 10.2. (a) Loss of activity following addition of 160 μM 5-OH-2-Me NQ at t=0 to 1μM RCs with 30μM DQ. The line the best fit to the first-order binding model E (see supporting information) with a k_{uni} of $1.7*10^{-2}s^{-1}$. (b) Restoration of DQ dependent activity following the addition of 30μM DQ to 1μM RCs preincubated with 160μM 5-OH-2-Me NQ for 30 minutes at pH 10.2. The solid line is the best fit to model C (see appendix) with a k_{off} of $2.0*10^{-4}s^{-1}$.

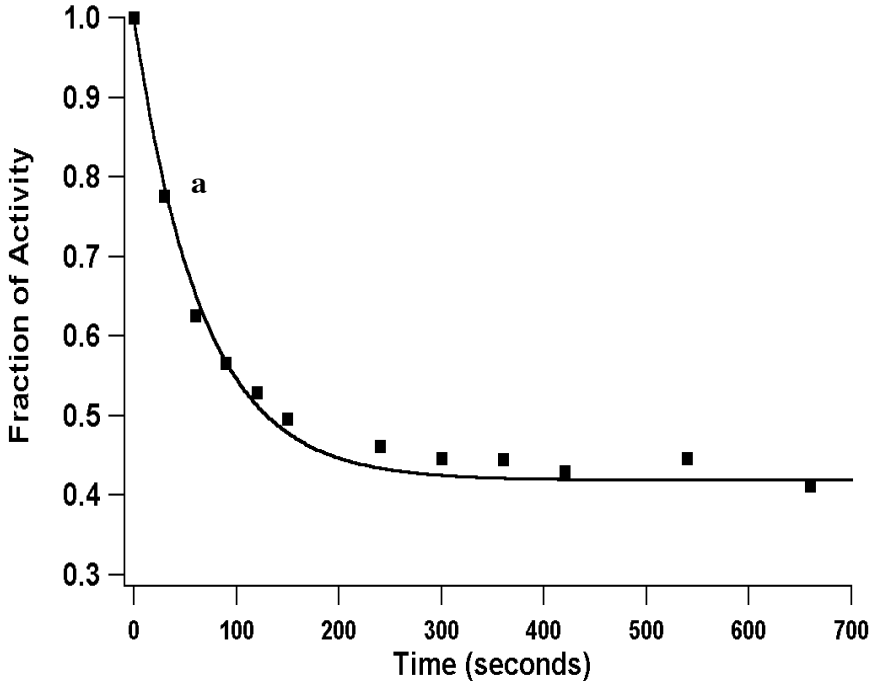

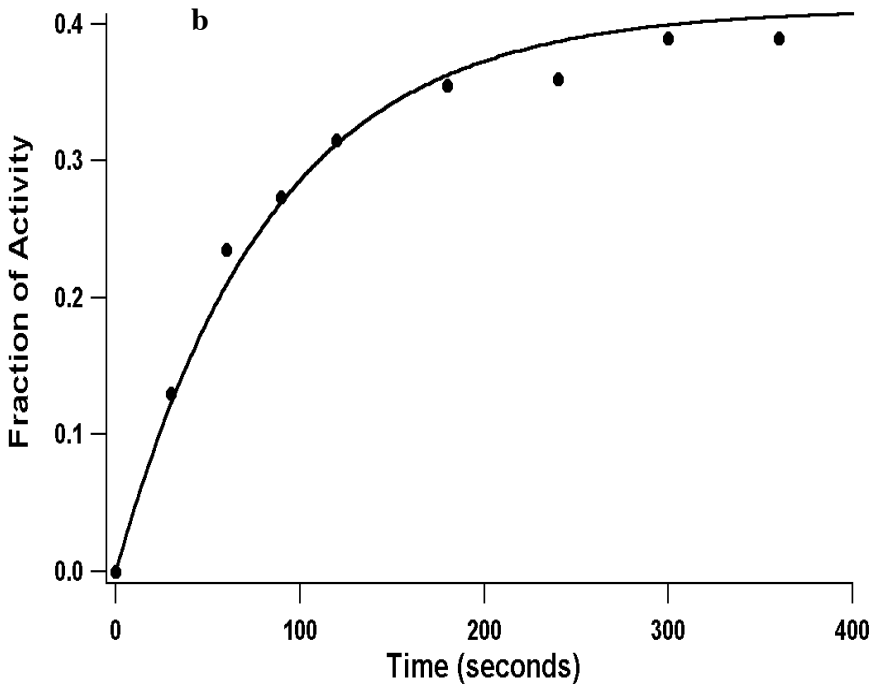

Determination of the binding mechanism: The anionic hydroxyl quinones bind in minutes, much slower than the 10^6 to 10^9 s^{-1} expected for a diffusion-dominated process. They bind at least 1000 times slower than the neutral quinones with comparable K_ds (Tables 2-1 and 2-2). The quinone concentration dependence of the rate constants can clarify whether the rate-limiting step is bi- or uni-molecular. For a second order rate-determining step, the association rate constant k_{on} ($M^{-1}s^{-1}$) is independent of quinone concentration, while the apparent first order rate constant k_{uni} (s^{-1}) is a linear function of concentration with $k_{uni} = k_{on}*[Q_T] + k_{off}$ (Duggleby and others 1982). On the other hand, for a first order rate-determining step, k_{uni} (s^{-1}) is independent of quinone concentration while the apparent k_{on} ($M^{-1}s^{-1}$) is a reciprocal function of concentration, $k_{on} = A +$

$k_{uni}/[Q_T]$, where A is the observed second order rate constant at saturating quinone concentration.

Concentration dependence of the neutral quinones association rate: For the active fast binding neutral quinones the change in amplitude on the second flash at 3 different delay times at a single concentration was fit to a second order model (A in supporting information), providing k_{on}, and with a first order model (D in supporting information), providing k_{uni}. The k_{on} for DQ measured in this way gives a mean value of $6.9*10^6$ $M^{-1}s^{-1}$ (Fig. 2-4a) in reasonable agreement with $5.5*10^6$ $M^{-1}s^{-1}$ found by a global fit of the data (Fig. 2-2). The neutral quinone k_{on}s are concentration independent, as shown for DQ (Fig. 4a), indicating a second order rate-determining step. As expected, k_{uni} is a linear function of quinone concentration. The slope of the concentration dependence of k_{uni} for DQ is $2.4*10^6$ $M^{-1}s^{-1}$ (Fig. 2-4b), which is in reasonable agreement with the measured k_{on} (Fig. 2-2). The y-intercept (Fig. 2-4b) is not in good agreement with the k_{off} obtained from K_d*k_{on} (Table 2-1). For example, 2-Me-NQ has a negative y intercept (data not shown). However, it is not unusual that this analysis does not provide accurate values for k_{off} (Duggleby and others 1982).

Concentration dependence of the hydroxyl quinone association rate: The association data for the slow binding anionic hydroxyl quinones (Fig. 3) was fit with a second order model (B in appendix) providing k_{on} and with a first order model (E in appendix) providing k_{uni}. 5-OH-NQ and 5-OH-2-Me-NQ show a first order rate-determining step. For 5-OH-2-Me-NQ k_{uni} is concentration independent (Fig 2-4d) with the average value of $0.017s^{-1}$ while k_{on} depends on $[Q_T]^{-1}$ (Fig. 4c). The k_{uni} derived from

fitting the concentration dependence of the observed second order rate (k_{on}) is $0.008s^{-1}$ in reasonable agreement with the directly determined value.

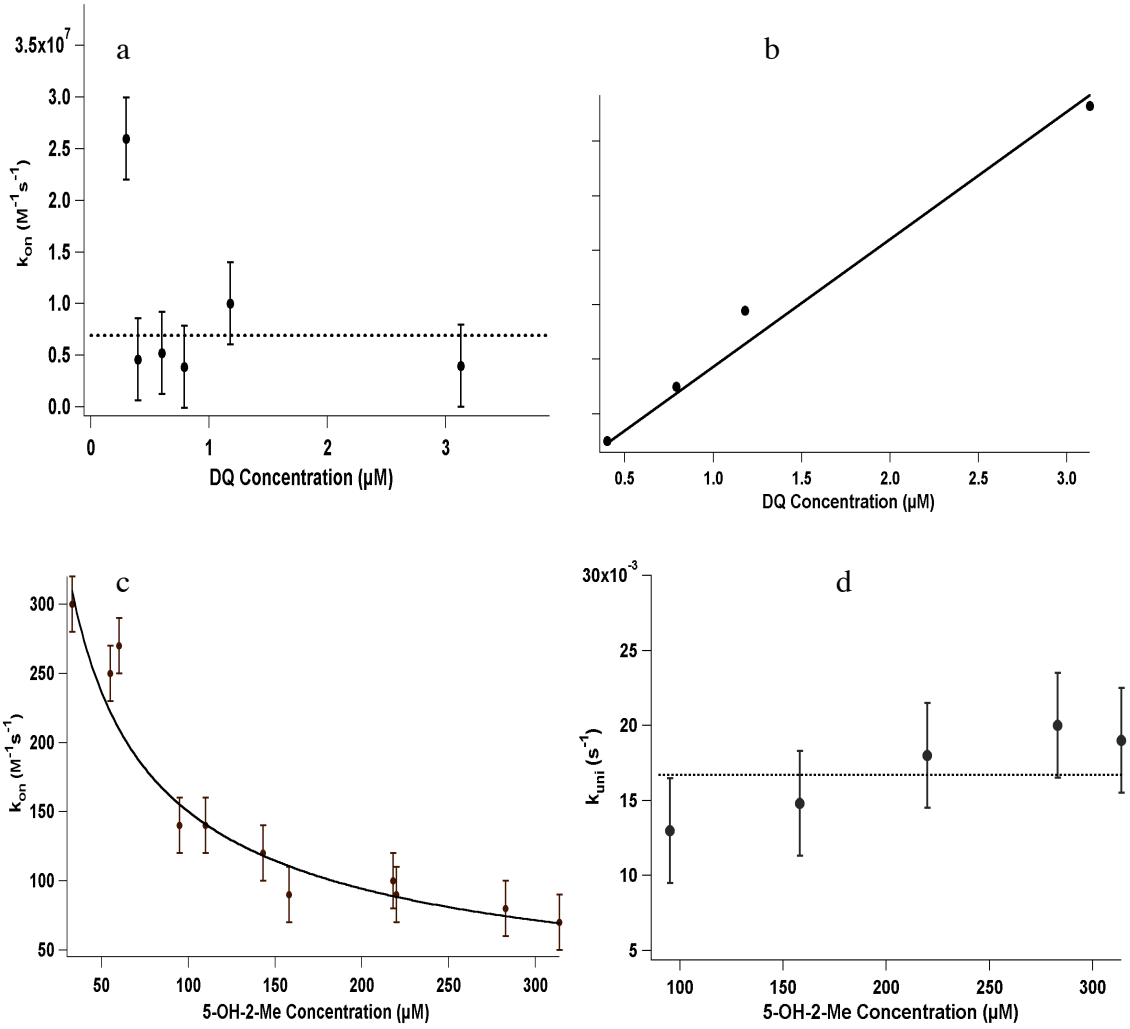

Figure 2-4: Dependence of the derived first and second order rate constants (k_{uni} and k_{on}) on quinone concentration. (a-b) DQ, a neutral quinone. The DQ concentrations tested yield 30-85% saturation of Q_A binding sites; (a) Concentration dependence of the second order association rate constant, k_{on} derived by fitting the double flash data at the three delay times (50, 100 and 200ms) at the given quinone concentration (A in supporting information). The dashed line is $6.9*10^6\ M^{-1}s^{-1}$, which is the mean value of 6 fits. (b) Fit

of data with first order model (D in supporting information) provided k_{uni}. The solid line is the best-fit obtained by linear regression with slope = $2.4*10^6$ $M^{-1}s^{-1}$ and y-intercept = $0.52s^{-1}$. The experimental conditions are 1 M RCs in 10mM Tris and 0.005% LDAO at pH 7.8. (c-d) 5-OH-2-Me-NQ, an anionic quinone inhibitor. (c) The second order rate constant (k_{on}), (B supporting information), displays a reciprocal concentration dependence, as expected for a first order rate-determining step. The solid line is $k_{on}(M^{-1}s^{-1}) = 26 + 0.008/[Q_T]$. (d) The first order rate constant (k_{uni}) (E supporting information) is independent of the hydroxyl quinone concentration. The dashed line at $0.017s^{-1}$ is the average k_{uni} for all the measurements. The experimental conditions are 1 M RCs in 10mM CAPS and 0.005% LDAO at pH 10.2.

Table 2-2: Binding Rates and Affinities for Anionic Hydroxyl Quinone at the Q_A Site of RCs

	Quinone	pH	K_I (M)	$k_{uni}x10^2$ (s^{-1})	$k_{off}x10^4$ (s^{-1})	pK_a	Wavelength* (nm)
9	2-OH –NQ	7.8	0.1 ± 0.05	7.0 ± 2.0**	3 ± 0.7	4.16	540
10	5-OH -NQ	10.2	0.6 ± 0.2	2.2 ±0.2	1 ± 0.5	9.12	530
11	2-OH-3-Iso –NQ	10.2	4.0 ± 2.3	0.7 ±0.1	2 ± 0.3	5.85	480
12	5-OH-2-Me–NQ	10.2	4.5 ± 1.4	1.7 ± 0.7	2 ± 0.6	9.4	520

Numbers are used as labels in figure 8. pH: K_Is and first order association and dissociation rate constants measured at a pH above the hydroxyl group pK_a. K_I is obtained from the concentration dependence of equilibrium DQ activity. *Wavelength used to measure absorbance difference between neutral and ionized hydroxyl quinone to determine the pK_a in aqueous solution. **Measured above 25 M where k_{on} is independent of quinone concentration (Fig 2-5). ND: Dissociation of 2-OH-3-Me could not be detected (Fig 2-6).

Both 5-OH quinones show completely reversible binding that is consistent with a first order rate-determining step. Thus, k_{on} can be determined by loss of activity after the quinone is added to RCs reconstituted with DQ (Fig. 3a), while k_{off} can be determined from the restoration of activity when DQ is added to RCs pre-incubated with the hydroxyl quinone (Fig. 2-3b). The same K_I is derived from the concentration dependence of the long time asymptote is both measurements and this is consistent with the value determined from k_{uni}/k_{off}.

The three quinones with an ortho-hydroxyl group present data that is more difficult to interpret. The apparent second order rate constant (k_{on}^{obs}) for 2-OH-NQ fits a model similar to 5-OH-2-Me-NQ (Fig. 4c) with $k_{on}^{obs} = 900M^{-1}s^{-1} + 0.05s^{-1}/[Q_T]$ (Fig. 2-5a) suggesting the rate-determining step is first order. On the other hand, the observed rate (k_{on}^{obs}) of 2-OH-NQ is quinone concentration dependent at low concentration, becoming independent at higher concentrations (Fig. 2-5b). This indicates that the rate-determining step itself is concentration dependent. Thus the rate was treated with a model consisting of two barriers, one is first order and the other second order (their sequence is unspecified) (Xu and Gunner 2002). At low concentration the second order association

process limits the rate, with k_{uni}^{obs} being concentration dependent (Fig. 5b). However, the reaction cannot proceed faster then the first order step, which is rate-limiting at high concentration. Thus $k_{uni}^{obs} = k_{uni}/(1+K_{bi}/[Q_T])$, where k_{uni} is true rate constant for the first order step and K_{bi} is the dissociation constant for the second order process (Fig. 5b). Fitting the data to this model yields $k_{uni} = 0.089s^{-1}$, comparable to the values found for the other anionic quinones, and K_{bi} = 4.5 μM. The affinity of the initial encounter is significantly weaker then the overall K_d of 0.1μM (Table 2), indicating that protein conformational changes in the subsequent first order step may tighten binding. There is reasonable agreement between the k_{uni} obtained from concentration dependence of the rate ($0.089s^{-1}$) and from the apparent second order model ($0.05s^{-1}$) (Fig. 2-5).

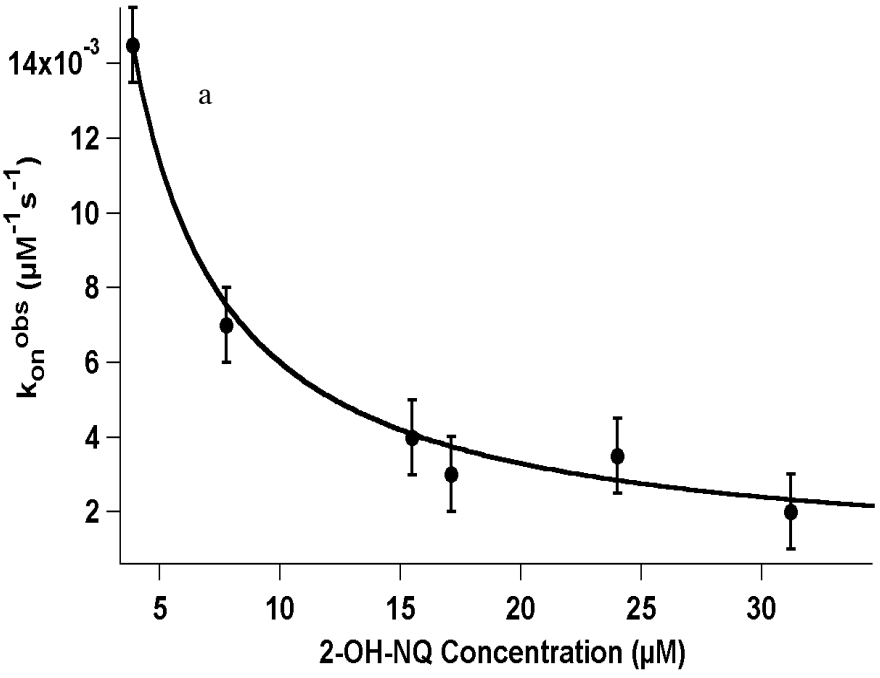

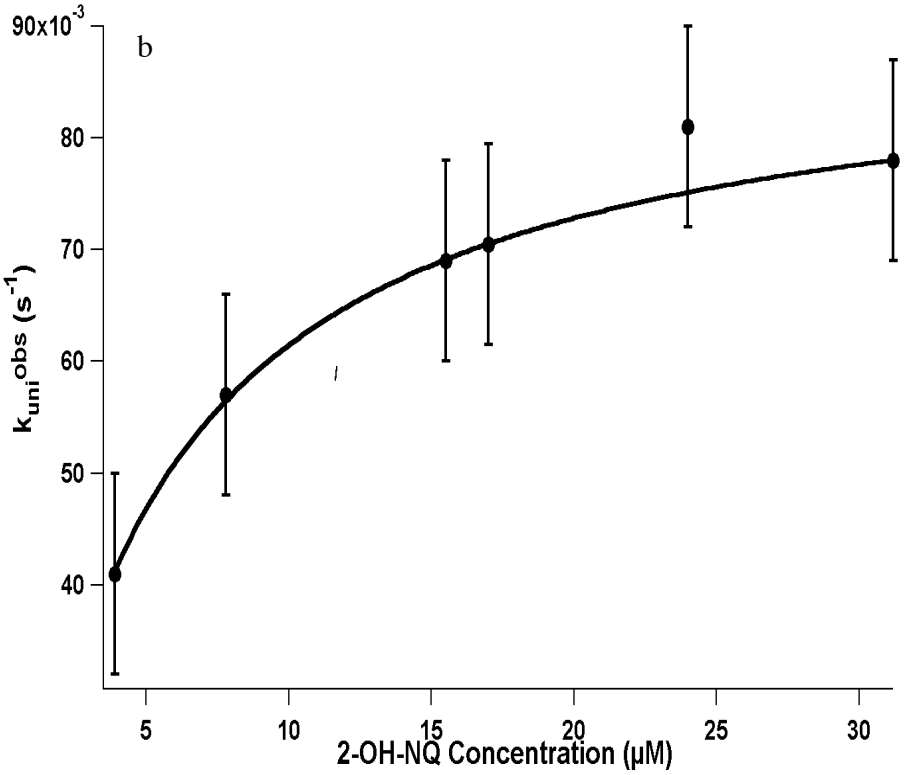

Figure 2-5: a) Concentration dependence of second order rate constant (k_{on}) for 2-OH-NQ. The solid line is the best-fit curve, $k_{on}^{obs} = 900M^{-1}s^{-1} + 0.05/[Q_T]$. b) Concentration dependence of first order rate constant (k_{uni}) for 2-OH-NQ. The solid line is $k_{uni}^{obs} = 0.089s^{-1}/(1+4.5/[Q_T])$. The rate-determining step becomes independent of concentration when $k_{uni} = 0.089s^{-1}$. The experimental conditions are 1□M RCs in 10mM Tris and 0.005% LDAO at pH 7.8.

If DQ is added to a sample pre-equilibrated with an anionic hydroxyl quinone, full activity can be recovered with 2-OH-NQ, 5-OH-NQ and 5-OH-2-Me-NQ (Fig. 3B). For these quinones the directly measured k_{off} matches the value derived from $k_{on}*K_I$. However, for 2-OH-3-Me-NQ, the addition of DQ does not restore any activity (Fig. 6).

This is consistent with K_I being in the sub-nanomolar range. There are no changes in RC spectra that would indicate significant changes in structure due to incubation with 2-OH-3-Me-NQ. Similar measurements with 2-OH-3-Iso-NQ shows only 50% of the activity is recovered and k_{off} is slower than $k_{on}*K_I$, indicating that the dissociation mechanism is not just the reverse of association.

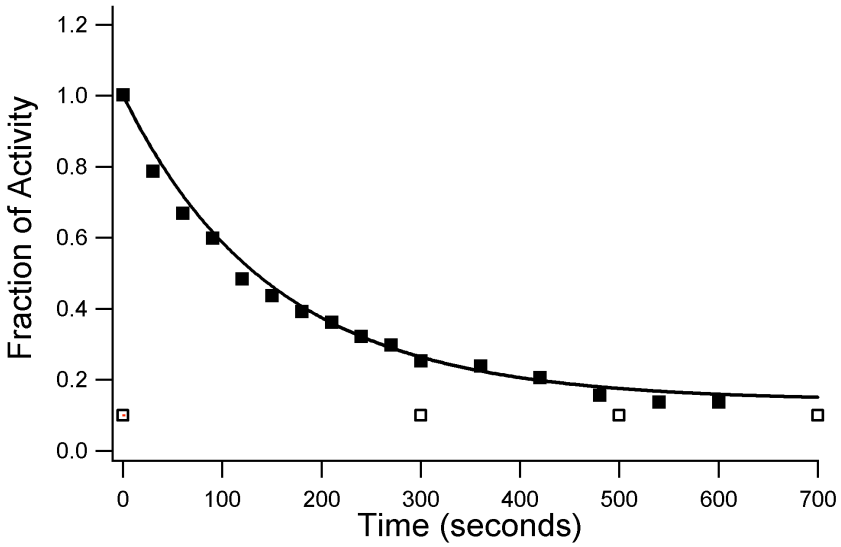

Figure 2-6: Binding of 2-OH-3-Me. Solid squares: At t=0 23μM of 2-OH-3-Me was added to 30μM DQ in equilibrium with 1μM RC_T (pH 7.8). The time course for the inhibition of DQ activity yielded the measured k_{uni} of $8*10s^{-1}$. Empty squares: 30μM DQ is added to a sample with 1μM RC_T pre-equilibrated for 30 minutes with 23μM 2-OH-3-Me (in 10mM Tris at pH 7.8). No DQ activity was detected.

Viscosity dependence of k_{on}: For a second order rate-determining step, diffusion plays a dominant role thus the rate constant is predicted to be inversely proportional to the

solvent viscosity (η) (Kramers 1940). Using glycerol as a solvent modifier, the viscosity dependence of k_{on} for DQ and 2-Me-NQ was determined (Fig. 2-7a). The dashed lines represent the ideal diffusion controlled reaction, where the product $k_{on}*\eta$ is constant. The k_{on}s for these two neutral quinones have strong viscosity dependence (Fig. 2-7a), consistent with a second order rate-determining step. For DQ the association rate becomes slower than expected as the viscosity increases, as k_{on} is above the dashed line in Fig. 2-7a. The reason for this is not clear but it may be due to solvent osmotic pressure, which has been observed previously when glycerol is used as a solvent modifier (Xavier and Willson 1998). On the other hand, the second order rate constants (k_{on}) for the anionic 5-OH-2-Me-NQ and 2-OH-NQ are independent of viscosity (Fig. 2-7b) supporting a first order rate-determining step for the hydroxyl-quinones.

Ionic Strength Dependence of k_{on} and k_{uni}: Binding kinetics were measured at NaCl concentrations of 0 to 300 mM. Ionic strength will affect the binding rate if electrostatic interactions between RCs and quinone are important for the rate-determining step. Neither k_{on}, for the neutral quinones, nor k_{uni}, for the anionic quinones depend on the ionic strength (data not shown). Thus, electrostatic interactions do not govern the rate-determining step. For the hydroxyl quinones, this is further evidence of a first order rate-determining step since solution counterions would be expected to shield electrostatic interactions between the anionic inhibitor and the RCs.

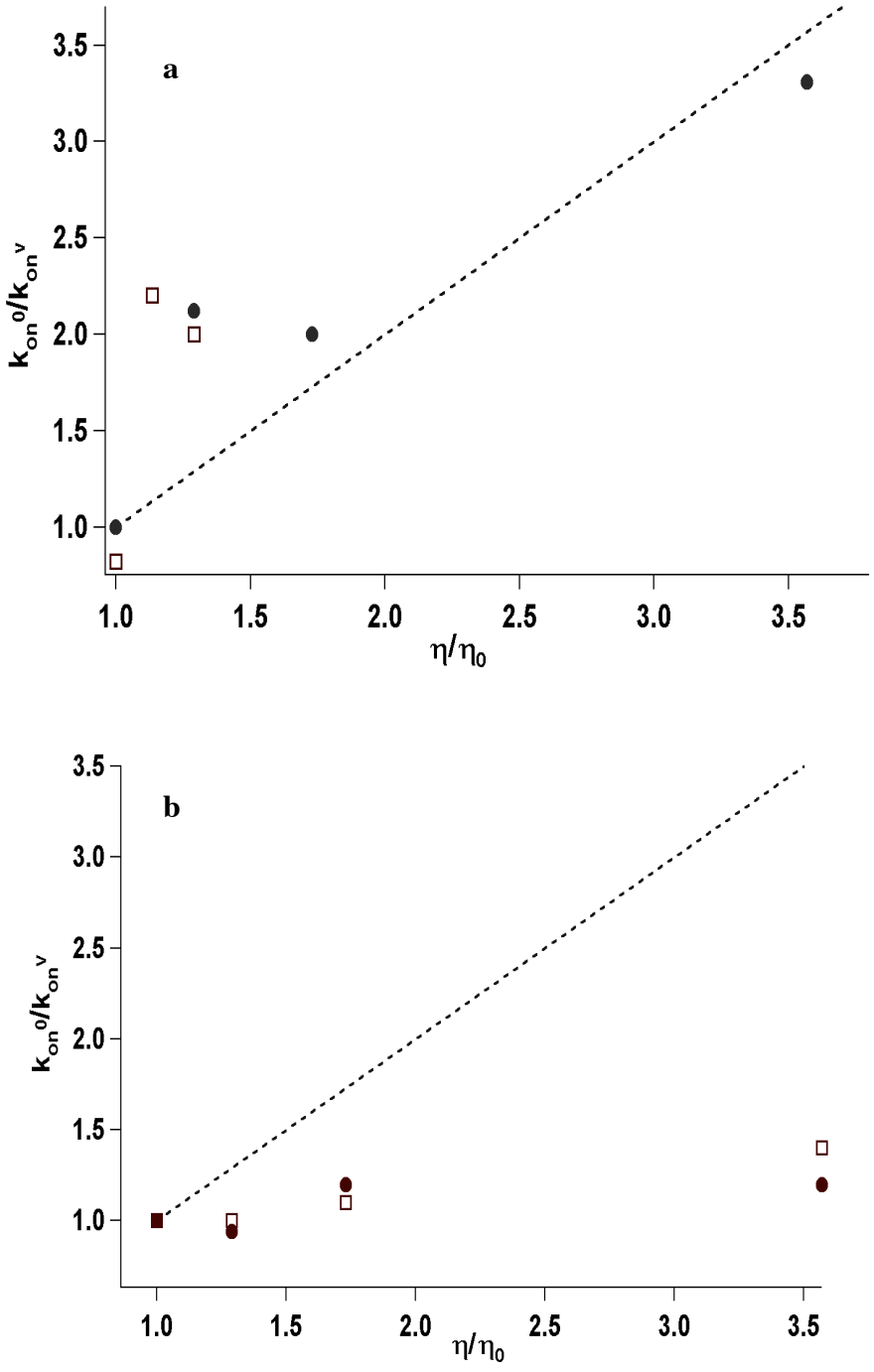

Figure 2-7: Viscosity dependence of the second order association rate constant (k_{on}). The dashed line has a slope of 1 representing the expected trend for a second order diffusion controlled association reaction (equation 6). Each data point represents the average k_{on}

measured with 1 M RC in 0.005% LDAO at 20%, 50% and 70% binding saturation for each quinone. (a) open squares: DQ, filled circles: 2-Me-NQ measured in 10mM Tris at pH 7.8. (b) open squares: 5-OH-2-Me-NQ (measured in 10mM CAPS at pH 10.2), filled circles: 2-OH-3-Me-NQ (measured in 10mM Tris at pH 7.8).

Comparing binding rates and equilibrium affinity: The K_ds for the fast binding neutral quinones and the K_Is for the slow binding hydroxyls are in the same range (0.1 to 90 M) yet their dissociation rates differ by 10^3 to 10^4-fold (Fig. 8a). For the neutral quinones the association rate (k_{on}) correlates with K_d, thus an increase in binding strength is predominately due to faster association (Fig. 2-8b). 2-MeOx-NQ deviates from this trend as its k_{on} is slower than expected given its K_d. Methoxy substituents lower the quinone partition coefficient, preferring the aqueous phase, which can increase the energy barrier for association (Rich and Bendall 1979). The Q_A site interacts strongly with the methoxy group keeping the K_d tight in spite of the association barrier.

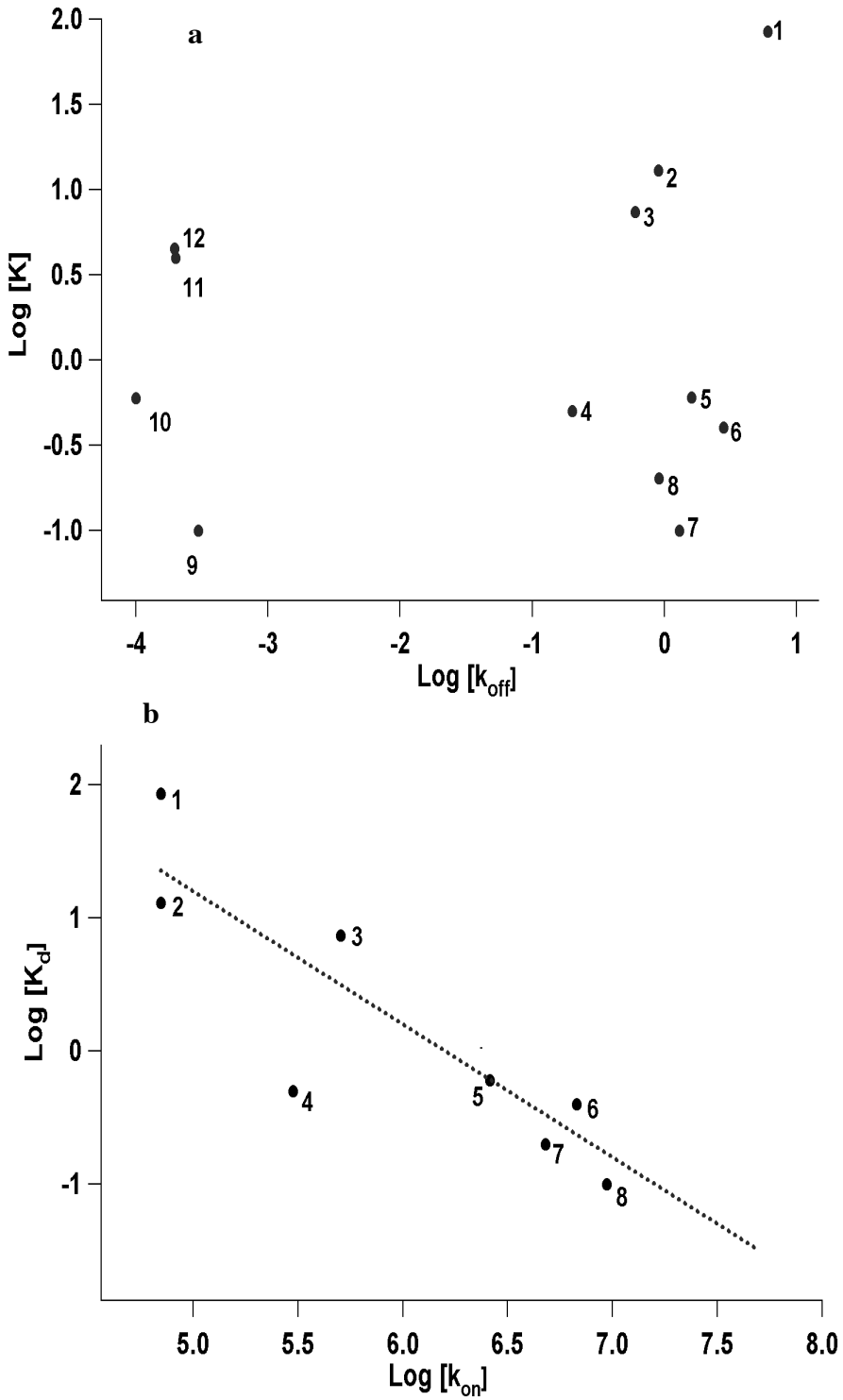

Figure 2-8: Binding affinity vs binding rate constants for neutral and anionic quinones. (a) Comparison of the dissociation rate (k_{off}, s^{-1}) and the binding affinity (K is K_d for

neutral quinones and K_I for hydroxyl quinones in units of □M). The anionic hydroxyl quinones (9-11) dissociate about 10,000-fold more slowly than neutral quinones (1-8) with comparable K_ds. (b) Comparison of the second order association rate (k_{on}, $M^{-1}s^{-1}$) and the binding affinity (K_d, □M) for the neutral quinones. The dashed line has a slope of –1 showing the correlation between Log[K_d] and –Log[k_{on}]. The quinone labels from Tables 1 and 2. 1: UQ_0, 2: 1,2-NQ, 3: 1,4-NQ, 4: 2-MeOx-NQ, 5: 2-Me-NQ, 6: DQ, 7: 2,3-diMe-NQ, 8: 2-Br-NQ, 9: 2-OH-NQ, 10: 5-OH-NQ, 11: 2-OH-3-Iso-NQ, 12: 5-OH-2-Me-NQ.

2-D) Discussion: The comparison of binding of neutral and anionic quinones to the Q_A site of RCs show that the negatively charged hydroxyl quinones dissociate about 10^4-times more slowly than neutral quinones with comparable K_ds (Fig. 8a). In addition these quinones have different mechanisms for binding. The linear dependence of the apparent first order rate constant (k_{uni}) on quinone concentration shows that the rate-determining step for the neutral quinones is second order (Fig. 4) (Kurz and others 1987; Steyaert and others 1991; Xavier and Willson 1998). The dependence of K_d on the second order k_{on} shows that the association rate plays the dominant role in controlling affinity (Fig. 8). The solvent viscosity dependence indicates this is a primarily diffusion-controlled process (Fig. 7). The measured rate constants of these quinones (10^5 to 10^7 $M^{-1}s^{-1}$) are typical of the association of large proteins with small ligands, where only a small fraction of the protein surface can form an active encounter complex (Schreiber 2002; van Holde 2002).

The anionic hydroxyl quinones are slow binding inhibitors at the Q_A site. In addition to binding more tightly, many transition-state analogs bind slowly, indicating that there are large barriers for binding these high-energy reaction intermediates (Bulow and others 2001; Dharmasena and others 2002; Jiang and others 2002; Lohse and others 2000; Merkler and others 1990; Morrison and Walsh 1988; Yiallouros and others 1998). While slow kinetics has been observed in systems with a single step, second order association mechanism (Bulow and others 2001; Lohse and others 2000), this is not a good description of the association of anionic hydroxyl quinones with the Q_A site. The concentration independence of k_{uni} (Fig. 2-4) and solvent viscosity independence of the second order rate constant k_{on} (Fig. 2-7) supports a first order rate-determining step for these quinones. This requires a two-step binding process, for which there are two possible paths (Figure 2-9). In one (P_1), unbound reaction centers exist in an equilibrium mixture of RC_F and RC_F^*. RC_F^*, which has very low equilibrium occupancy binds rapidly and tightly to the anionic inhibitor, I_F^-. Here the rate-determining step is the slow conformational change from RC_F to RC_F^*. Along P_2, an initial encounter complex, RCI^-, is formed rapidly. This is followed by the slow change from RCI to RCI^{-*}, the more thermodynamically stable complex. The RCI complex samples many conformational states until the one that can best stabilize the anion is found. Protein rearrangement as the source of slow binding kinetics is commonly observed for enzyme inhibition (Dash and others 2002; Pandhare and others 2003). Both pathways have been found in studies of other proteins (Dash and others 2002; Merkler and others 1990). In either case the measured K_ds reflect the overall affinity for formation of RCI^{-*} from RC_F and I^-_F.

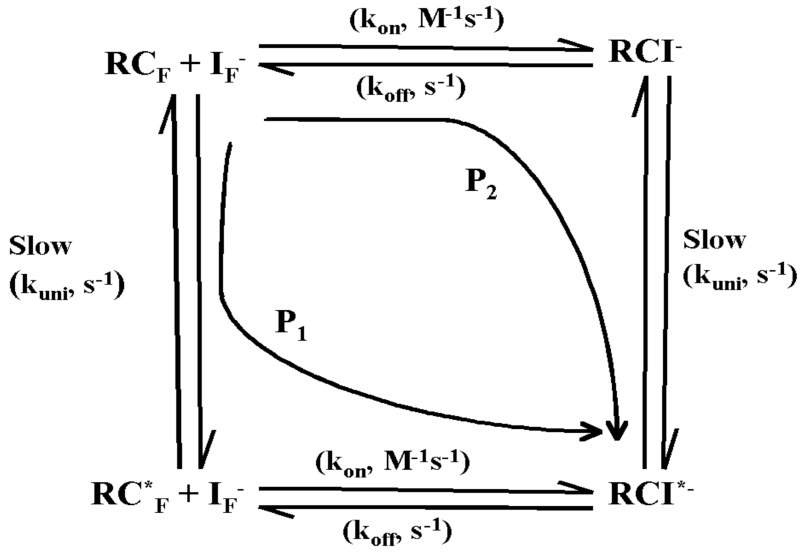

Figure 2-9: Two pathways (P_1 and P_2) for the binding of anionic hydroxyl quinones with a slow first order rate-determining step (k_{uni}). The fast, reversible binding process is governed by the second order rate constant k_{on}.

The quinone concentration and solvent viscosity dependence of the rate establish the order of the rate-determining step but cannot distinguish between P_1 and P_2. However, the correlation between k_{uni}, k_{off} and K_d can provide some clues. P_2 should show an initial burst phase of inhibition due to the rapid formation of RCI^- before the slow isomerization to form RCI^{-*}. This is not observed but cannot be ruled out given the difficulty of obtaining early time measurements. The amplitude of the burst would be dependent on the affinity of I^- for RC_F, which may be low. Along P_1, the slow conformational rearrangements only involve RC_F. Here the anionic hydroxyl quinones behave as

transition-state analogs that bind rapidly to the high-energy configuration (RC_F^*). Since RC_F^* has a low equilibrium occupancy, the overall association rate is slow. The inhibitor affinity depends on the rate at which the RCI^{*-} changes back to the low affinity RCI^-. A similar mechanism was used to describe the results for the slow-onset inhibition of Yeast AMP deaminase (Merkler and others 1990).

The binding of 5-OH-NQ and 5-OH-3-Me-NQ show a first order rate-determining step indicating that quinone association is too fast to be observed. On the other hand, the binding of 2-OH-NQ shows kinetic evidence for both steps in formation of RCI^{-*}. Here the second order process is rate limiting at low quinone concentration while the first order process becomes rate limiting at higher concentrations (Fig. 2-5).

2-OH-3-Me binds irreversibly to the Q_A site (Fig. 2-6). Slow irreversible binding could imply the formation of a covalent bond in the active site (Bretscher and others 2003), or that the encounter complex denatures at a rate faster than dissociation. No change in the RC near-IR absorbance spectra is found after incubation with this quinone thus denaturation is unlikely. The observed irreversible binding could also indicate that the affinity is in the sub-nanomolar range. Adding a methyl group at the 3 position would need to increase the affinity of 2-OH-NQ (K_I=0.1 M) by at least 100-fold to keep DQ from displacing it under the experimental conditions employed here. The neutral diortho-substituted 2,3dMe-NQ does bind ≈6 fold more tightly than the mono-substituted 2-Me-NQ (Table 1), showing that the addition of an ortho-methyl group tightens binding. In contrast, 2-OH-3-Iso-NQ (K_I=4.2 M) binds more weakly than the mono-substituted 2-OH-NQ (Table 2). However, it is likely that the branched isopropyl group weakens

affinity (Gunner unpublished results). Continuum electrostatic calculations do indicate that ionized 2-OH-3-Me-NQ binds 40-fold tighter than 2-OH-NQ.

Anionic hydroxyl quinones as models for the semiquinone: Previous studies of difference FTIR (Breton and others 1994a; Breton and others 1994b), electrochromatic shifts following $Q_A^{\bullet-}$ formation (Steffen and others 1994), E_m shifts in replacement compounds (Warncke and Dutton 1993a) and mutational analysis (Takahashi and others 2001; Wells and others 2003) indicate that it is the negative charge on the quinone that causes the protein response following formation of $Q_A^{\bullet-}$. Thus, even though the anionic hydroxyl quinones are not radicals, they can serve as models for the study of semiquinone binding. The results presented here show that a negative charge causes slow binding kinetics at the Q_A site. At pH 7.8, neutral 5-OH-2-Me-NQ with a pK_a of 9.4 is a fast binding neutral compound that can reconstitute Q_A activity (manuscript in preparation), while at high pH the anionic quinone dissociates slowly Semiquinones dissociate slowly from the Q_A and Q_B sites (Diner and others 1984). Ferrocene, an external electron donor of $P^{\bullet+}$, creates RCs in the state $PQ_A^{\bullet-}$. For a number of tailess semiquinones in the Q_A site this state is trapped for seconds (Kalman and Maroti 1994). Semiquinone disappearance was attributed to the accessibility of external oxidants, and preliminary results indicate that in O_2 depleted samples the semiquinone lifetime increases (data not shown). These results put an upper limit on semiquinone k_{off} of $0.5s^{-1}$ for $DQ^{\bullet-}$, 1000-fold faster than the anionic hydroxyl quinones but 10-fold slower then the neutral DQ (Table 2-1). Thus, the slower dissociation of the hydroxyl quinones could provide a better limit for the semiquinone lifetime in the absence of external oxidants.

The observed rate of anionic hydroxyl quinone binding is slow. Physiologically, slow conformational changes cannot be required for formation of the $Q_A^{\bullet-}$, which accepts an electron from bacteriopheophytin in 150ps (Kirmaier and others 1985). However, relaxation stabilizes the $RCQ^{\pm}$ charge separated state once it is formed (Brzezinski and others 1992; Okamura and Feher 1992; Tiede and Hanson 1992; Xu and Gunner 2000; Zachariae and Lancaster 2001). Events such as proton uptake, internal charge transfer and the reorganization of internal dipoles have been proposed to stabilize $Q_A^{\bullet-}$ (Alexov and Gunner 1999; McPherson and others 1988; Nabedryk and others 1990). Furthermore, changes in a cluster of acidic residues near the Q_B site help stabilize $Q_A^{\bullet-}$ (Kalman and others 1998; Miksovska and others 1996), perhaps though shifts in their ionization (Alexov and Gunner 1999).

The relative affinity of quinone and semiquinone for the Q_A site determines how the *in situ* E_m differs from that found in solution (Fig. 2-10). While it is difficult to measure E_ms for single electron reductions of quinone in water, some have been estimated (Rich 2004; Rich and Bendall 1979; Swallow 1982a). The $E_{m,sol}$ for $UQ/UQ^{-\square}$ is ≈–145 mV (Swallow 1982b; Wraight 1998; Zhu and Gunner 2005) while it is –45 (Dutton and others 1973) to –75 mV (Rutherford and Evans 1980) in the Q_A site at pH 7. This 70 to 100 mV E_m shift indicates the semiquinone binds 15 to 45 times more tightly then the quinone. Inhibitor binding at the Q_B site also shows that the semiquinone binds more tightly than the quinone or dihydroquinone (Diner and others 1984). The work presented here allows comparison of the relative affinity of neutral and anionic quinones. The k_{off}s for the anionic hydroxyl quinones are 10^4 times slower than the neutral compounds (Fig. 8a). If the semiquinone off rate slowed this much with no change in association kinetics,

this would corresponds to an E_m shift of +240mV. However, the results presented here show that anionic compounds also associate slowly. The anionic hydroxyl and neutral quinones have different binding mechanisms, so their association rate constants cannot be directly compared. However, a comparison of the rate of formation of the bound complex at 50% saturation shows the average k_{on} for the neutral quinones is in the range of 10^6 to 10^7 $M^{-1}s^{-1}$ (Table 2-1) while, using 5-OH-2-Me-NQ as an example, $k_{uni}/[Q_T]$ is 3500 to 5500 $M^{-1}s^{-1}$. Thus, the anionic quinones associate 180 to 2800 times more slowly, while k_{off} slows by 10^4 compared to the neutral quinones. Assuming the same shift in the binding kinetics of the quinone and semiquinone predicts a ~33 to 100mV increase in E_m, in good agreement with the measured E_m shift. Since there is no free semiquinone in either membrane or solution, slow semi-quinone association would not affect RC activity. The slow k_{off} helps preserve the unstable, high energy semiquinone $Q_A^{\bullet -}$, minimizing energy loss and free radical damage. This analysis assumes all anionic quinones are stabilized by the same amount. The E_m shift moving from the aprotic solvent dimethylformamide (Prince and others 1983) to the Q_A site is not the same for all compounds indicating that specific protein interactions can also play an important role (Warncke and Dutton 1993a; Woodbury and others 1986).

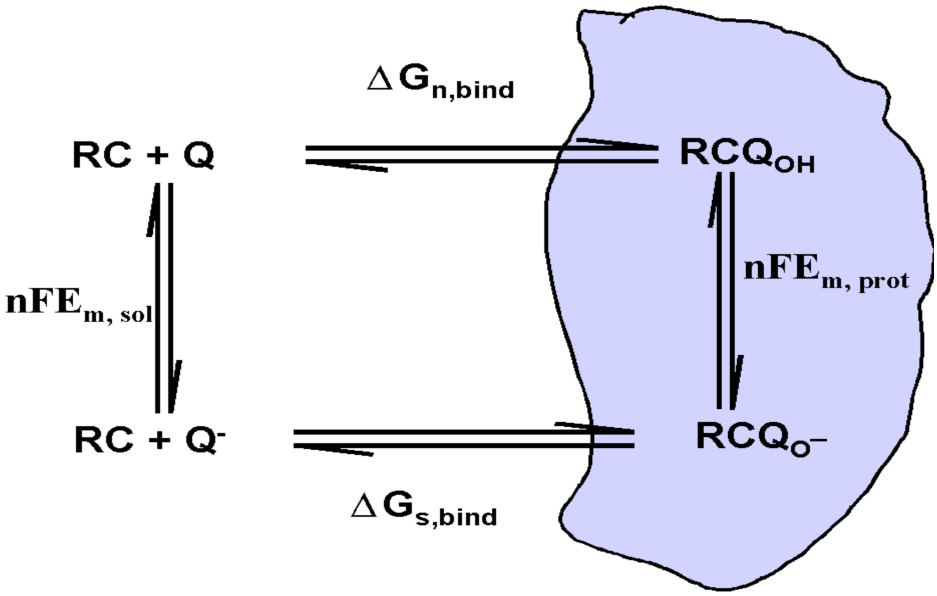

Figure 2-10: Relationship between quinone binding energy and redox midpoint potential. $\Delta G_{s,bind}$ and $\Delta G_{n,bind}$ are the association free energies for the semiquinone and neutral quinone. $nFE_{m,prot}$ and $nFE_{m,sol}$ are the free energies for semiquinone formation in the protein and in aqueous solution, n is the number of electrons transferred (here n=1) and F is Faraday's constant. $\Delta G_{s,bind} = nRTlog(k_{on,\,semi}/k_{off,\,semi}) = \Delta G_{n,bind} - nF(E_{m,prot} - E_{m,sol})$.

The measured K_ds for the neutral and anionic hydroxyl quinone (Tables 2-1and 2-2) reflect the free energy difference of the quinone in solution and in the Q_A site. There is a loss of solvation energy incurred by transferring the quinone from the high dielectric environment of water (ε=80) into the low dielectric protein, and loss of motional degrees

of freedom in the binding site (Zhu and Gunner 2005). Charged compounds interact with water more favorably than neutral ones do. Thus the anionic hydroxyl quinones need to have additional favorable interactions with the protein to have K_ds that are similar to the neutral quinones. The partition coefficient (P) provides a quantitative measure of the energy of transferring the quinone out of water and into a non-interacting solvent such as cyclohexane ($\Delta G_{trans} = 2.3RT\log P$) (Radzicka and Wolfenden 1988). While some neutral quinones have measured partition coefficients (Braun and others 1986; Rich and Bendall 1979) anionic quinones do not. The difference in the partition coefficient ($\Delta\log P$) of ionized and neutral forms of 5-OH-NQ in octanol was calculated with a fragment-based method (www.molinspiration.com) (Abraham and Leo 1987; Hansch and others 1991). Octanol is a more polar solvent than cyclohexane thus this provides a lower limit of the free energy for transferring the anionic quinone from water. The $\Delta\log P$ was 2.2 corresponding to a $\Delta\Delta G_{trans}$ of –3 kcal/mol (130 meV). Previous electrostatic calculations have shown that the protein interacts –2.5 kcal/mol more favorably with $Q_A^{\bullet-}$ compared to Q_A, corresponding to a 72-fold tighter K_d favoring anion binding (Zhu and Gunner 2005). Favorable interactions with protein side chains, the backbone dipoles and the non-heme iron were found to stabilize anion binding.

Anthraquinone (AQ) and substituted derivatives have smaller E_m shifts from solution values in the Q_A site than benzo and naphthoquinones (Woodbury and others 1986). These semiquinones should therefore be more weakly bound relative to the neutral quinone and could show faster dissociation rates. Preliminary results using the double flash method with 1-Cl-AQ and 2-Cl-AQ showed that the amplitude decreases rather than increases on the second flash, consistent with semiquinone dissociating between flashes.

These low potential quinones have fast charge recombination kinetics making it difficult to model the binding kinetics on the same timescale as the other neutral quinones in this study.

Chapter 3: Quinone pK_a and E_m Shifts in the Q_A site of Bacterial Reaction Centers

3-A) Introduction Photosynthetic bacterial reaction centers (RCs) use bound co-factors to transfer electrons over long distances. Thus the co-factor binding sites are able to accommodate both the neutral and charged forms during activity. The role of the protein environment in determining the relative stability of the neutral and deprotonated species of three hydroxyl quinones bound at the Q_A site of RCs from *Rhodobacter sphaeroides* was investigated and compared with the native Q_A (ubiquinone-10). The neutral species of 5-hydroxyl-2-methyl-naphthoquinone (5-OH-2-Me-NQ) is an active electron acceptor, while its deprotonated species is an anionic competitive inhibitor. Thus the formation of the charge-separated state ($P^+Q_A^-$) was used to experimentally determine the pK_a in the Q_A site (7.6 ± 0.3). The measured pK_a is downshifted by about 1.8 pH units relative to the value measured in aqueous solution (pK_a = 9.4) indicating that the Q_A site favors the anionic species. In addition to experiment, Multi-Conformational Continuum Electrostatics (MCCE) was used to calculate the *in situ* pK_a, $pK_{a,protein}$, of 5-OH-2-Me-NQ ($pK_{a,protein}$ = 7.1), 2-hydroxyl-naphthoquinone (2-OH-NQ, $pK_{a,protein}$ = 0) and 2-hydroxyl-3-methy-naphthoquinone (2-OH-3-Me-NQ, $pK_{a,protein}$ = 1.2) based on the pK_a shift relative to solution. While the K_ds for ionized 2-OH-NQ and 5-OH-2-Me-NQ at the Q_A site were previously determined experimentally, the K_d for ionized 2-OH-3-Me-NQ could not be determined presumably because it binds too tightly to detect dissociation from competitive inhibition with duroquinone (Madeo). Here MCCE was used to compare the relative affinities of these three ionized quinones and results are compared with experiment. The good agreement between experimental and theoretical results found here

indicate that electrostatics is the dominant principle governing how the Q_A site modifies quinone chemistry and thus allows a more detailed analysis of the important interactions.

Proteins are heterogeneous and thus contain local environments specifically designated for different functions. By controlling the local electrostatic environment of bound co-factors and ligands proteins can change physical properties, such as pK_a and redox midpoint potential (E_m), which characterize the energetics of a change in charge state. Factors such as long-range electrostatic interactions, dipolar interactions, hydrogen bonding and differential solvation energy losses for the reactant and product (desolvation penalty) regulate the free energy of protein-mediated charge transfer reactions. The polarizability of the local environment can also play a role. Characterizing the energetics of these processes with an atomic level structural model is an ongoing effort in structural biology.

RCs are important electron-transfer proteins that mediate the conversion of solar energy to chemical energy during photosynthesis. By catalyzing a series of redox reactions between bound co-factors, RCs store the energy of a photon in the form of charge separation. The bacterial RC from *Rhodobacter sphaeroides* is an integral membrane protein consisting of three protein subunits, L, M and H and 10 co-factors including two ubiquinones (Q_A and Q_B). Absorption of a photon (860nm) excites the primary donor P, a bacteriochlorophyll dimer, and sub sequentially changes the protein from a redox state where all of the co-factors are neutral to a state with a charge separation of 25A across the cell membrane. Q_A is singly reduced by the lower potential cofactor, bacteriopheophytin (H_A), which lives for only a few nanoseconds. Q_A^- donates

its electron to the terminal acceptor, ubiquinone-10 bound at the Q_B site (Blankenship and others 1995; Feher and others 1989).

The protein environment of the Q_A binding site tunes the energy levels of the negatively charged (reduced semi-quinone) and neutral (oxidized) states of the bound quinone. The relative energy level between these two states ensures that electron transfer is favored in the forward direction, thus the differential affinity of the quinone redox states is an important factor that regulates the free energy of electron transfer. The semi-quinone binds more tightly than the neutral state (Diner and others 1984; Warncke and Dutton 1993b), thus the protein stabilizes the reduced state more than the oxidized raising the redox potential (E_m) relative to solution. A larger the difference in affinity causes a larger shift in the E_m in going from solution to protein. Previous MCCE calculations have shown that the protein stabilizes Q_A^- by 108 meV relative to the neutral species thus indicating that the anionic species binds 63-fold more tightly (Zhu and Gunner 2005). This difference in affinity is caused by differential desolvation penalties and specific interactions between the quinone and the Q_A binding pocket. The backbone amides of residues M260-271 have been shown to be important for stabilizing the negatively charged species in the Q_A site (Zhu and Gunner 2005). Interactions with the backbone dipoles are known to be important for stabilizing buried charges, especially anions since the average electrostatic potential from the backbone is generally positive (Gunner and others 2000).

Since both the pK_a and the E_m are thermodynamic parameters that express the ratio of charged to neutral species at equilibrium, the same electrostatic interactions that shift the quinone E_m will shift its pK_a. Since the Q_A site raises the quinone E_m by favoring

the reduced anionic state, it is expected that the pK_a will be lowered due to favoring the deprotonated anionic state. Previous calculations have shown that the Q_A site lowers the pK_a of the semi-quinone by 1.5 units indicating that it takes 90meV more energy to protonate Q_A^- in the protein compared to in solution (Zhu and Gunner 2005). This explains why the semi-quinone does not pick up a proton during eletron transfer. Previous experiments measuring the rate of hydroxyl quinone binding at the Q_A site have indicated that ionized hydroxyl quinones are good semi-quinone models (Madeo). The work presented here experimentally measures the pK_a of the hydroxyl quinone, 5-OH-2-Me-NQ, in solution and in the Q_A site of bacterial reaction centers from *Rhodobacter sphaeroides*. This experimental shift in pK_a (ΔpK_a) is compared with the calculated ΔpK_a of 5-OH-2-Me-NQ and the native semi-quinone in the Q_A site using MCCE. Furthermore MCCE is used to calculate the ΔpK_a of the two ortho-hydroxyl quinones 2-OH-NQ and 2-OH-3-Me-NQ. The relative affinity of the ionized species of these three quinones is compared to experiment. The good agreement between experimental and computational results confirms the MCCE method (Georgescu and others 2002; Mao and others 2003) and supports the idea that the Q_A site is designed to stabilize a negative charge (Warncke and Dutton 1993b).

3-B) Methods and Materials

RC Isolation and Native Quinone Removal: The isolation of *Rb. sphaeroides* engineered poly-histidine-tagged RCs has been described previously (Goldsmith and Boxer 1996). The RCs were purified on Ni-NTA (nitrilotriacetic acid) resin. The Ni-NTA column was washed with 0.05% LDAO in 10mM Tris buffer and the RCs were eluted with 40mM

imidazole in 0.05% LDAO at pH 8. Q_A removal (Okamura and others 1975; Woodbury and others 1986) yielded RCs with less than 10% of the native ubiquinone left in the Q_A site and empty Q_B sites. The RC concentration was determined given $\varepsilon_{802} = 0.288\ \mu M^{-1}cm^{-1}$. The Q_A charge recombination activity was measured as described previously (Madeo).

Measurement of 5-OH-2-Me-NQ pK_a: The solution pK_a was measured previously by difference absorbance spectroscopy at 520nm. The difference absorbance band was measured from pH 4 to pH 10.5. To control pH the buffers Tris (pH 7.2-8.5), Ches (pH 8.5-10) and Caps (pH 10.5-11.5) were used at a concentration of 10mM

To determine the *in situ* pK_a of 5-OH-2-Me-NQ, the charge separated $P^+Q_A^-$ amplitude was recorded over the pH range from 7.2 to 10.2 by measuring the maximum absorbance at 430nm. The amplitude due to the residual ubiquinone left in the Q_A site was subtracted out. Since only the neutral species can form the semi-quinone at the Q_A site, the charge-separated amplitude ($P^+Q_A^-$) is proportional to the *in situ* fraction of protonated quinone. The titration was done with 80 μM 5-OH-2-Me-NQ, 0.8 μM RCs in .005% LDAO. Under these conditions the Q_A site will be saturated with ionized quinone ($K_d = 4.5\mu M$), thus the total amplitude was determined from the total RC concentration with the fraction of Q_A sites still occupied by native quinone (due to less than 100% Q_A removal) subtracted out. The difference between the total amplitude and the equilibrium amplitude represents the fraction of ionized species (fi). The fraction of ionized species (fi) was measured as a function of pH and fit with the equation:

$$fi(pH) = \frac{10^{\frac{pH}{n}}}{10^{\frac{pH}{n}} + 10^{\frac{pK_a}{n}}}$$

pH dependence of the reaction time course: Previous results have shown that the inactive ionized form of 5-OH-2-Me-NQ associates slowly with the Q_A site with the measured rate constant $0.02s^{-1}$, while the protonated species equilibrates in seconds. The disappearance of the $P^+Q_A^-$ amplitude was followed in time in a sample containing 80 M 5-OH-2-Me-NQ and 0.8 M RCs in 0.005% LDAO. Amplitude measurements were taken at 0.5 to 1 minute intervals, in the pH range of 7.2 to 10.2, until equilibrium was reached. The data was fit with a first order rate-determining model describing the slow single exponential decay (rate constant, k_{uni}) of the $P^+Q_A^-$ amplitude (RCQ^-) to its equilibrium configuration:

$$\frac{d}{dt} RCQ^-(t) = -k_{uni} \cdot \left[RCQ^-(t) \right]$$

Theoretical Method: Multi conformational continuum electrostatics (MCCE) (Georgescu and others 2002; Mao and others 2003; Zhu and Gunner 2005) calculates the equilibrium distribution of ionization and conformational states of protein side chains, buried waters, ions and co-factors at a defined solution E_h and pH. MCCE combines continuum electrostatics and molecular mechanics to calculate shifts in the free energy of proton and electron transfer reactions in going from water to the protein interior ($\Delta\Delta G_{protein}$). The starting coordinates used in this study are 1AIG (Stowell and others 1997), a 2.6A crystal structure of the reaction center from *Rhodobacter sphaeroides* frozen in the light ($P^+Q_B^-$ state). Side chain conformers are added providing alternative positions for the hydroxyl protons of Ser, Thr, Tyr and water, His tautomers and the different ionization states of the acids Asp, Glu and Tyr and the bases Arg, Lys and His. Backbone and non-polar side chains are fixed. Look-up tables are calculated for the electrostatic and non-electrostatic pair-wise interactions between residues (ΔG_{res}), between backbone and residues (ΔG_{pol})

and reaction field energies (ΔG_{rxn}). The DelPhi program solves the Poisson-Boltzmann equation to calculate the electrostatic components (Nicholls and Honig 1991). The non-electrostatic energy components include torsion ($\Delta G_{torsion}$) and Lennard-Jones interactions (ΔG_{nonel}). MCCE is a multi-conformational approach, thus the electrostatic energy of several side chain positions (rotamers) is determined during the calculations. Monte Carlo is used to sample the possible microstates (a microstate has one conformer for every side chain, co-factor and water) of the system at a defined pH and E_h. The interior dielectric constant is 4 and 80 is used for the solution with a salt concentration of 150 mM. The free energy of microstate x (ΔG_x), at a given pH and E_h, is the sum of the electrostatic and non-electrostatic energy terms (Mao and others 2003).

$$\Delta G_x = \sum_{i=1}^{M} \delta_x(i)\{\gamma(i)[2.3k_bT(pH - pK_{sol,i}) - nF(Eh - Em_{sol,i})]$$
$$+(\Delta\Delta G_{rxn,i} + \Delta G_{torsion,i} + \Delta G_{pol,i} + \Delta G_{nonel,i})\}$$
$$+\sum_{i=1}^{M} \delta_x(i) \sum_{j=i+1}^{M} \delta_x(j)[\Delta G_{ij}^{el} + \Delta G_{ij}^{nonel}]$$

Calculation of the free energy of quinone protonation reactions: MCCE was used to calculate the *in situ* pK_a of 5-OH-2-Me-NQ, 2-OH-3-Me-NQ and 2-OH-NQ. The free energy of a proton transfer reaction is related to the pK_a, thus $\Delta\Delta G_{protein}$ (the shift in free energy in going from water to protein) is related to the difference in pK_a (ΔpK_a) between the reaction in water and protein ($\Delta pK_a = pK_{a,protein} - pK_{a,sol}$) through (Mao and others 2003; Zhu and Gunner 2005). The relationship is $\Delta\Delta G_{protein} = -2.3RT\Delta pK_a$.

Quinone pK_a values obtained by Monte Carlo sampling as a function of pH (Georgescu and others 2002) do not yield the correct free energy of protonation because of pH dependent protein ionizations and conformational changes. This is because the protein overall charge changes with pH thus changing the electrostatic potential at the sites of interest. Thus the free energy of ionization does not change simply as pK_a – pH as expected in aqueous solution. These changes make the quinone pK_a pH dependent when bound to the protein. The effective pK_a at pH 7 (pK_a') is how far away the protonation free energy at pH 7 (ΔG_7) is from zero (what it is when pH = pK_a). This is different from the $pK_{a,protein}$ because it eliminates pH dependent changes in the protein that could affect the proton transfer reaction. The pK_a' is calculated from $pK_a' = 7 - \Delta G_7/RT$

Relative binding affinities of the three quinones: The $pK_{a,protein}$ is governed by the relative stability of the neutral and ionized quinone in the Q_A site, which in turn is related to their differential binding affinities ($K_{d,neutral}$ and $K_{d,ion}$). Given the dissociation free energy, $\Delta G_d = -2.3RT\log(K_d)$, the relationship is

$$pK_{a,protein} - pK_{a,sol} = \log\left(\frac{K_{d,ion}}{K_{d,neutral}}\right)$$

The K_ds for the ionized hydroxyl quinones at the Q_A site were determined previously by competitive inhibition with duroquinone. Here MCCE was used to estimate their relative affinities using the difference in the free energy of interactions for the ionized states.

$$\Delta G_{b,2} - \Delta G_{b,1} = -RT \ln\left(\frac{K_{d,2}}{K_{d,1}}\right)$$

The quantity $\Delta G_{b,2} - \Delta G_{b,1}$ is the difference of the free energy of protein interactions and desolvation energy between 2 ionized quinones (1 and 2) bound at the Q_A site.

Partial atomic charges: The non-heme iron between Q_A and Q_B was fixed with a +2 charge and all other native co-factors were fixed as neutral. For both ionization states, the partial atomic charges for the three quinones used in this study (2-OH-NQ, 5-OH-2-Me-NQ and 2-OH-3-Me-NQ) were obtained by the Hartee-Fock type *ab initio* method with a 6-31G** basis set. The electronic density was partitioned into atomic charges by the method of charges from electrostatic potential (CHELPG charges) implemented in Gaussian 98 (Ohno and others 2001). Each quinone has a total of three ionization states, two neutral and one ionized. The degenerate neutral conformers have their acidic protons lying in the plane of the ring 120° apart from each other (Fig. 3-1). The partial charges for all other co-factors are from (Parson and others 1990). PARSE charges and radii were used for all other groups (Sitkoff and others 1994).

Quinone orientations in the Q_A site: The quinones were docked at the Q_A site in four basic orientations. Two of the orientations (left and right) are related by a 180-degree rotation about the axis connecting the 1 and 4 positions (A-1, Fig. 3-1). This shifts ring 1 either within vander Waals distance (2-3 angstroms) of Met-M218 (left) or Ala-M248 (right) as shown in figure 3-3-2. The next two orientations (up and down) are related by a 180-degree rotation about an axis connecting the midpoint between C6 and C7 to the midpoint between C2 and C3 (A-2, Fig. 3-1). This rotation exchanges positions 5, 4 and 3 (down) for 8, 1 and 2 (up), respectively (Fig. 3-1). These four orientations are illustrated with

ionized 5-OH-2-Me-NQ in the Q_A site (Fig. 3-2). Each orientation has two neutral and one ionized conformer (Fig. 3-1), thus a total of 12 quinone conformers were sampled in the Monte Carlo simulation. Each orientation has an oxygen atom in the 1 and 4 positions (Fig. 3-1), which make important hydrogen bonds with the side chain of His-M219 and the backbone amide of Ala-M260 (Stowell and others 1997).

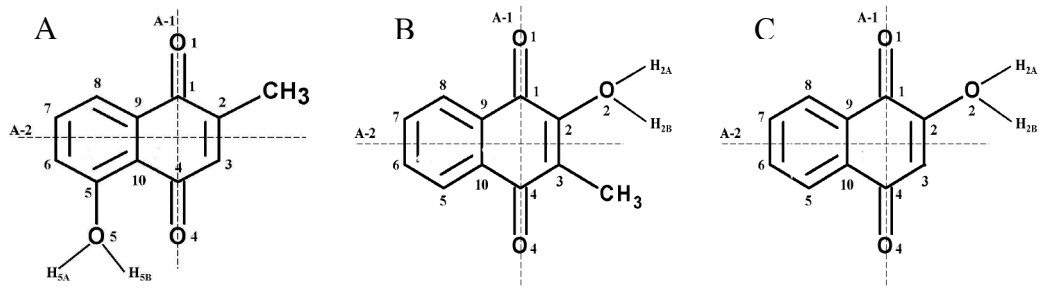

Figure 3-1: Structure and atomic nomenclature for the three quinones tested in this study. To show both neutral conformers, only the acidic hydrogen atoms are labeled explicitly. These two degenerate conformers have their hydrogen atoms positioned in the plane of the ring 120 degrees apart. The quinones are docked in the Q_A site in four orientations related by 180-degree rotations about the axes A-1 and A-2. These rotations maintain the important hydrogen bonds between the quinone carbonyls A) 5-OH-2-Me-NQ, B) 2-OH-3-Me-NQ C) 2-OH-NQ.

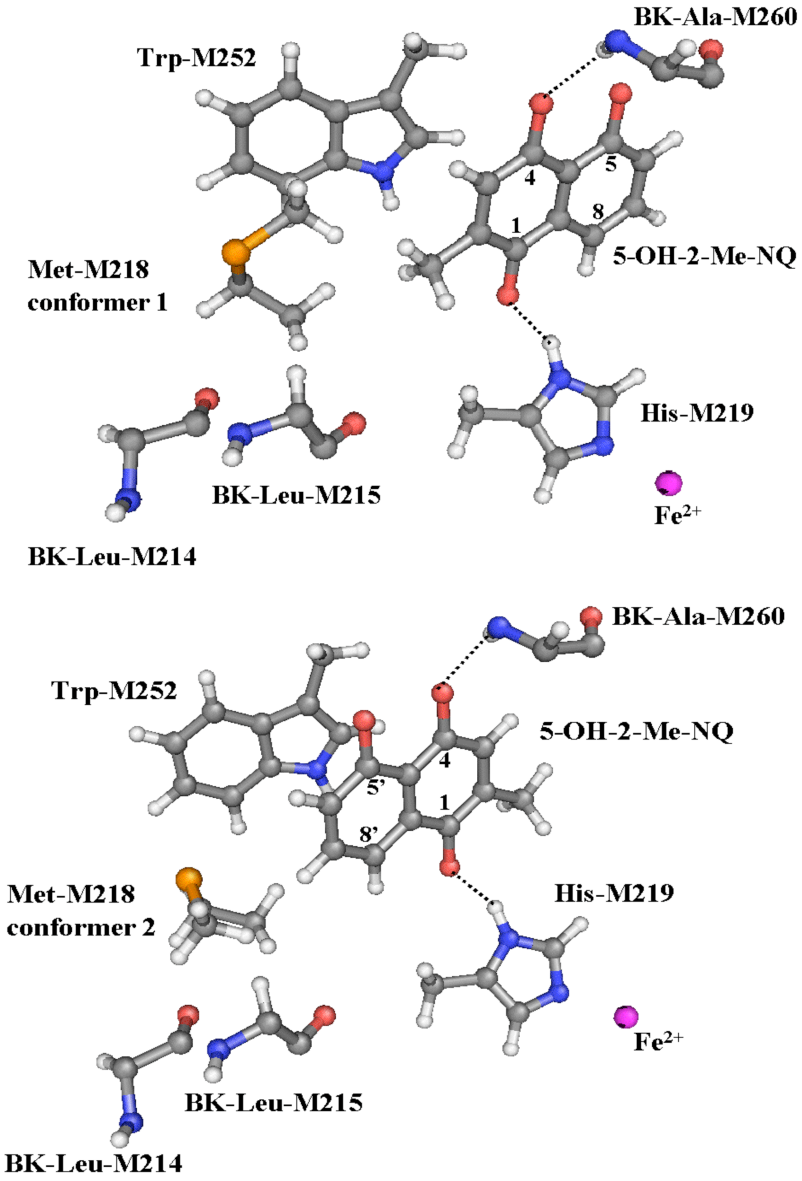

Figure 3-2: Atomic position nomenclature for 5-OH-2-Me-NQ docked in the Q_A site. These positions also correspond to the ortho-hydroxyls. In the primed position of the quinone rings moves closer to residue Met-M218 due to a rotation about an axis connecting positions 1 and 4.

3-C) Results

Experimental pK_a and pH Dependence of the Binding Rate for 5-OH-2-Me-NQ: The solution pK_a for 5-OH-2-Me-NQ was determined by difference absorbance spectroscopy at 520nm. The absorption peak at 520nm is proportional to the fraction of ionized species (fi) thus the pH dependence of the difference peak yields the pK_a. The titration was done in the pH range of 6 to 10.2 and the data was fit with equation 1 yielding the solution pK_a of 9.4 (Fig. 3-3).

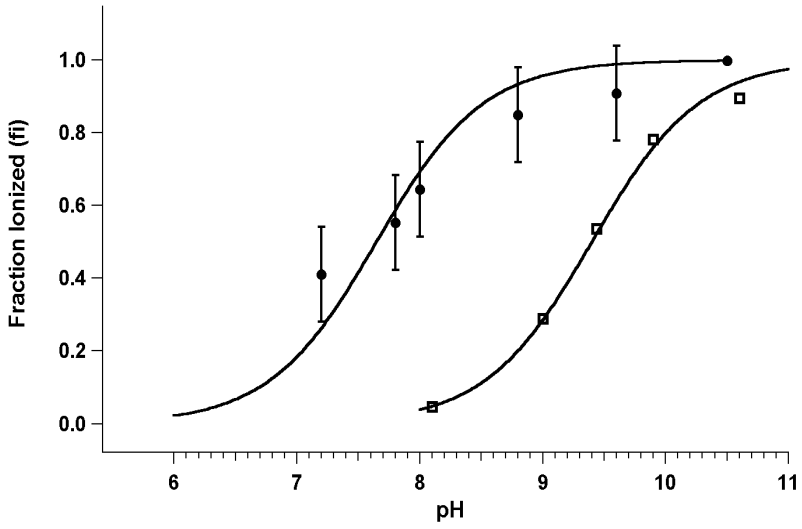

Figure 3-3: Experimental pK_a measurements of 5-OH-2-Me-NQ

Open squares: pK_a measured in aqueous solution by difference absorbance spectroscopy at 520nm. The pK_a is 9.4; filled circles: pK_a measured in the Q_A site of bacterial RCs by the pH dependence of the $P^+Q_A^-$ amplitude. The pK_a is 7.6. The solid lines are the best fit to equation 1.

The pK_a of 5-OH-2-Me-NQ in the Q_A site was determined by the pH dependence of the amount of charge separated state ($P^+Q_A^-$) formed by a flash of actinic light. Only

the neutral species can accept an electron at the Q_A site to form the charge separated state, thus the amplitude at any given pH is proportional to the fraction of neutral species. The activity was titrated in the range of 7.2 to 9.6 under saturating conditions. The pH dependence provided the *in situ* pK_a of 7.6 ± 0.13, a downshift of 1.8 pH units relative to solution (fig. 3-3). In support of this, previous continuum electrostatics calculations have shown that the pK_a for ubiquinone semi-quinone in the Q_A is downshifted by 1.5 pK units (Zhu and Gunner 2005).

The sample took several minutes to reach equilibrium at each pH tested. This slow rate is attributed to the slow dissociation of the anionic quinone. It has been previously established that protonated 5-OH-2-Me-NQ associates and dissociates rapidly from the Q_A site (on the order of milliseconds) while the ionized form displays very slow binding kinetics (on the order of minutes) (Madeo). The observed slow loss of $P^+Q_A^-$ amplitude, even at pHs well below 9.4, confirms that the ionized species is formed in the Q_A site, thus the pK_a is downshifted relative to solution. The binding mechanism of the ionized species was previously determined to have a first order rate-determining step and the first order rate constant (k_{uni}) is obtained by solving equation 2. k_{uni} is pH independent in the range of 7.2 to 10.2 (Fig. 3-4) providing evidence that the time dependent loss of activity is due dissociation of the anionic quinone.

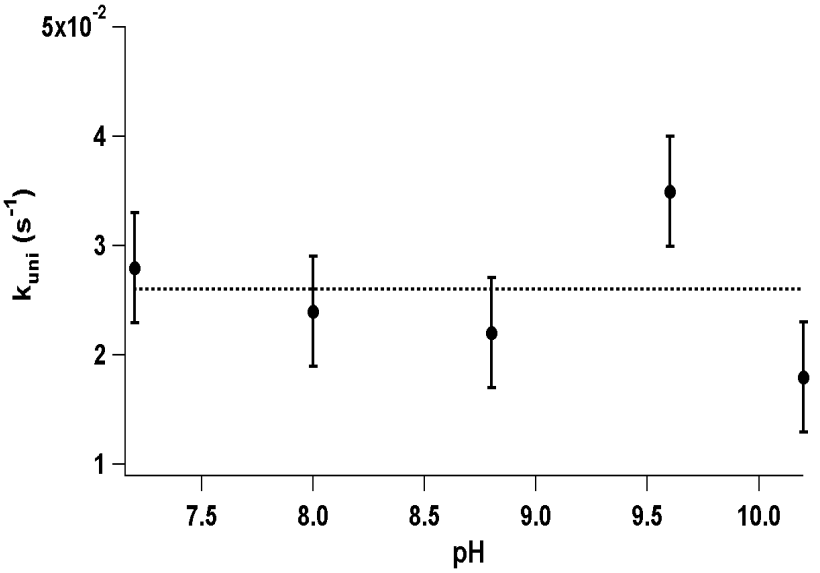

Figure 3-4: pH dependence of the rate to reach the equilibrium amplitude of $P^+Q_A^-$

The unimolecular rate constant (k_{uni}) was obtained by fitting the time dependent loss of $P^+Q_A^-$ amplitude with equation 2. The dashed line is the average value, 0.026 s^{-1}.

Theoretical Determination of in situ pK_a for 5-OH-2-Me-NQ: MCCE was used to determine the *in situ* pKa of 5-OH-2-Me-NQ in the Q_A site. Monte Carlo sampling was done over the pH range of 6-10. The energy difference between the ionized and neutral species was determined to yield a pK_a of 7.2. This is a downshift of 2.2 pH units from the solution in reasonable agreement with the experimental results shown above. Thus the Q_A site stabilizes the ionic species by about 3kcal/mol relative to the neutral (equations 1 and 2). This energy difference is broken up into the unfavorable loss of solvation due to moving a charge from water into the protein ($\Delta\Delta G_{rxn}$), the electrostatic pair-wise interactions with the protein backbone (ΔG_{pol}) and the residues ($\Delta G_{residues}$) and the non-electrostatic torsion and backbone Lennard-Jones interactions (ΔG_{nonel}) (Table 3-1). All of the favorable interactions come from polar interactions with the backbone and pair-wise

electrostatic interactions with the other residues. The unfavorable reaction field energy component is nearly cancelled out by the favorable interactions with the backbone, as is commonly observed with anionic groups (Gunner and others 2000; Kim and others 2005)

Table 3-1: Comparison of energy contributions for the pK_a shift relative to solution for the three quinones used in this study to that of the native quinone

reaction	$\Delta\Delta G_{rxn}$	ΔG_{pol}	$\Delta G_{residues}$	ΔG_{nonel}	Solution pK_a/E_m	*In situ* pK_a/E_m	pK_a'
5-OH-2-Me-NQ proton transfer	5.4	-4.8	-3.3	0.5	9.4	7.1	7
2-OH-NQ proton transfer	4.7	-2.8	-6	0	4.0	0.5	2.1
2-OH-3-Me-NQ proton transfer	4.3	-2.6	-4.8	0	5.0	1.81	3.4
Q_A^* electron transfer	6.5	-4.6	-4.1	0	-145mV	-37mV	
Q_A^* Proton transfer	6.7	-4.6	-3.9	0	4.9		3.4
Q_B^* (proximal) Electron transfer	6.4	-6.5	-2.3	0	-145mV	-7mV	
Q_B^* (proximal) Electron transfer				0	4.9		2.7

The negative sign for the pK_a shift indicates a downshift due to the stabilization of the ionized species relative to the neutral. *Native quinone values are from (Zhu and Gunner 2005). E_m values are given at pH 7.

The primary contribution to ΔG_{pol} is from residues M250-260 and (Fig. 3-5) in agreement with what is found with the native ubiquinone-10 (Zhu and Gunner 2005). The residues most important for electrostatic stabilization of the ionized quinone (and thus directly contribute to the ΔpK_a) are the non-heme iron (due to the +2 charge, iron contributes the highest stabilization energy for the ionized quinone), HisM219, ArgM241, ArgM247 and ArgM253 (Table 3-2, Fig. 3-5). These 3 Arg, about 13-15 A away from O5, remain ionized over the entire pH range of the titration and they contribute 5.5kcal/mol of the favorable electrostatic energy stabilizing the anionic quinone. Thus, as expected for a buried hydrophobic environment long-range electrostatic interactions are significant (Kim and others 2005).

Theoretical Determination of in situ pK_a for the ortho-hydroxyl quinones: The calculated pK_a for 2-OH-3-Me-NQ is 1.2, a downshift of 2.8 pK units from the solution value. Thus the Q_A site stabilizes the ionic species by about 3.8 kcal/mol relative to the neutral (equations 1 and 2). The calculated pK_a for 2-OH-NQ is 0, a downshift of 4 pK units from the solution value. Thus the Q_A site stabilizes the ionic species by about 5.4 kcal/mol relative to the neutral (equations 1 and 2). The breakdown of the energy contributions is shown in Table 3-1. The same residues that make the strongest

contribution to the pK_a shift of 5-OH-2-Me-NQ also make the strongest contributions for the ortho-hydroxyl quinones (Table 3-2, Fig. 3-5).

Table 3-2: Residues with the largest contribution to the ΔpK_a in the Q_A site of the three quinones used in this study.

	ΔpK_a		
Residue	5-OH-2-Me-NQ	2-OH-3-Me-NQ	2-OH-NQ
Fe^{2+}	-4.5	-4.3	-5.1
His-M219	-1.2	-1.2	-1.7
Arg-M233	-0.8	-0.5	-0.5
Arg-M241	-1.5	-0.7	-0.7
Arg-M247	-1.1	-0.7	-0.8
Arg-M253	-1.5	-0.8	-0.9
Asn-M259	-1.0	-0.2	-0.3

All ionizable residues are in their ionized form except His-M219. The negative sign for the pK_a shift indicates a downshift due to the stabilization of the ionized species relative to the neutral.

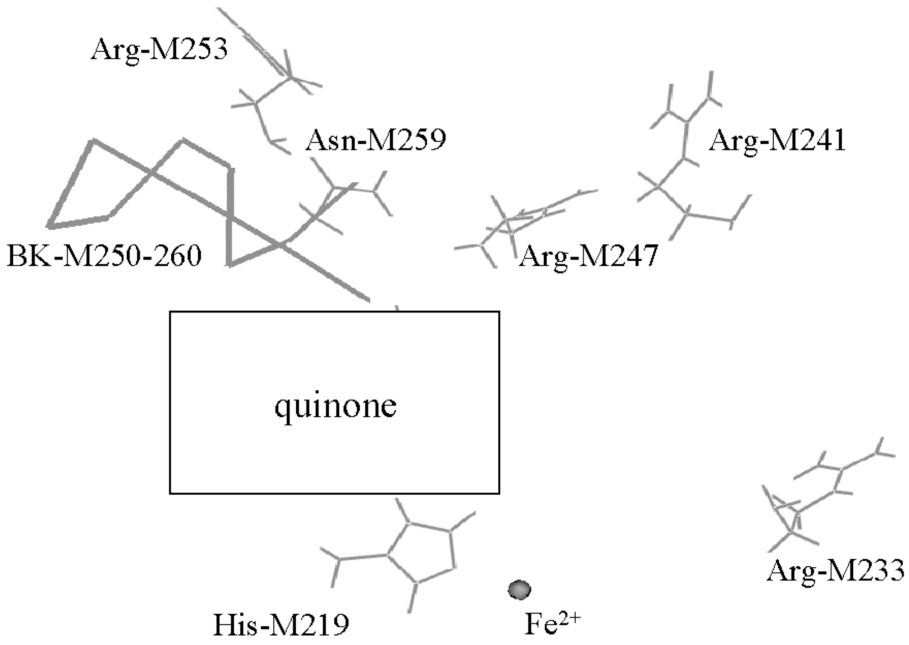

Figure 3-5: Residues that make the strongest contributions to shifting the pK_a of the three hydroxyl quinones used in this study. All of the Arg residues have a positive charge and are located 12-15 angstroms away from the quinone. The box labeled 'quinone' represents the net space taken up by all four of the possible quinone orientations. The amount that the side chain each of these residues shifts the pK_a is given in Table 3-2.

Stabilization of 5-OH-2-Me-NQ with different orientations in the Q_A site: Table 3-4 shows the energy components contributing to the pK_a shift of 5-OH-2-Me-NQ in the four different orientations (see Methods for a description). In the neutral state 5-OH-2-Me-NQ prefers the down, right orientation relative to the up, right orientation because the hydroxyl group interacts more favorably with the side chain of His-M219 (making $\Delta G_{residues}$ more favorable) and in the up, right orientation the hydroxyl group has a more

unfavorable LJ interaction with the backbone of residues Ala-M248 and Ala-M260 (making ΔG_{nonel} less favorable).

For 5-OH-2-Me-NQ, the left orientation is occupied only in the ionized state thus pK_a values could only be obtained for the right orientation (Table 3-3). This is because in the left orientation there is a LJ clash with the most favored conformer (conformer 1) of Met-M218 (Fig. 3-6). Conformer 1 of Met-M218 is favored because it has 1.2kcal/mol more favorable LJ interactions with the backbone (residues Leu-M215 and Leu-M214) and 1.35kcal/mol more favorable pair-wise interaction with Trp-M252 than conformer 2 (Fig. 3-6). In order for the quinone to occupy the left orientation Met-M218 must adopt the unstable conformer 2. Despite this ionized 5-OH-2-Me-NQ occupies the left position by 12%, forcing Met-M218 to occupy conformer 2 (the occupancy changes from 10% to 25% at the end of the titration). The energetic cost of moving Met-M218 into the position of conformer 2 is paid back by the lower desolvation penalty of the ionized quinone in the left orientation. A lower desolvation penalty is more important for a charged species.

The pK_a in the down, right orientation is 7.8, which is 2 pH units higher than the up right orientation (pK_a = 5.8). Thus the up right orientation favors the ionized state relative to the neutral 100-times more than the down right orientation. Different residue pair-wise interactions ($\Delta\Delta G_{residues}$) in the up and down right orientations accounts for this. The important residue interactions are with Fe^{2+}, His-M219 and Glu-L212 (Table 3-4). Despite that the up right orientation moves the hydroxyl oxygen (O5, Fig. 3-1) 4.6A further away from Fe^{2+} than the down, right orientation (Fig. 3-2), interactions with Fe^{2+} lowers the pK_a by 0.3 units more in this orientation (Table 3-4). This is because the acidic protons have a partial positive charge that interacts unfavorably with the Fe^{2+}.

Interactions with His-M219 lowers the pK_a by 0.8 units more in the up, right orientation because the neutral quinone interacts with His-M219 2.5-times favorably in the down, right orientation making it harder for the quinone to be ionized in this position. Lastly, Glu-L212 interacts appreciably only in the down, right orientation because the negatively charged hydroxyl oxygen comes close to the ionized acid. Glu-L212 has a pK_a of about 8 and it is an important residue for regulating the electrochemistry at the Q_B site (Alexov and Gunner 1999). Thus Glu-L212 titrates in the same region as 5-OH-2-Me-NQ in the down, right orientation and the unfavorable interaction between the two ionized species raises the quinone pK_a by 0.5 units in this orientation (Table 3-5).

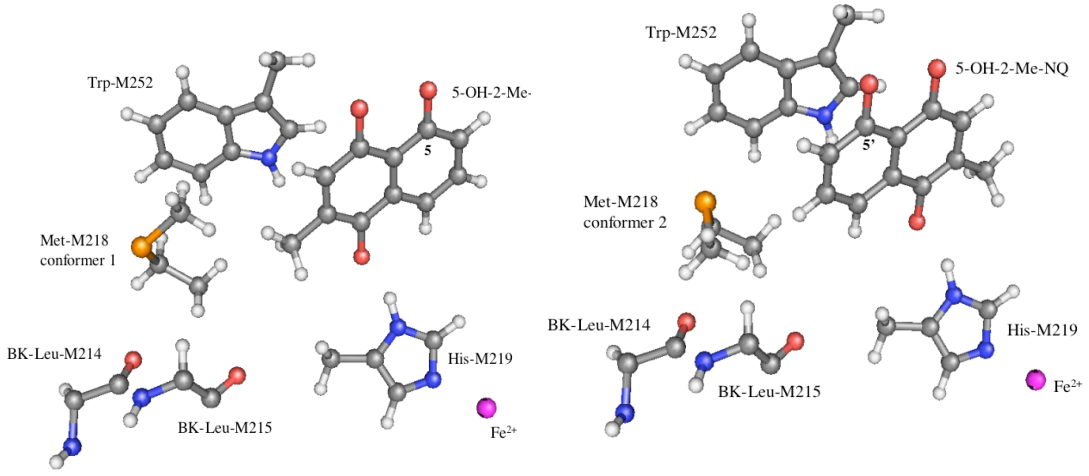

Figure 3-6: Interactions between 5-OH-2-Me-NQ and Met-M218.

When 5-OH-2-Me-NQ occupies a right orientation (either up or down, although up is illustrated here), Met-M218 occupies its most stable conformer (conformer 1). Conformer 1 is a more stable conformer for Met-M218 because it avoids the LJ clash with the backbone of residues Leu-M214 and Leu-M215 and interacts more favorably with Trp-M252. 5-OH-2-Me-NQ can occupy the left position only if Met-M218 moves out of the

way and occupies conformer 2. Despite this conformer 2 increases its occupancy from 10% to 25% due to the ionization of 5-OH-Me-NQ.

Table 3-3: Comparison of the energies of occupied conformers for 5-OH-2-Me-NQ

net crg	OH position	ΔG_{rxn}	ΔG_{pol}	ΔG_{res}	ΔG_{nonel}	Occ.	BK
0	8	6.1	-0.7	-6.3	-17-3	81%	-3.7
0	5	5.7	-2.7	-4.5	-14-1	19%	-3.7
–1	8	14	-6.6	-9.8	-17-3	48%	-9.4
–1	5	13	-7.6	-8.7	-14-1	40%	-8.6
–1	5'	10.4	-5.8	-9.5*	-13-0	12%	-5.8

*After the clash with Met-M218 is subtracted out.

Reported occupancies and $\Delta G_{residues}$ are given at pH 5.3 for the neutral and pH 9 for the ionized conformers.

Table 3-4: Comparing the residue interactions contributing to the pK_a of 5-OH-2-Me-NQ in the Q_A site in the down and up right orientations

Residue	pK_a (OH 8')	pK_a (OH 5)
Fe^{2+}	-7	-7.3
His-M219	-1.5	-2.3
Glu-L212	+0.5	0
Sum	-8	-9.6

All numbers are given in pK units. Negative values indicate that the residue favors interactions with the ionized quinone thus lowering the pK_a. The calculated pK_a for the down, right orientation is 7.8 and the up, right is 5.8.

Stabilization of the ortho-hydroxyls with different orientations in the Q_A site: Unlike 5-OH-2-Me-NQ, the left orientation is never occupied for either ionization state of the 2-OH quinones. The stronger preference of ionized 2-OH-3-Me-NQ for the up, right orientation (the preference is not as strong for ionized 5-OH-2-Me-NQ) makes it less favorable to shift into the left orientation, thus it cannot pay back the energetic cost of moving Met-M218 into conformer 2 (Table 3-5). The reason for this strong preference is the comparably small desolvation penalty of ionized 2-OH-3-Me-NQ in the up, right orientation ($\Delta\Delta G_{rxn}$ in Table 3-5). When 2-OH-3-Me-NQ occupies the up, right orientation the hydroxyl oxygen is sitting in a cavity treated as a continuum of dielectric 80, thus in the ionized state, where O2 carries a partial charge of –0.76, this conformation is stabilized. In the down, right orientation the methyl group is sitting in this cavity instead, thus contributing to the large difference in occupancy of these two orientations in the ionized state.

In the ionized state of 2-OH-NQ the preference for up, right relative to down, right is not as strong (Table 3-6). The reason for that is that when 2-OH-NQ occupies the down, right position a hydrogen atom resides in the cavity as opposed to a methyl group for 2-OH-3-Me-NQ. Thus the desolvation penalty for ionized 2-OH-NQ is not as large as for ionized 2-OH-3-Me-NQ in the down, right orientation and as a result 2-OH-NQ can more freely sample this orientation.

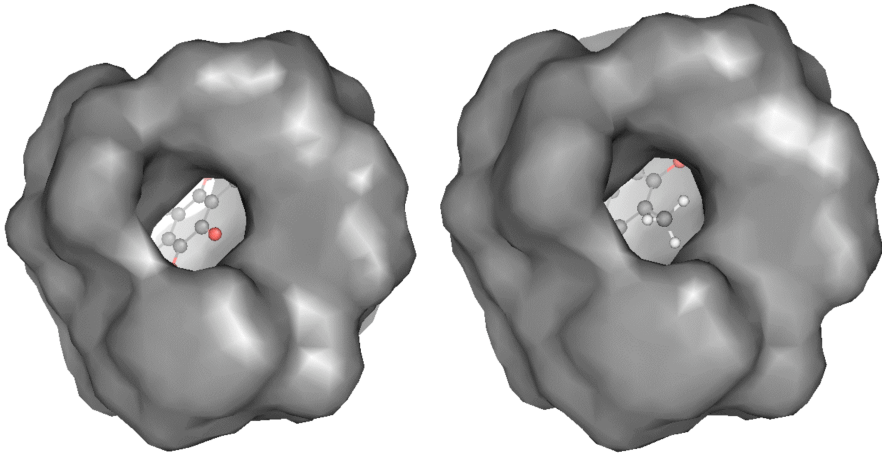

Figure 3-7: Space-filling surface model with ionized 2-OH-3-Me-NQ bound. This shows the position of the high dielectric cavity.

A) The up, right orientation has a relatively low desolvation penalty (8.6 pK units) because O2 sits in this cavity. B) In the down, right orientation the methyl group occupies this position thus the desolvation penalty is larger (12.4 pK units). This difference explains the large difference in occupancy for these two conformers (Table 3-5).

Table 3-5: Comparison of the energies of occupied orientations for 2-OH-3-Me-NQ

net crg	OH position	$\Delta\Delta G_{rxn}$	ΔG_{pol}	ΔG_{res}	ΔG_{nonel}	Occ.
0	2’	3.3	-0.9	-7.0	-20	76%
0	3’	2.7	-0.7	-6.0	-20	24%
–1	2’	12.4	-5.3	-11	-20	8%
–1	3’	8.6	-4.4	-10	-20	92%

Reported occupancies are given at pH 0 for the neutral and pH 3 for the ionized conformers.

Table 3-6: Comparison of the energies of occupied orientations for 2-OH-NQ

net crg	OH position	$\Delta\Delta G_{rxn}$	ΔG_{pol}	ΔG_{res}	ΔG_{nonel}	Occ
0	2’	2.9	-0.7	-4.3	-19	51%
0	3’	2.9	-0.6	-5.5	-18	49%
–1	2’	10.4	-5.0	-11.5	-19	28%
–1	3’	9.5	-4.5	-11.5	-18	72%

Relative binding affinities of the three quinones: The dissociation constants (K_d) for the anionic species of 5-OH-2-Me-NQ and 2-OH-NQ at the Q_A site were previously measured experimentally. For 2-OH-3-Me-NQ dissociation could not be observed, thus

the K_d could not be determined. Thus it was concluded that 2-OH-3-Me-NQ binds at the sub-nanomolar level, which is too tight to be measured experimentally. The neutral species could not be measured due to the low solution pK_as of the ortho-hydroxyl quinones. Although MCCE cannot calculate the absolute binding affinity of a bound co-factor, it can determine their relative binding energies (see Methods). Thus MCCE was used to determine the relative binding energies of the three hydroxyl-quinones used in this study.

Table 3-7 compares the experimental and theoretical relative binding energies. The experimental value is $\log(K_{d,1}/K_{d,2})$, which gives the free energy difference of binding for between two ionized quinones (1 and 2) in pK units. For 2-OH-3-Me-NQ the K_d is assumed to be 1nM (the smallest value that would be observed experimentally), thus the smallest value of $\log(K_{d,1}/K_{d,2})$ is obtained. The MCCE value is obtained from difference of $\Delta G_{protein}$ in the ionized states of the respective hydroxyl quinones. The theoretical comparison between 5-OH-2-Me-NQ and 2-OH-3-Me-NQ (1 and 2) shows that ionized 2-OH-3-Me-NQ binds 6.8 pK units more favorably which corresponds to a K_d 10^6-fold tighter. This could explain the reason why dissociation could not be observed experimentally. Most of the additional binding energy comes from the comparably small desolvation penalty (ΔG_{rxn}) and more favorable LJ interactions with the backbone.

Table 3-7: Comparison of experimental and theoretical free energy differences between the binding affinities for ionized hydroxyl quinones.

	Experiment	MCCE
$\Delta G_{b,1} - \Delta G_{b,2}$	at least 3.6	6.8±1
$\Delta G_{b,1} - \Delta G_{b,3}$	1.65 ± 0.4	3±1
$\Delta G_{b,3} - \Delta G_{b,2}$	at least 2	1.5±1

Energy values given in pK units.

1: 5-OH-2-Me-NQ with experimental K_d = 4.5 ± 1.4 μM; 2: 2-OH-3-Me-NQ with experimental too tight to be determined; 3: 2-OH-NQ with experimental K_d = 0.1 ± 0.05 μM.

3-D) Discussion: In photosynthetic reactions centers electron transfer reactions are initiated by a photon of light. The reactions take place between bound co-factors embedded in a protein medium resulting in the conversion of light energy to charge separation across biological membranes. Quinones are important biological redox agents whose chemistry is modified significantly by the protein environment in which it is bound. In bacterial RCs, both quinone binding pockets (Q_A and Q_B) are occupied by ubiquinone-10. Despite this electron transfer is favorable only from Qa to Qb with nearly 100% quantum yield. Thus the protein environment is of critical importance. Studying the protein-quinone interactions that take place in the binding sites is a necessary step for characterizing the role of the protein environment. Since semi-quinones are unstable free

radicals it is difficult to work with them directly. Thus in this study, the deprotonated species of 5-OH-2-Me-NQ was used as a stable negatively charged quinone and the pH dependence of its binding to the Qa site was characterized. The results presented here supports the idea that the net negative charge on the quinone is the most important feature used by the protein to regulate quinone electrochemistry at the Qa site.

In the Qa site, the bound quinone is deeply buried, about 20 A from the protein surface. Through specific interactions with surrounding residues, the negatively charged and neutral quinone species are differentially stabilized and properly orientated for electron transfer. This differential stabilization is characterized by the difference in the dissociation equilibrium constant (Kd) for the neutral and reduced species. Although the Kd of the semi-quinone (Kd_{ion}) cannot be measured directly, it can be calculated using equation 2, if the Kd of the neutral species (Kd_{neu}), the Em of the electron transfer in the protein (Em_{pro}) and in solution (Em_{sol}) are known. By substituting pKa for Em in equation 2, the shift in pKa can be used to compute the Kd of the deprotonated species relative to the neutral. The form of the equation is unchanged because both processes are driven by the equilibrium occupancy of a neutral and ionized species. The equation relating this thermodynamic cycle is $K_{d,\,ion} = 10^{pKa,\,prot\,-\,pKa,\,sol}(K_{d,\,neu})$

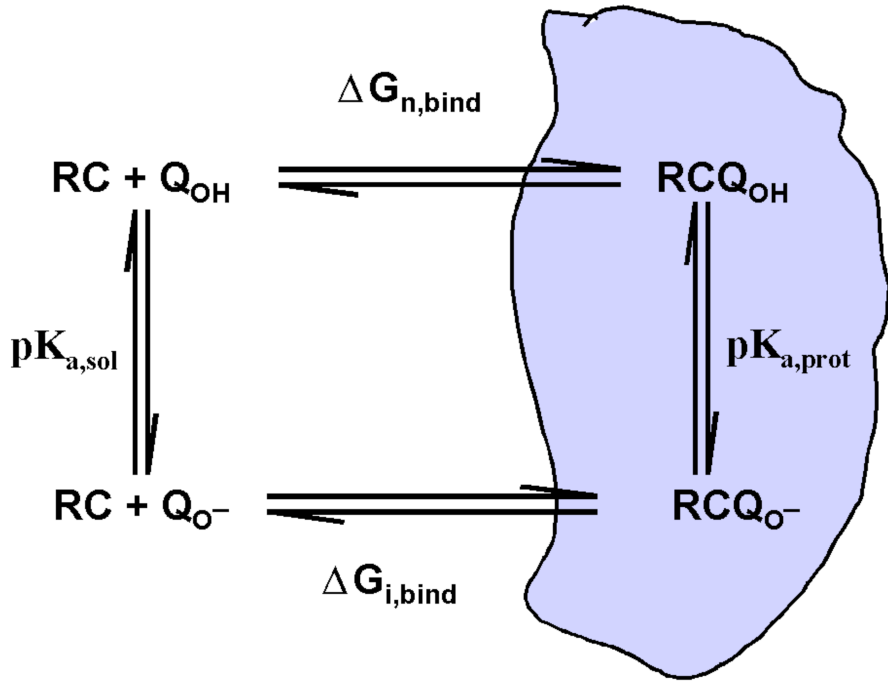

Figure 3-8: Thermodynamic cycle showing the relationship between the quinone pK_a shift and relative affinities of the ionized and neutral species.

Thus, according to equation $K_{d,\ ion} = 10^{pKa,\ prot\ -\ pKa,\ sol}(K_{d,\ neu})$, a shift in Em (or pKa) is directly related to a shift in Kd and can therefore be used to characterize the differential stability of the quinone species. A large Em or pKa shift indicates a large difference in stability. The direction of the shift indicates which species has become more stable relative to the other. For example, a downshift in pKa indicates that the deprotonated species has become more stable relative to the protonated while a downshift in Em indicates that the oxidized species has become more stable relative to the neutral.

The Qa site is a hydrophobic environment with no ionizable residues within a 12 A radius of the native quinone. The negatively charged semi-quinone bound to the Qa site of bacterial RCs is the first stable species during photosynthesis, having a lifetime on

the order of seconds. Thus, despite the hydrophobic nature of the environment a buried negative charge is stabilized. The Qa site is also non-polarizable. The response of the protein to the change in charge upon Qa reduction are believed to occur at distant sites, such as the H subunit where proton transfer takes place and the residues surrounding Qb. The Qa site is, therefore, a low dielectric medium, thus long-range electrostatic interactions are important. The desolvation penalty is the energy loss due to the unfavorable reaction of transferring a charged or polar species from the high dielectric medium of water to the low dielectric medium of the protein interior. Thus the desolvation penalty is larger for the charged species because it interacts more strongly with water. Depending on how buried the binding site is, this desolvation penalty alone can shift pKas up to 5 pK units or Ems up to 300mV. Favorable interactions between the anionic semi-quinone and the protein compensate for this. Although the quinone reaction studied here is a proton transfer, the energetics are similar to the differential stability of ubiquinone-10 in its reduced and oxidized forms, where the ionized species binding energy is about 2 kcal/mol more favorable than the neutral.

Binding affinities for the hydroxyl quinones:

Although the quinone concentration dependence of the $P^+Q_A^-$ amplitude is the standard way to measure the dissociation constant (K_d) for functional quinones it could not be applied for neutral 5-OH-2-Me-NQ for two reasons: 1) even at pH 7.2, the charge recombination amplitude decreases with time due to formation of the ionized species in the Q_A site, thus the relationship between total quinone concentration and charge recombination amplitude was not directly proportional 2) the charge recombination rate

changes as a function of quinone concentration indicating that some of the quinone may be binding at the Q_B site.

The ionized species for all three hydroxyl quinones act as Q_A site competitive inhibitors, thus their dissociation constants (K_I) were measured previously by determining the concentration dependence DQ activity (Madeo). The K_I for 2-OH-3-Me-NQ could not be determined because association appeared to be irreversible. It was concluded that the added methyl group at the 3 position would need to increase the affinity of 2-OH-NQ by at least 100-fold (equivalent to two pK units) in order to not observe DQ displacement. This is in very good agreement with the comparison found with MCCE calculations (Table 3-7). The additional binding energy for 2-OH-3-Me-NQ comes from about a 10-fold smaller desolvation penalty and another 10 to 100-fold more favorable LJ interactions with the backbone (Tables 3-5 and 3-6).

Chapter 4: Applying Multi-Conformational Continuum Electrostatics to Evaluate the Redox Potentials of the Co-factors in PSI and PSII

4-A) Introduction: Photosystem I (PSI) and photosystem II (PSII) use similar co-factors in a similar orientation to conduct electrons across the membrane. Despite these similarities the redox potentials of the embedded co-factors is different in the two photosystems. The E_m of the primary donor of (P_{700}) PSI is 450mV while for PSII (P_{680}) is 1100mV. The higher potential of PSII is necessary because it must oxidize water (E_m =820mV). The primary donor of both photosystems is a chlorophyll a (Chla) dimer, thus the protein environment plays the important role of fine tuning these potentials. MCCE (Multi-Conformational Continuum Electrostatics) is a computational method that can calculate the shift in E_m of a co-factor in moving from the high dielectric environment of water to the low dielectric environment inside the protein. MCCE was used to calculate the redox potentials of the primary donors of both PSI and PSII. The potential of each monomer was also determined. In agreement with experimental results from the literature the A chain monomer of PSI (P_A) is higher potential. This indicates that the electron is asymmetrically distributed in P_{700} and is more likely to be found on P_A. The role of electrostatics in tuning the environment is investigated. In addition both PSI and PSII contain quinones as part of their electron transfer chain. PSI contains 2 phylloquinoes (A_{1A} and A_{1B}) in the A and B co-factor branches. These quinones are very low potential (about –600mV). PSII contains 2 plastoquinones (Q_A and Q_B) at potentials near 0mV. In PSII the protein raises the quinone potential relative to solution, while in PSI the protein

lowers the potential. The role of electrostatics in tuning these potential was also investigated using MCCE.

The reaction centers of photosystem I (PS I) and photosystem II (PS II) are the two membrane–bound protein pigment complexes responsible for the conversion of solar energy into chemical energy during photosynthesis in cyanobacteria, green algae and higher plants (Nelson and Ben-Shem 2004). Numerous pigments harvest light and funnel it to the primary electron donors; P_{700} for PS I and P_{680} for PS II. P_{700} and P_{680} are specialized pairs of chlorophyll molecules whose geometry and redox potential are finely tuned by their protein environments. The harvested photon excites these primary donors, greatly decreasing their redox potentials and thus initiating a chain of electron transfer (ET) reactions between bound redox active co-factors. In PS I the excited electron of P_{700} is transferred in sequence to A_0 (a monomeric chlorophyll a, Chla), A_1 (phylloquinone) and the three Fe_4S_4 clusters F_x, F_A and F_B. In PS II the excited electron of P_{680} is transferred in sequence to a pheophytin ($Pheo_{D1}$), Q_A (plastoquinone) and Q_B (plastoquinone). The final electron acceptor for PS II is the bound plastoquinone (Q_B), which is doubly reduced to plastoquinol and subsequently dissociates from the reaction center (Diner and Babcock 1996). For PS I the final acceptor, ferredoxin, is a separate iron-sulfur protein that docks to the reaction center and uses the electron to reduce NAD to NADPH. P_{700} is re-reduced by the mobile electron carrier plastocyanin. P_{680} is re-reduced by the PS II residue $Tyr161_{D1}$, which is subsequently reduced by the bound oxygen-evolving center (OEC) where the ultimate source of electrons comes from water.

Crystal structures of PS I (2.5 A) (Jordan and others 2001) and PS II (3.5 A) (Ferreira and others 2004) from cyanobacteria reveal that the redox-active co-factors in

both photosystems are arranged in two symmetric branches related by a pseudo-axis perpendicular to the membrane (Fig. 4-1). Each branch is bound to a particular membrane-spanning subunit; PsaA and PsaB in PS I and D_1 and D_2 in PS II. Electron transfer can take place along both branches in PS I, although at different rates, until the electron reaches F_x located on the pseudo-symmetry axis (Fig. 4-1). In PS II ET always occurs along D_1 until $Q_A^{\bullet -}$ passes the electron to Q_B, bound to D_2. The Chla monomers that make up the special pairs are named according to the branch they are closest to; P_A and P_B for P_{700} and P_{D1} and P_{D2} for P_{680}.

Despite their similar geometry, the redox active co-factors of PS I and PS II have very different potentials. PS II, with its ability to extract electrons from water (E_m = 820mV), is the most powerful oxidizing agent known in biology, while the role of PS I is to generate strong reducing equivalents, thus its co-factors are much lower potential. The redox potential of P_{700} is 470mV (Webber and others 1996) while P_{680} is on the order of 1150 to 1260 mV (Nugent 1996; Rappaport and others 2002). Thus these photosystems provide very different environments for their co-factors. The electronic structure of the oxidized primary donor and interactions with the protein environment determine the redox potential in both photosystems (Rutherford and Faller 2002; Webber and Lubitz 2001). The crystal structures have shown that the major organizational difference between P_{700} and P_{680} is the distance between the chlorophylls (6.34A for P_{700} and 8.15A for P_{680}). Thus P_{680} is less coupled and may be monomeric (Mulkidjanian 1999; Rutherford and Faller 2002; Rutherford and Nitschke 1996) while P_{700} behaves more like a dimer. Furthermore P_{700} is a heterodimer where P_A is Chla', the C-13^2 epimer of P_B (Chla) (Jordan and others 2001). No chlorophyll isomers are found in PS II.

The reasons why P_{680} is about 600mV higher potential than P_{700} and plastoquinones in PS II are about 500mV higher potential that the phylloquinones bound to PS I are a mystery. Factors that could play a role include electrostatic interactions with the surrounding protein, ring torsion, hydrogen bonding and the dimeric quality of the primary donors. The work presented here uses multi-conformational continuum electrostatics (MCCE) to investigate the role of electrostatics in tuning the redox potential of P_{700}, A_{1A} and A_{1B} in PS I and P_{680}, Q_A and Q_B in PS II. The differential interactions between these co-factors and their protein environment have a significant effect on their electrochemistry. About 50% of the potential gaps between PS I and PS II can be accounted for by electrostatics.

4-B) Methods: Atomic charges: For all oxidation states of chlorophylls and quinones and the two protonation states of 1,2-dipalmitoyl-phosphatidyl-glycerole (LHG in PS I, PDB 1JB0) and bicarbonate (BCT) the partial atomic charges were obtained by the Hartee-Fock type *ab initio* method with a 6-31G** basis set. The electronic density was partitioned into atomic charges by the method of charges from electrostatic potential (CHELPG charges) implemented in Gaussian 98. The net charge for LHG and BCT was –1 for all redox titrations. For the Mn_4O_4 cluster (PS II) each oxygen atom was assigned a charge of –2, two of the Mn atoms were assigned +4 and the other two +3 and +2 as suggested for the S_0 state in the Babcock hydrogen-atom abstraction model (Tommos and Babcock 1998). PARSE charges and radii were used for all other groups (Sitkoff and others 1994).

Reference E_m values: MCCE calculates the shift in the free energy of ionization when moving from water (ε=80) to protein ($\Delta\Delta G_{protein}$). The *in situ* E_m is given by $E_m = E_{m,sol} - \Delta\Delta G_{protein}/nF$. $E_{m,sol}$ is the reference redox potential of the group in solution. For Chla, $E_{m,sol}$ for the one electron oxidation reaction is 500mV (Suponeva and others 1995). The $E_{m,sol}$ of a one-electron reduction, in a protic solvent, for plastoquinone (Q_A and Q_B of PS II) is –170mV and for phylloquinone (A_{1A} and A_{1B} of PS I) is –240mV (Swallow 1982a).

4-C) Results:

Redox potential of P_{700} of PS I: The calculated E_m for P_{700} is 565mV, a shift of +65mV ($\Delta\Delta G_{protein}$ = +65meV) relative to the solution value. Table 4-4-1 shows the energy components that contribute to the E_m of $P_{700.}$ ($\Delta\Delta G_{protein}$ is broken up into the loss of charge stabilization in moving from the high dielectric environment of water into the low dielectric of the protein ($\Delta\Delta G_{rxn}$), the electrostatic pair-wise interactions with the backbone (ΔG_{epol}), the torsion and Lennard-Jones interactions ($\Delta G_{nonelec}$) and the residue pair-wise interactions with other conformers ($\Delta G_{residues}$). The positive values in Table 4-4-1 indicate contributions that destabilize the ionized species, thus raising the potential for P_{700}. The reported values are the average between the two monomers. Table 4-4-1 shows that ($\Delta\Delta G_{epol}$ destabilizes the oxidized primary donors, thus contributing to raising their potentials. This is not surprising because the backbone dipoles tend to stabilize anions not cations (Gunner and others 2000). ($\Delta G_{residues}$ is the only energy component that lowers P_{700} potential. Thus favorable electrostatic interactions between P_{700} and the surrounding side chains significantly stabilize the oxidized state overcoming the unfavorable repulsion of the backbone and the desolvation penalty. Buried ionized

residues in the P_{700} binding site can account for this. Electrostatic interactions are effective over long ranges in the low dielectric medium of the protein, thus buried charges are important for maintaining functional pK_as and E_ms in many protein systems (Kim and others 2005). Interactions up to 25 A away influence the E_m of P_{700}. Our calculations show that the His ligands (His-A680 and His-B660) lower the potential of their respective chlorophyll monomers by about 80mV, in agreement with mutational analysis in *Chlamydomnas reinhardtii* (Krabben and others 2000).

Redox potential of P_{680} of PS II: The calculated E_m for P_{680} is 820mV, a shift of +320mV relative to solution. At the end of the titration, P_{D1} was almost fully oxidized (96%), while P_{D2} was only 4% oxidized. Thus P_{D1} is appears to be the primary donor in PS II. Since essentially only P_{D1} was oxidized when both monomers were free, P_{D1} and P_{D2} were titrated independently and while one was titrating the other was fixed in its neutral state. These are the values reported in Table 4-1.

The main difference influencing the gap between P_{700} and P_{680} is the pair-wise interactions with other residues (Table 4-1). The OEC, with a net charge of +6, has the largest pair-wise interaction raising the potential of P_{680} (300mV).

Table 4-1: Summary of energy components for primary donors and quinones

Co-factor	E_m (mV)	$\Delta\Delta G_{rxn}$	ΔG_{pol}	ΔG_{nonel}	$\Delta G_{residues}$
P_{700} (PS I)	565	+236	+84	0	-246
P_{D1} (PS II)	822	+211	+127	0	-30
P_{D2} (PS II)	907	+225	+114	0	+65
Q_A (PS II)	-43	+218	-111	0	-233
Q_B (PS II)	0	+271	-151	0	-291
A_{1A} (PS I)	-221	+345	-227	0	-134
A_{1B} (PS I)	-227				

All calculations were done at pH 7 and 100mM salt. Energy values are given to the nearest millielectrovolt (meV). Negative values indicate a more favorable interaction with the ionized species, thus contribute to lowering the potential of the primary donors and raising the potential of the quinones.

Redox potentials of P_A and P_B of P_{700}: At the end of the titration for P_{700}, P_B is 83% oxidized while P_A is 16% oxidized indicating that P_B is lower potential than P_A. To get a better understanding of how the protein environment contributes to lowering the potential of P_B relative to P_A, the E_m of each monomer was calculated independently by switching off the charges of the other monomer (Table 4-2). The difference in E_m between the two monomers is 36mV with ΔG_{pol} contributing 67% and pair-wise interactions with the residues contributing the other 33%.

The most important residue for direct hydrogen bonding to P_A is Thr-A743. When the hydroxyl hydrogen of Thr-A743 is fixed in the position with the best orientation for hydrogen bonding to P_A the E_m of P_A is 640mV (38mV higher than when it is free to sample all positions), thus this hydrogen bond acts to raise the potential of P_A relative to P_B. The only likely hydrogen bond donor to P_B is hydroxyl hydrogen of Thr-B726, which is 4.68A from the 13^3-ester carbonyl. Fixing this hydrogen in the most optimal hydrogen bonding position raised the E_m of P_B by only 9mV. Thus hydrogen bonding is more important for tuning the potential of P_A as compared to P_B, in agreement with other studies (Breton and others 2005).

Table 4-2: Difference in environment between the monomers of P_{700}

Co-factor	E_m (mV)	$\Delta\Delta G_{rxn}$	ΔG_{pol}	ΔG_{nonel}	$\Delta G_{residues}$
P_A	603	+236	+96	0	-232
P_B	566	+238	+72	0	-244

Redox potential of Q_A and Q_B in PS II: PS II contains the benzoquinone plastoquinone (PL9) as both Q_A and Q_B. Q_A is lower potential than Q_B thus permitting forward electron transfer. In these calculations, each quinone was titrated independently while the other was fixed in the neutral reduced state (Table 4-4-1).

The calculated E_m for Q_A is -43mV in good agreement with published values (Johnson and others 1995; Krieger and others 1995; Rappaport and others 2002) and

about 168mV higher than the reference value. The structure of the Q_A site resembles that of purple bacteria. Similar to the reaction centers in *Rhodobacter sphaeroides* one carbonyl oxygen of Q_A is hydrogen bonded to the non-heme iron ligand His-D214 (His-M219 in *Rhodobacter sphaeroides*) and the other to the backbone (Allen and others 1988). In our calculations the electrostatic pair-wise interaction between His-D214 and Q_A is stronger in the reduced state, thus this hydrogen bond contributes to raising Q_A potential. The backbone hydrogen bond is formed with Phe-D261. In our calculations the interaction between Q_A and the backbone dipole of Phe-D261 is unchanged upon Q_A reduction. The geometry of the Q_A site is suitable for π-π interactions between the quinone ring and Trp-D253. The importance of these interactions for setting the Q_A E_m is unknown. FTIR studies suggest that these interactions do not influence the E_m (Noguchi 1999).

It appears that Tyr-D244 uptakes a proton upon Q_A reduction. Upon Q_A reduction Tyr-D244 changes from 68% ionized to 16% ionized. Ser-D262 and Thr-D217 change their preferred hydroxyl hydrogen positions upon Q_A reduction. These alterations do not have a significant effect on the E_m but may be important for facilitating proton motions and protein relaxations due to the change in charge. PS II uptakes a total of 0.6 protons upon Q_A reduction.

Similar to the reaction centers of purple bacteria, larger conformer occupancy changes were observed upon Q_B reduction compared to Q_A (Alexov and Gunner 1999). In the reduced state (Q_B^-), the most occupied conformer of Ser-A264 (95%) has the hydroxyl hydrogen in the most optimal position for forming a hydrogen bond with the quinone carbonyl oxygen (Fig.). In the oxidized state the occupancy of this conformer is

reduced to 7% and the interaction energy is reduced from -2.4 to -1.2 kcal/mol. Thus the hydrogen bond between Q_B and Ser-A264 is important for stabilizing the semi-quinone (raising the Q_B E_m) and it plays a role similar to Ser-L223 in the reaction centers of *Rhodobacter sphaeroides* (Alexov and Gunner 1999). The ionization of His-A252 changes from 0 to 28% in going from oxidized to reduced Q_B. In addition the proton positions of His-A252 reorganize such that the position most optimal for hydrogen bonding with Ser-A264 (Fig.) changes its occupancy from 7% to 67% upon forming Q_B^-.

To better understand the effect of the proton positions of Ser-A264 and His-A252 on the E_m of Q_B, monte carlo sampling with the hydroxyl proton of Ser-A264 fixed in the hydrogen bonding position (Fig). The E_m when the proton is free to sample all possible positions is –63mV, which is 20mV lower potential than Q_A (Table 4-4-1) thus forward electron transfer would be unfavorable. With the Ser-A264 proton fixed the E_m is raised to 0.0mV permitting forward electron transfer. This 43mV gap between Q_A and Q_B is in good agreement with experiments, thus we assume that 0.0mV is the correct E_m for Q_B and the energy results for this calculation is reported (Table 4-4-1). It is likely that the hydrogen bond between Ser-A264 and Q_B^- is stronger than the electrostatic interaction. Table 4-1 shows that the potential gap between Q_A and Q_B can be account for by the differential interactions with the residues ($\Delta G_{residues}$) in the different binding sites.

The ionization of His-A252 changes from 0 to 28% in going from oxidized to reduced Q_B and this is independent of the proton positions on Ser-A264. This is also similar to the reaction centers of purple bacteria where a proton transfer was observed in the Q_B site upon Q_B^- formation (Alexov and Gunner 1999). In addition the proton

positions of His-A252 re-orientate due to Q_B reduction, which may be important for protein relaxation in response to the change in charge.

Redox Potential of A_{1A} and A_{1B} in PS I: Electron transfer in PS I occurs from A_1 to F_x and currently there is conflicting data about the relative importance of electron transfer down the A and B branches. Despite the EPR studies suggesting that only the A-branch is active in electron transfer (Bittl and Zech 1997; Yang and others 1998), there is a lot of experimental evidence supporting the bidirectional electron transfer model (both branches are active) (Guergova-Kuras and others 2001; Hastings and Sivakumar 2001; Joliot and Joliot 1999; Santabarbara and others 2005). Our calculations show that the redox potential of A_{1A} are both –230mV, thus supporting the bidirectional model.

FTIR experiments suggested that Glu-A699 and Glu-A702 are affected by A_{1A}^- formation and Glu-B679 and Glu-B682 are affected by A_{1B}^- formation (Hastings and Sivakumar 2001). Thus these conserved glutamic acid residues are likely to be important for modifying the phylloquinone E_ms. Our calculations show that Glu-A699 and Glu-A702 are ionized and lower the potential of A_{1A} by 170mV (Fig). Glu-B679 is ionized and lowers the potential of A_{1B} by 100mV while Glu-B682 is 90% neutral thus does not significantly affect the potential. Glu-B679 is ionized because of favorable electrostatic interactions with the positively charged residues Lys-A569 (-13kcal/mol) and Lys-A555 (-12kcal/mol). Glu-B682 is not involved in such favorable pair-wise interactions thus its driving force for ionization is not as strong.

Previous electrostatic calculations by Ishikita et. al. suggested that Asp-B575 is predominantly (85%) ionized and hydrogen bonded to the crystal water (HOH-37) when A_{1A} is neutral (Ishikita and Knapp 2003). The hydrogen bond between Asp-B575 and HOH-37 was necessary to keep the acid ionized and the resulting interactions lowered the potential of A_{1A} by 100mV and A_{1B} by 85mV (Ishikita and Knapp 2003). In our calculations Asp-B575 is never more than 2% ionized, even with HOH-37 modeled explicitly, because of unfavorable interactions with ionized Asp-B580. These two Asp residues are coupled and cannot be ionized at the same time. Asp-B580 prefers to be ionized (rather than Asp-B575) because it has more favorable interactions with Arg-B712 and LysB-556 and less unfavorable interactions with the nearby anionic Cys residues that ligate F_X (Fig.). The unfavorable interaction energy between reduced A_{1A} and ionized Asp-B580 is 44% less than for ionized Asp-B575 thus Asp-B580 is less able to influence the redox potential.

To address the influence of the electrostatic interaction between ionized Asp-B575 on the redox potential of A_1, this acid was fixed in the ionized state during A_1 titration. The presence of ionized Asp-B575 changed the occupancy of the HOH-37 conformer optimal for forming a hydrogen bond with its carbonyl from 11% to 90%. This agrees with the idea that a hydrogen bond with this crystal water is important for maintaining the ionized state of Asp-B575 (Ishikita and Knapp 2003). Furthermore, the ionized Asp lowered the potential of A_{1A} by 100mV (E_m = -335) and A_{1B} by 60mV (E_m = -291mV).

The crystal structure of PS I (1JB0) contains three bound 1,2-dipalmitoyl-phosphatidyl-glycerole molecules in the vicinity of the phylloquinones (Saenger 2002).

These lipids are intrinsic structural components of PS I which are important for reaction center oligomerization and binding antenna to the reaction center (Domonkos and others 2004; Saenger 2002). The lipids were modeled explicitly and the negatively charged phosphate moiety of lipid I lowered the redox potential of A_{1A} by 85mV (Fig), while not significantly changing the E_m of $A_{1B.}$

4-D) Discussion

Redox potential of P_{700}: MCCE calculated an E_m of 565mV for the P_{700} dimer, a shift of +65mV relative to aqueous solution and close to the expected value (470mV). At the end of the titration P_A is 16-18% oxidized while P_B is 82-84% oxidized indicating that P_B is in a higher potential environment. High field EPR of $P_{700}^{\bullet+}$ studies have indicated that the unpaired electron is mostly localized on P_B (Petrenko and others 2004). Molecular orbital calculations also indicate that hydrogen bonding will stabilize P_A suggesting that the unpaired electron resides predominately on P_B (Webber and Lubitz 2001). ENDOR experiments have estimated that P_B has 5-times more radical character than P_A (Kass and others 2001). Lastly, using FTIR difference spectroscopy in chlamydomonas PS I it was found that P_B carries the bulk of the positive charge in the P_{700} oxidized state (Wang and others 2003).

To get a better understanding of how the protein environment contributes to lowering the potential of P_B relative to P_A, the E_m of each monomer was calculated independently by switching off the charges of the other monomer (Table 4-4-2). Under these conditions the E_m of P_A is 602mV and P_B is 566mV. Thus there is approximately a 40mV difference between the two environments.

Importance of asymmetry in P_{700}: P_A and P_B of P_{700} are interacting with different local environments. The PS I crystal structure shows that P_A is involved in an extensive hydrogen-bonding network while no such network is observed for P_B (Fromme and others 2001; Jordan and others 2001). This hydrogen-bonding network involves a water molecule (HOH-19), Thr-A743, SerA-607, Tyr-A603 and the backbone of Gly-A739 (residues numbers from cyanobacteria, PBD 1JB0) (Fig.). In particular, Thr-A743 is an important residue because its hydroxyl oxygen is 2.98 A away from the 13^1 carbonyl oxygen of P_A, thus it should make the strongest hydrogen bonds directly to the chlorophyll. FTIR difference spectroscopy has indicated that the hydrogen-bond network is perturbed due to cation formation (Wang and others 2004). The hydroxyl hydrogen position of Thr-A743 that is the most optimal for making a hydrogen bond (position 3, Fig.) with the 13^1 carbonyl oxygen is always the most preferred, decreasing slightly from 94% occupancy to 90% occupancy upon cation formation. The interaction energy is –1.2kcal/mol. This is mostly due to the fact that in our calculations P_A is never more than 18% oxidized. The difference in the interaction energy between Thr-A743 and the neutral versus the fully oxidized P_A is +0.79 kcal/mol (interaction is stronger in the neutral state), thus a stronger perturbation should be observed if P_A carried more of the charge in the oxidized state. The most occupied HOH-19 conformers are orientations suitable for hydrogen bonding with Thr-A743 (Fig.), which helps to maintain the right orientation for the hydrogen bond between Thr-A743 and P_A and Tyr-A603.

The largest change in this hydrogen bonding network due to cation formation is the position of the hydroxyl hydrogen of Ser-A607 (Fig). The occupancy ratio of the two

occupied positions change from 2:1 to 3:1 in the neutral and oxidized states respectively. The preferred position interacts more favorably with HOH-19 (modeled explicitly) and is in the best position for hydrogen bonding with Tyr-A603 (0.86 kcal/mol interaction energy). Despite this its occupancy is lowered upon P_{700} oxidation due to electrostatic repulsions with the cationic P_A.

Asymmetry in P_{680}: There is evidence that the primary electron donor in PS II is a chlorophyll monomer rather than a dimer in which the most likely candidate is the chlorophyll adjacent to Ph_{D1} (Fig) (Rutherford and Faller 2002) (more ref therein with experimental evidence of a monomeric primary donor).

Redox potentials of A_{1A} and A_{1B}: In PS I, the two phylloquinones are symmetrically arranged and are the last electron acceptors in the PsaA and PsaB protein subunits respectively. Each quinone is π-stacked with trytophan residues (Trp-A697 for A_{1A} and Trp-B677 for A_{1B}). Since π-stacking does not influence the electrostatic field around the quinone it does not affect the quinone E_ms calculated here. The physiological importance of π-stacking interactions in determining the *in situ* E_m of A_1 is not known. FTIR studies have suggested that they are not important (Hastings and Sivakumar 2001), while quantum chemical calculations suggest that they can lower the potential of A_1 by up to 150mV (Kaupp 2002). Thus this may be a source of error in the calculations presented here.

In contrast to PS II, only one of each of the carbonyl oxygen atoms of the phylloquinones in PS I accepts a hydrogen bond (Fromme and others 2001; Jordan and

others 2001). This is supported by density functional calculations (O'Malley 1999), EPR (Pushkar and others 2004) and FTIR studies (Hastings and Sivakumar 2001). The hydrogen bond donors are the amide backbones of Leu-A722 (A_{1A}) and Leu-B706 (A_{1B}). The favorable electrostatic interaction between A_{1A} and the backbone of Leu-A722 is 1.6kcal/mol and between A_{1B} and the backbone of Leu-B706 it is 1.5kcal/mol. These interactions do not change significantly upon quinone reduction. FTIR difference spectroscopic studies have indicated that the backbone amides are perturbed due to A_{1A} reduction (Sivakumar and others 2005). The MCCE calculations for PSI do not match the literature values as well as PSII (Fig. 4-7). In MCCE the backbone is fixed thus if error is imparted in these calculations if the backbone alters its conformation due to A_{1A} reduction. DFT calculations have suggested that each hydrogen bond to the semi-quinone can increase the reduction potential by as much as 250mV (O'Malley 1999), thus the lack of hydrogen bonds in A_{1A} and A_{1B} could contribute to their low potential. The effect of the loss of solvent-quinone hydrogen bonds on the shift in E_m in going from solution to the A_1 binding site is not considered in our calculations. This energetic penalty could lower the potential by up to 500mV (Kaupp 2002) making the E_m in the aprotic solvent DMF (-460mV (Prince and others 1983)) a better reference value for calculating the phylloquinones in PS I. Using –460mV as a reference potential the calculated E_ms for A_{1A} and A_{1B} would be –460mV, which is closer to the expected value.

4-E) Figures for Chapter 4

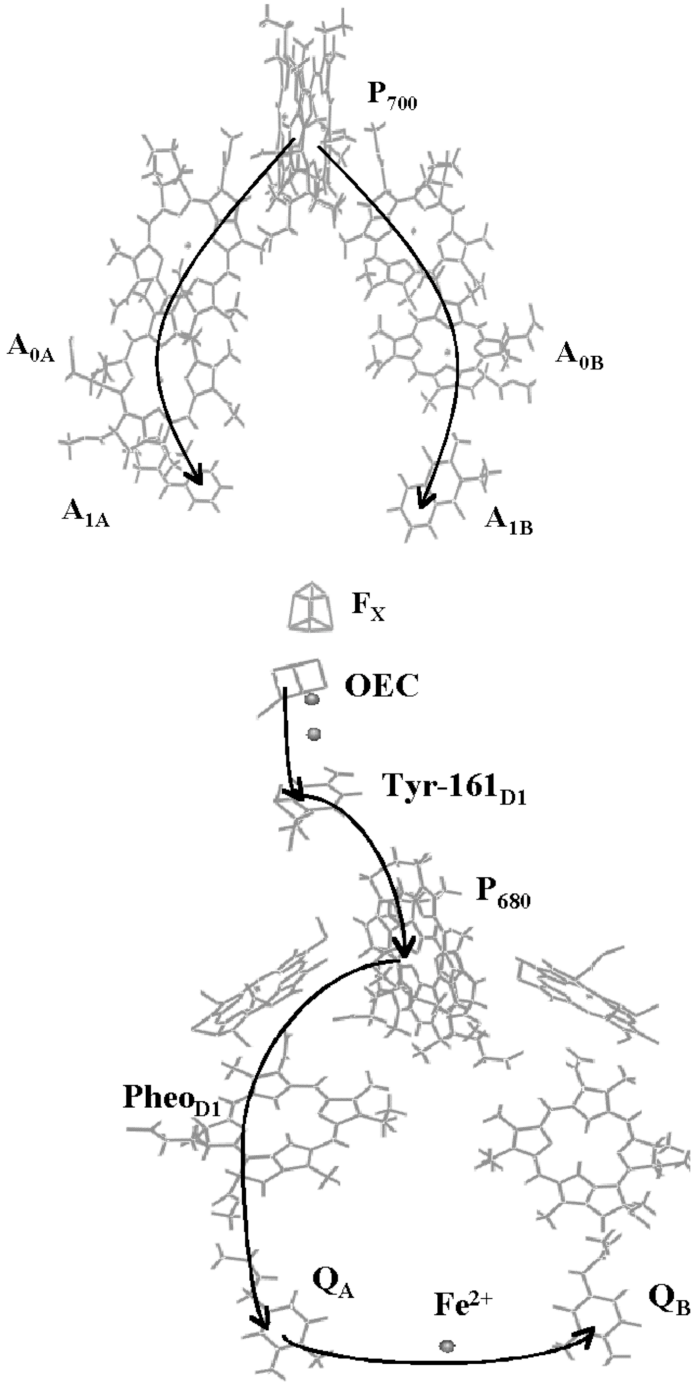

Figure 4-1: Electron transport chains in PS I and PS II.

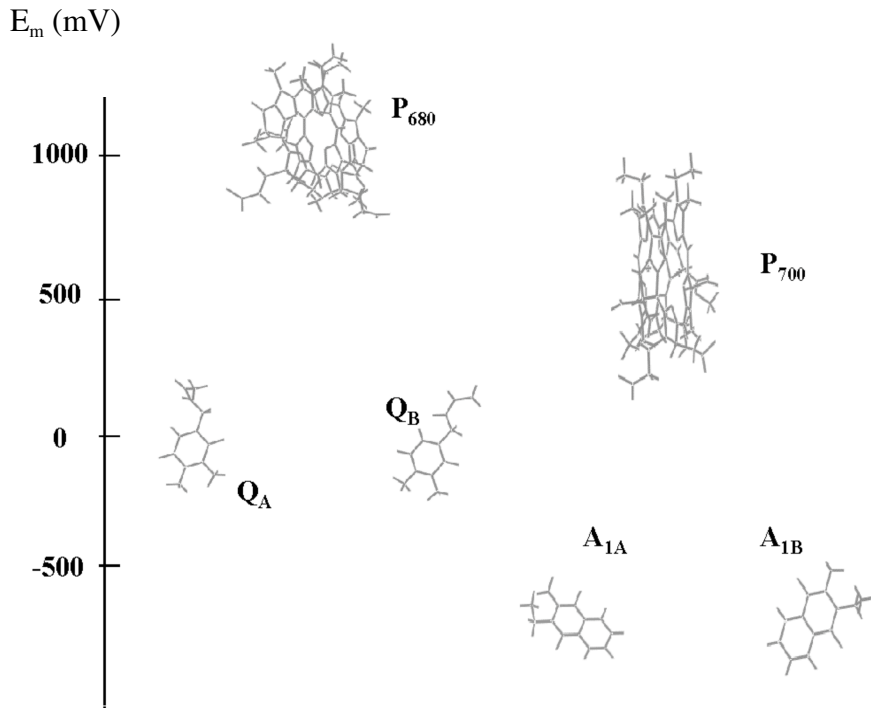

Figure 4-2: Approximate redox potentials of the primary donors and quinones of PS I and PS II.

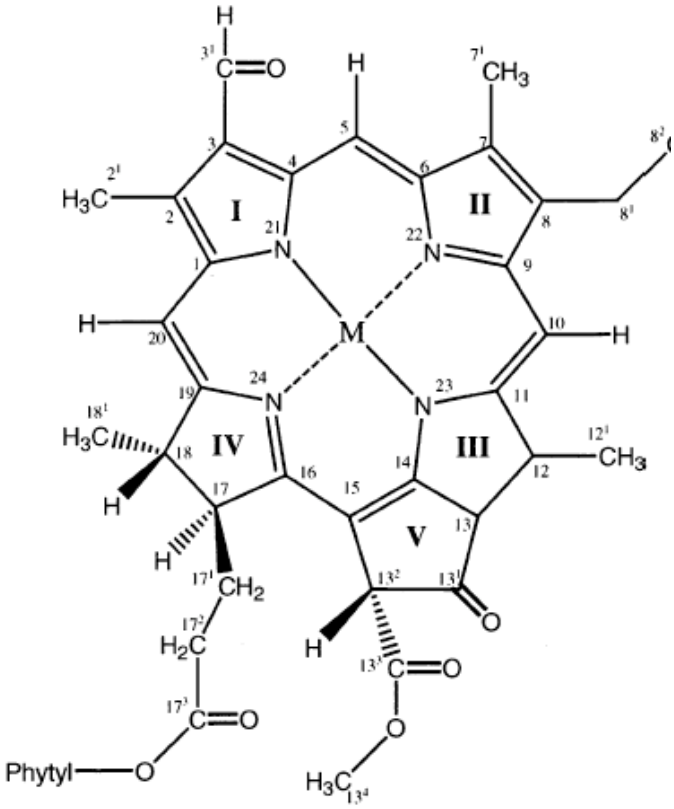

Figure 4-3 Chlorophyll molecule with the IUPAC nomenclature system

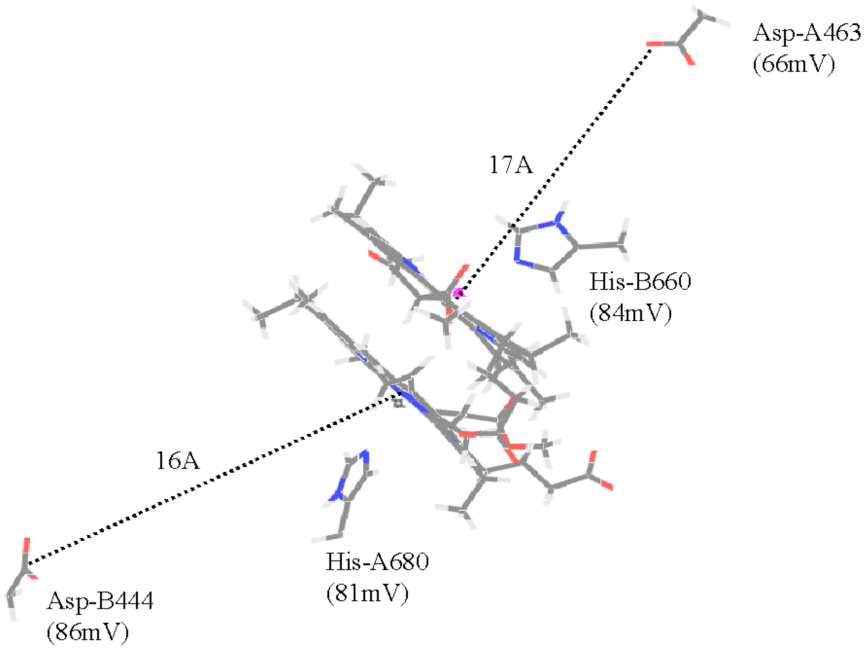

Figure 4-4: Important residue interactions that contribute to lowering the E_m of P_{700}. Numbers in the parathesis indicates the shift in redox potential due to the differential pair-wise interaction between the respective residue with the oxidized and reduced states of P_{700}.

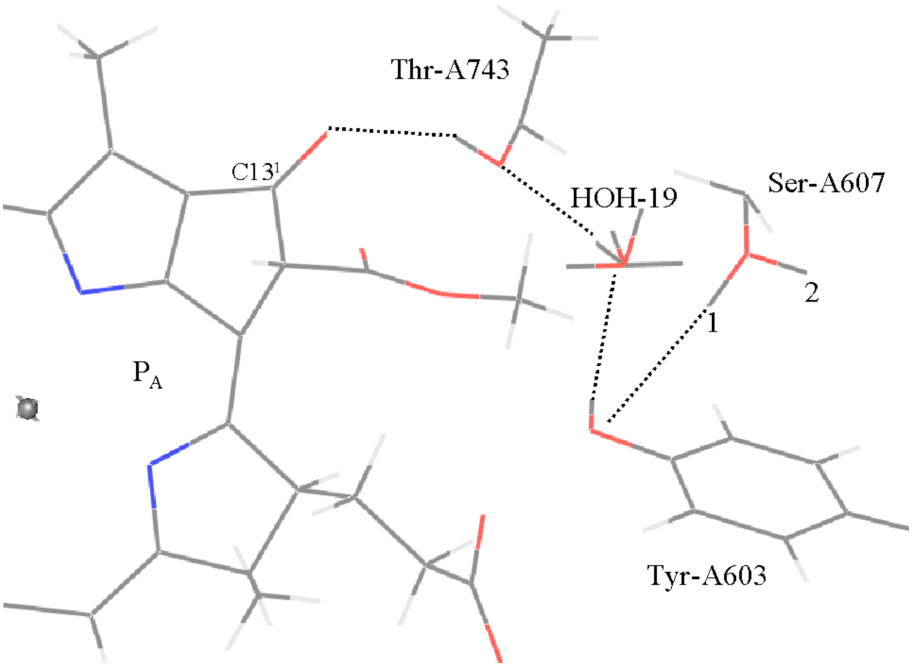

Figure 4-5: Hydrogen bonding network surrounding P_A (P_{700}).

Only hydogens that are involved in the network are shown in dark color. The dashed lines indicate hydrogen bonds. The proton positions shown are the most occupied in the Monte Carlo sampling (there are three HOH-19 conformers and two Ser-A607). Thr-A743 has a strong interaction (-1.2 kcal/mol) with the oxygen of the $C13^1$ carbonyl, which does not change significantly upon P_{700} oxidation. The hydroxyl hydrogen of Ser-A607 has two occupied positions (1 and 2). The occupancy ratio of 1 to 2 changes from 1:2 to 1:3 upon P_{700} oxidation. Thus despite the hydrogen bonding in position 1, position 2 is more favored because it shifts away from electrostatic repulsion with the chlorophyll, which becomes more unfavorable upon oxidation.

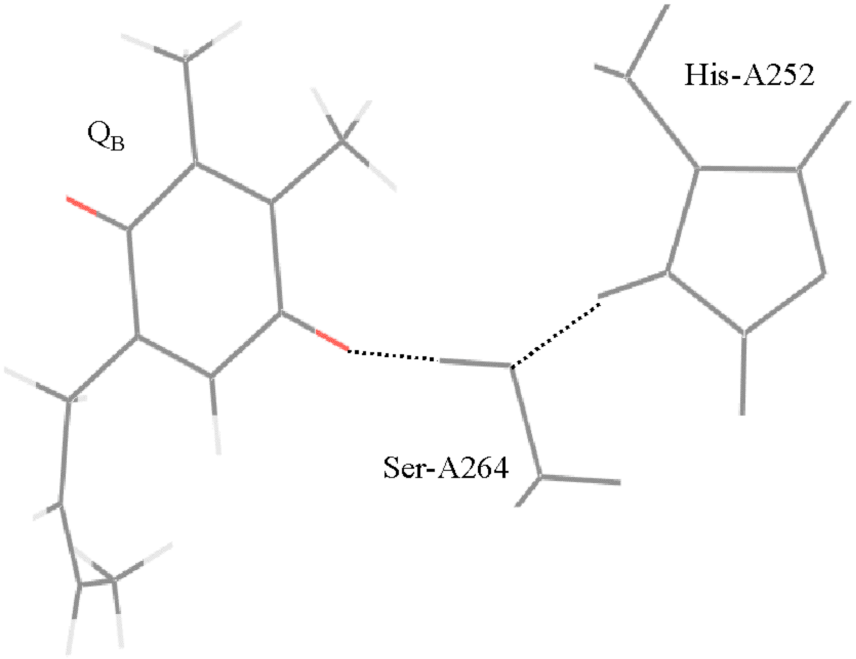

Figure 4-6: Hydrogen bonding network that raises the redox potential of Q_B (PS II).

Hydrogen bonding with Ser-A264 plays an important role in stabilizing the semi-quinone permitting forward electron transfer from Q_A^-.

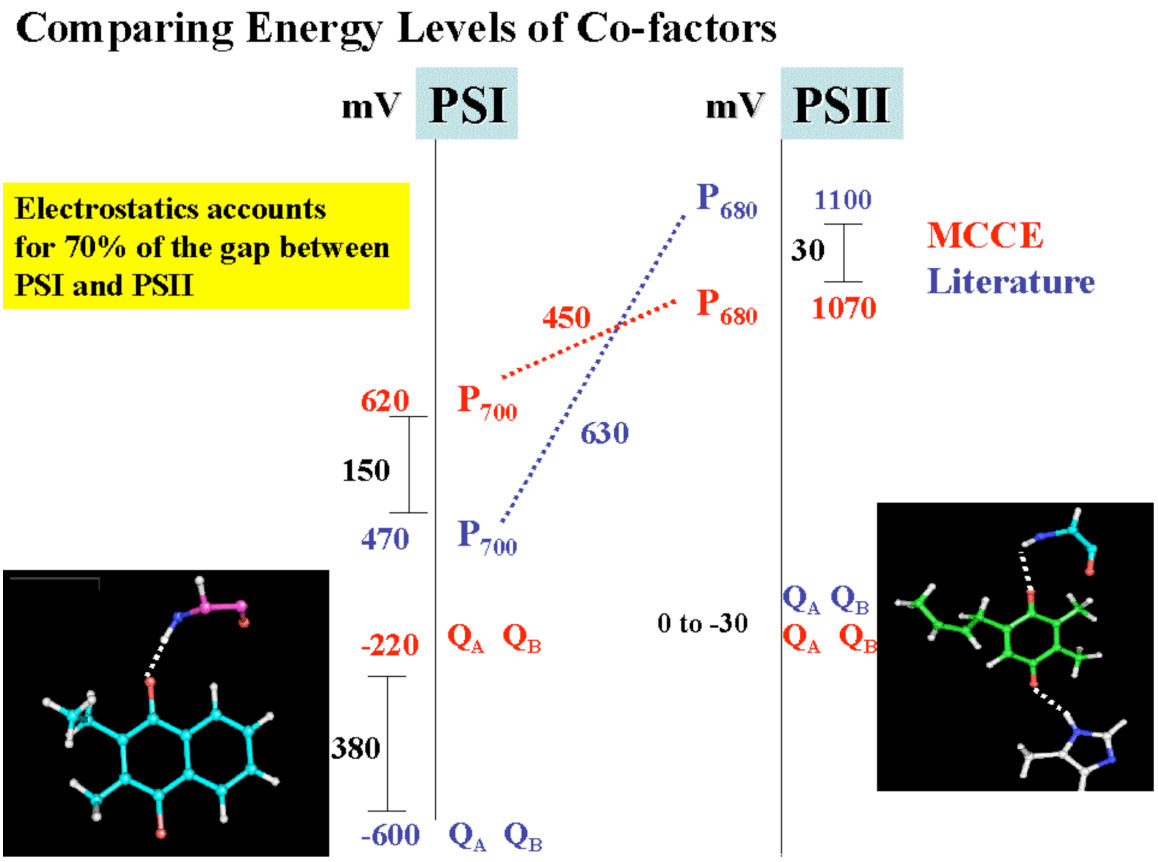

Figure 4-7: Comparing MCCE calculated redox potentials of PSI and PSII to other published values. MCCE can account for about 70% of the gap between the primary donors of PSI (P_{700}) and PSII (P_{680}). The rest may come from non-electrostatic contributions such as hydrogen bonding and quantum mechanical effects that do not greatly affect the electric field surrounding the co-factors. MCCE calculates the co-factors for PSII reasonable well, but is significantly far off for PSI. This could partially be due to using the wrong reference E_m value in solution (see text).

APPENDIX

Model A, Second order analysis of fast binding active quinones at 100% light saturation (□ = 1): In the double flash method the depletion of RCQ by an actinic flash of light causes quinone association to be much faster than dissociation (k_{on}*[Q_F][RC_F] >> k_{off}*[RCQ]), thus additional RCQ is formed, denoted RCQ_{bind}, which is detected by a second flash. The difference in amplitude between the flashes is used to derive the association rate constant (k_{on}). The data is fit assuming a second order reaction (A1). Since K_d, the dissociation constant, is measured independently and k_{off}=Kd*k_{on}, the only free parameter is k_{on}. The mathematical model is a first order nonlinear differential equation that is solved to obtain RCQ_{bind} as a function of time:

RCQ_{eq} = concentration of RCQ excited by the first flash at a given quinone concentration thus forming the $RCQ^{\pm}$ state

k_{AP} = rate constant for the larger phase of Q_A charge recombination (the smaller phase is due to the residual native quinone in the Q_A site which does not participate in the binding), measured from the exponential decay of P^+ at 430nm.

Given

$$RC_F + Q_F \underset{koff}{\overset{kon}{\rightleftharpoons}} RCQ_{bind}$$

The rate of change of RCQ is:

$$\frac{d}{dt}RCQ_{bind}(t) = kon \cdot \left(RC_F(t) \cdot Q_F(t) - K_d \cdot RCQ_{bind}(t)\right)$$

Conservation equations for RC_F (t) and Q_F (t) are:

$$RC_F(t) = RC_T - RCQ_{eq} - RCQ_{bind}(t)$$

$$Q_F(t) = Q_T - RCQ_{eq} - RCQ_{bind}(t)$$

After the first flash, the formation of RCQ by charge recombination from the $RCQ^{\pm}$ state (RCQ_{back}):

$$RCQ_{back}(t) = RCQ_{eq} \cdot \left(1 - e^{-k_{AP} \cdot t}\right)$$

Putting the model together gives:

$$\frac{d}{dt}RCQ_{bind}(t) = k_{on} \cdot \left[(RC_T - RCQ_{eq} - RCQ_{bind}(t)) \cdot (Q_T - RCQ_{eq} - RCQ_{bind}(t)\right]$$
$$-K_d \cdot \left[RCQ_{bind}(t) + RCQ_{eq} \cdot \left(1 - e^{-k_{AP} \cdot t}\right)\right]$$

Setting the initial condition to $[RCQ_{bind\ t=0}]=0$, Mathematica 4.2 was used to find numerical solutions to this equation for values of Q_T ranging from 0 to the concentration needed to completely saturate the Q_A sites at equilibrium. The solutions give RCQ_{bind} as a function of time at each quinone concentration. Plotting RCQ_{eq} + RCQ_{bind} against Q_T for each time point generates a set of sigmoidal curves. The k_{on} used to generate plots that best fit for the data is the measured k_{on} of the quinone. Figure A1 illustrates the time

course of model A. Assuming 100% light saturation the initial conditions: $[RCQ_{bind\ t=0}] = 0$.

Modifications due to incomplete light saturation ($\lambda < 1$): Each flash of actinic light excites approximately 80-85% of the RCQ ($\lambda = 0.80$-0.85) leaving the other 20% in the ground state. Thus there is an increase in amplitude on the second flash even in the absence of quinone binding. λ is measured from the extra amplitude formed by the second flash at saturating quinone concentrations. The absorbance change on the first flash (ΔA_1) is proportional to $\lambda * [RCQ_{eq}]$, where λ is the light saturation (the fraction of RCQ that received at least one photon) and $[RCQ_{eq}]$ is the equilibrium concentration of RCs with active quinone bound before a flash perturbs the system. On a second flash, given at time t $\Delta A_2(t)$ is proportional to $[RCQ_{bind}(t)] * \lambda + [RCQ^{\pm}(t)] + (1-\lambda) * [RCQ_{eq}]$, where $[RCQ^{\pm}(t)]$ is the amount of charge separated RCs remaining at time t. $\lambda < 1$ is accounted for in the theoretical model by fixing the initial conditions for solving equation A6 to: $[RCQ_{t=0}] = (1-\lambda) * [RCQ_{eq}]$, $[RCQ^{\pm}_{t=0}] = [RCQ_{eq}] * \lambda$ and $RCQ_{bind\ t=0} = 0$. Thus equation A6 is transformed to:

$$\frac{d}{dt} RCQ_{bind}(t) = k_{on} \cdot \left[(RC_T - RCQ_{eq} - RCQ_{bind}(t)) \cdot (Q_T - RCQ_{eq} - RCQ_{bind}(t) \right]$$
$$- K_d \cdot \left[RCQ_{bind}(t) + (1-\lambda) \cdot RCQ_{eq} + \lambda \cdot RCQ_{eq} \cdot \left(1 - e^{-k_{AP} \cdot t}\right) \right]$$

where,

λ = percent light saturation (measured when the Q_A site is fully occupied

Accounting for the light saturation in the model means that the data can be fit without any modifications. The effect that $\lambda < 1$ has on the theoretical curves is shown in figure A1.

On the other hand, $\lambda < 1$ can be corrected for in the data rather than the model. The change in amplitude between the flashes (A_2 -A_1) can be modified to correctly reflect the change in amplitude strictly due to association. The modified change in amplitude is computed as $\Delta A = A_2 - p*A_1$

The correcting factor p is:

$$p = e^{-k_{AP} \cdot t} + \lambda \cdot ((1-\lambda) + (1-e^{-k_{AP} \cdot t}))$$

Correcting the data for light saturation and then fitting it to the model is important for the analysis of the quinone concentration dependence of k_{on}.

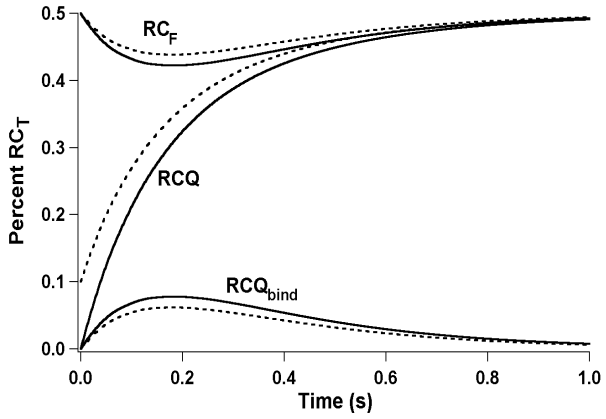

Figure A1: Effect of $\lambda < 1$ on the time course for the double flash assay

The solid lines represent the time course for RC_F, RCQ (total concentration of bound RCs) and RCQ_{bind} (the additional RCQ formed due to association) during the double flash analysis when $\lambda = 1$ and the dashed lines are for $\lambda = 0.80$. The conditions chosen here fix

Q_T so the Q_A sites are 50% saturated, thus $RCQ_{eq} = RC_F = \frac{1}{2}RC_T$ and $Q_T = \frac{1}{2}RC_T + K_d$; K_d=0.6□M, $k_{AP} = 3.5s^{-1}$ and RC_T=1□M. The derived k_{on} is $8*10^6\ M^{-1}s^{-1}$.

Model B, Second order model for slow inhibitor binding: The inhibitor binding of the anionic hydroxyl quinones (RCI) is monitored by the disappearance of DQ charge recombination activity. Since K_I, the inhibitor dissociation constant, is measured independently, the only free parameter is the association rate constant (k_{on}). DQ binding kinetics occurs 1000 times faster and thus are ignored in the model.

RCQ_{eq} = concentration of DQ bound RCs at equilibrium given that the K_d for DQ is 05.

The rate of change of RCI is:

$$\frac{d}{dt}RCI(t) = k_{on} \cdot \left(RC_F(t) \cdot I_F(t) - K_I \cdot RCI(t)\right)$$

The conservation equations for RC_F (t) and I_F (t) are:

$$RC_F(t) = RC_T - RCQ_{eq} - RCI(t)$$

$$I_F(t) = I_T - RCI(t)$$

Putting the model together yields:

$$\frac{d}{dt}RCI(t) = k_{on} \cdot \left[(RC_T - RCQ_{eq} - RCQ(t)) \cdot (I_T - RCI(t) - K_I \cdot RCI(t)\right]$$

This equation is solved with initial condition $RCI_{(t=0)}$= 0. The best fit to the data yields the second order k_{on} ($M^{-1}s^{-1}$).

Model C, Dissociation of anionic hydroxyl quinones: The dissociation rate constant (k_{off}) for the hydroxyl quinones was measured directly by adding DQ to a pre-equilibrated sample of hydroxyl quinone-bound RCs. The increase in DQ charge recombination activity was followed with time. Again, DQ binding kinetics are neglected.

Given that $k_{on} = k_{off}/K_I$, the rate of change of RCI is:

$$\frac{d}{dt}RCI(t) = \frac{k_{off}}{K_I} \cdot \left(RC_F(t) \cdot I_F(t) - k_{off} \cdot RCI(t)\right)$$

Incorporating equations B2 and B3 gives the final model:

$$\frac{d}{dt}RCI(t) = \frac{k_{off}}{K_I} \cdot \left[(RC_T - RCQ_{eq} - RCI(t)) \cdot (I_T - RCI(t) - k_{off} \cdot RCI(t)\right]$$

Since the sample starts off with hydroxyl quinone bound at the Q_A site, the initial condition is $RCQ_{(t=0)} = fRC_T$, where *f* is a number from 0 to 1 equal to the fraction of saturation.

Model D, First order model for fast binding active quinones: With a first orderrate-determining step, the rate of binding is independent of quinone concentration. Thus the rate-determining step only involves changes in the RCQ complex and the apparent first orderrate constant (k_0). The initial complex RCQ relaxes to the final equilibrium state, RCQ^*.

The first order reaction is:

$$RCQ \xleftrightarrow{ko} RCQ^*$$

The rate of change of RCQ is:

$$\frac{d}{dt} RCQ^*(t) = k_0 \cdot [RCQ(t) - RCQ^*(t)]$$

The second order step is assumed to be too fast to contribute to the rate, thus RCQ*(t) is modeled as the RC_F (t) (equation A2). Furthermore, since the data is obtained from the double flash method, RCQ(t) is the same as in model A (equation A4). Putting this together gives the final model:

$$\frac{d}{dt} RCQ(t) = k_0 \cdot \left[(RC_T - RCQ_{eq} - RCQ(t)) - \left[RCQ(t) + RCQ_{eq} \cdot \left(1 - e^{-k_{AP} \cdot t}\right) \right] \right]$$

Model E, First order model for slow binding inhibitor: The first ordermodel for the hydroxyl quinones describes a process in which the initial encounter complex (RCI) undergoes a first-order isomerization to form the most stable complex configuration (RCI^*). The model is a single exponential decay used to fit the observed disappearance DQ activity with time. The rate constant describing this process is the sum of the forward and reverse rates but the rate of the formation of RCI from RCI^* is much smaller than the forward rate, thus it is neglected in this model. The rate of change of RCI is:

$$\frac{d}{dt} RCI(t) = k_0 \cdot \left[RCI(t) \right]$$

Bibliography

Abbamonte P, Finkelstein KD, Collins MD, Gruner SM. 2004. Imaging density disturbances in water with a 41.3-attosecond time resolution. Phys. Rev. Lett. 92:237401-237404.

Abraham DJ, Leo AJ. 1987. Extension of the fragment method to calculate amino acid zwitterion and side schain partition coefficients. Proteins: Struct. Funct. Genet. 2:130-152.

Abrahams JP, Leslie AGW, Lutter R, Walker JE. 1994. Structure at 2.8Å resolution of F1-ATPase brom bovine heart mitochondria. Nature 370:621-628.

Abresch EC, Stowell MHB, McPhillips TM, Rees DC, Soltis SM, Feher G. 1997. A crystallographic investigation of light-induced structure changes in reaction centers of *Rb. sphaeroides*. Biophys. J. 72(2):A8.

Adir N, Axelrod HL, Beroza P, Isaaxson RA, Rongey SH, Okamura MY, Fher G. 1996. Co-crystallization and characterization of the photosynthetic reaction center-cytochrome c_2 complex from *Rhodobacter sphaeroides*. Biochemistry 35:2535-2547.

Ahlström P, Teleman O, Jönsson B. 1988. Molecular dynamics simulation of interfacial water structure and dynamics in a parvalbumin solution. J. Am. Chem. Soc. 110:4198-4203.

Alexov E. 2003. Role of the protein side-chain fluctuations on the strength of pair-wise electrostatic interactions: comparing experimental with computed pK_as. Proteins: Struct. Funct. Genet. 50:94-103.

Alexov E, Miksovska J, Baciou L, Schiffer M, Hanson DK, Sebban P, Gunner MR. 2000. Modeling the effects of mutations on the free energy of the first electron transfer from QA- to QB in photosynthetic reaction centers. Biochemistry 39(20):5940-52.

Alexov EG, Gunner MR. 1999. Calculated protein and proton motions coupled to electron transfer: electron transfer from Q_A^- to Q_B in bacterial photosynthetic reaction centers. Biochemistry 38(26):8253-70.

Allen JP, Feher G, Yeates TO, Komiya H, Rees DC. 1988. Structure of the reaction center from *Rhodobacter sphaeroides* R-26: Protein-cofactor (quinones and Fe+2) interactions. Proc. Natl. Acad. Sci. USA 85:8487-8491.

Allen JP, Williams JC, Graige M, Paddock ML, Labahn A, Feher G, Okamura MY. 1998. Free energy dependence of the direct charge recombination from the primary and

secondary quinones in reaction centers from *Rhodobacter sphaeroides*. Photosynth. Res. 55:227-233.

Baciou L, Rivas E, Sebban P. 1990. $P^+Q_A^-$ and $P^+Q_B^-$ charge recombinations in *Rhodopseudomas viridis* chromatophores and in reaction centers reconstituded in phosphatidylcholine liposomes. Existence of two conformational states of the reaction centers and effects of pH and o-phenanthroline. Biochemistry 29:2966-2976.

Bader JS, Cortis CM, Berne BJ. 1997. Solvation and reorganization energies in polarizable molecular and continuum solvents. Journal of Chemical Physics 106(6):2372-2387.

Barber J. 2002. Throwing light on photosynthesis. Trends in Biochemical Sciences 27(8):433.

Barter LM, Durrant JR, Klug DR. 2003. A quantitative structure-function relationship for the Photosystem II reaction center: supermolecular behavior in natural photosynthesis. Proc Natl Acad Sci U S A 100(3):946-51.

Bashford D, Case DA. 2000. Generalized born models of macromolecular solvation effects. Annu Rev Phys Chem 51:129-52.

Baxter RHG, Ponomarenko N, Srajer V, Pahl R, Moffat K, Norris JR. 2004a. Time-resolved crystallographic studies of light-induced structural changes in the photosynthetic reaction centers. Proc. Natl. Acad. Sci. USA 101:5982-5987.

Baxter RHG, Seagle BL, Ponomarenko N, Norris JR. 2004b. Specific radiation damage illustrates light-induced structural changes in photosynthetic reaction centers. J. Am. Chem. Soc. 126:16728-16729.

Berman HM, Westbrook J, Feng Z, Gilliland G, Bhat TN, Weissig H, Shindyalov IN, Bourne PE. 2000. The protein data bank. Nucleic Acids Research 28:235-242.

Bianchet MA, Pedersen PL, Amzel LM. 2000. Notes on the mechanism of ATP synthesis. Bioenergetics and Biomembranes 32:517-521.

Bittl R, Zech G. 1997. Pulsed EPR study of spin-coupled radical pairs in photosynthetic reaction centers: measurement of the distance between $P^{\bullet+}_{700}$ and $A^{\bullet-}_{1}$ in photosystem I and between $P^{\bullet+}_{865}$ and $Q_A^{\bullet-}$ in bacterial reaction center. J.Phys.Chem.B 101:1429-1436.

Blankenship RE, Madigan MT, Bauer CE. 1995. Anoxygenic Photosynthetic Bacteria. Govindjee, editor: Kluwer Academic Publishers. 1283 p.

Blankenship RE, Prince RC. 1985. Excited-state redox potentials and the Z scheme of photosynthesis. TIBS 10:382-383.

Boxer SG, Goldstein RA, Lockhart DJ, Middendorf TR, Takiff L. 1989. Exited states, electron transfer reactions, and intermediates in bacterial photosynthetic reaction centers. J. Phys. Chem. 93:8280-8294.

Braun BS, Benbow U, Lloyd-Williams P, Bruce JM, Dutton PL. 1986. Determination of partition coeffieients of quinones by high-performance liquid chromatography. Methods Enzymol 125:119-129.

Breton J, Burie J, Berthomieu C, Berger G, Nabedryk E. 1994a. The binding sites of quinones in photosynthetic bacterial reaction centers investigated by light-induced FTIR difference spectroscopy: Assignment of the Q_A vibrations in *Rhodobacter sphaeroide*s using ^{18}O- or ^{13}C-Labeled ubiquinone and vitamin K_1. J. Am. Chem. Soc. 33:4953-4965.

Breton J, Burie J, Boullais C, Berger G, Nabedryk E. 1994b. Binding sites of quinones in photosynthetic bacterial reaction centers investigated by light-induced FTIR difference spectroscopy: Binding of chainless symmetrical quinones to the Q_A site of Rhodobacter Sphaeroides. Biochemistry 33:2-24.

Breton J, Chitnis PR, Pantelidou M. 2005. Evidence for hydrogen bind formation to the PsaB chlorophyll of P700 in photosystem I mutants of synechocystis sp. PCC 6803. Biochemistry 44(14):5402-5408.

Bretscher EL, Li H, Poulos LT, Griffith WO. 2003. Structural characterization and kinetics of nitric-oxide synthase inhibition by novel N^5-(Iminoalkyl) and N^5-(Iminoalkenyl)-ornithines. The Journal of Biological Chemistry 278(47):46789-46797.

Brettel K, Leibl W. 2001. Electron transfer in photosystem I. Biochim Biophys Acta 1507:100-114.

Brixner T, Stenger J, Vaswani HM, Cho H, Blankenship RE, Fleming GR. 2005. Two-dimensional spectroscopy of electronic couplings in photosynthesis. Nature 434:625-628.

Brzezinski P, Okamura MY, Feher G. 1992. Structural changes following the formation of D+QA- in bacetrial reaction centers: measurement of light-induced electrogenic events in RCs incorporated in a phospholipid monolayer. Brenton J, Vermeglio A, editors. New York: Plenum Press. 321-330 p.

Bulow A, Plesner I, Bols M. 2001. Slow Inhibition of almond glucosidase by azasugars: determination of activation energies for slow binding. Biochim Biophys Acta 1545:207-215.

Colominas C, Luque FJ, Orozco M. 1999. Monte carlo mst new strategy for representation of solvent configurational space in solution. J.Comp.Chem. 20:665-678.

Cramer WA, Crofts AR. 1982. Electron and proton transport. In: Govindjee, editor. Photosynthesis: Energy Conversion by Plants and Bacteria. New York: Academic. p 387-467.

Cramer WA, Zhang H, Yan J, Kurisu G, Smith JL. 2004. Evolution of photosynthesis: time-independent structure of the cytochrome b6f complex. Biochemistry 43(20):5921-9.

Das T, Bratko D, Bhuiyan LB, Outwaite CW. 1995. Modified poisson-Boltzmann theory applied to linear polyelectrolyte solutions. J. Phys. Chem. 99:410-418.

Dash C, Vathipadiekal V, George SP, Rao M. 2002. Slow-Tight Binding Inhibition of Xylanase by an Aspartic Protease Inhibitor. The Journal of Biological Chemistry 277:17978-17986.

David L. 1995. Handbook of Chemistry and Physics: CRC.

Dharmasena SP, Wimalasena DS, Wimalasena K. 2002. A Slow-Tight Binding Inhibitor of Dopamine B-Monooxygenase: A Transition State Analogue for the Product Release Step. Biochemistry 41:12414-12420.

Diner BA, Babcock GT. 1996. Structure, dynamics and energy conservation efficiency in photosystem II. In: Ort DR, Yocum CF, editors. Oxygenic Photosynthesis: The Light Reactions. Dordrecht: Kluwer Academic Publishers.

Diner BA, Schenck CC, DeVitry C. 1984. Effect of inhibitors, redox state and isoprenoid chain length on the affinity of ubiquinone for the secondary acceptor binding site in the reaction centers of photosynthetic bacteria. Biochim. Biophys. Acta 766:9-20.

Domonkos I, Malec P, Sallai A, Kovacs L, Itoh K, Shen G, Ughy B, Bogos B, Sakurai I, Kis M and others. 2004. Phosphatidylglycerol is essential for oligomerization of photosystem I reaction center. Plant Physiology 134(4):1471-1478.

Draber W, Tietjen K, Kluth JF, Trebst A. 1991. Herbicides in photosynthesis research. Angew. Chem. 30:1621-1633.

Duggleby RG, Attwood PV, Wallace JC, Keech DB. 1982. Avidin is a slow binding inhibitor of Pyruvate Carboxylase. Biochemistry 21:3364-3370.

Dutton PL, Leigh JS, Wraight CA. 1973. Direct measurement of the midpoint potential of the primary electron acceptor in *Rhodopsuedomonas sphaeroides* in situ and in

the isolated state: some relationships with pH and o-phenathroline. FEBS Lett. 36:169-173.

Elcock AH, McCammon JA. 1997. Continuum solvation model for studying protein hydration thermodynamics at high temperatures. Journal of Physical Chemistry B 101(46):9624-9634.

Feher G, Allen JP, Okamura MY, Rees DC. 1989. Primary processes in bacterial photosynthesis:
Structure and function of bacterial photosynthetic reaction centres. Nature 339:111-116.

Feher G, Okamura MY, Kleinfeld D. 1985. Electron transfer reactions in bacterial photosynthesis: Charge recombination kinetics as a structure probe.1-20.

Ferreira KN, Iverson TM, Maghlaoui K, Barber J, Iwata S. 2004. Architecture of the photosynthetic oxygen-evolving center. Science 303:1831-1838.

Fleming GR, van Grondelle R. 1997. Femtosecond spectroscopy of photosynthetic light-harvesting systems. Curr Opin Struct Biol 7(5):738-48.

Freindorf M, Gao J. 1996. Optimization of Lennard-Jones parameters for a combined Ab initio quantum mechanical and molecular mechanical potential using the 3-21G basis set. J. Comp. Chem. 17(3):386-395.

Fromme P. 1996. Structure and function of photosystem I. Curr Opin Struct Biol 6 no.4:473-484.

Fromme P, Jordan P, Krauß N. 2001. Structure of photosystem I. Biochim Biophys Acta 1507:5-31.

Fyfe PK, Jones MR, Heathcote P. 2002. Insights into the evolution of the antenna domains of Type-I and Type-II photosynthetic reaction centres through homology modelling. FEBS Lett. 530:117.

Gao J-L, Shopes RJ, Wraight CA. 1990. Charge recombination between the oxidized high-potential c-type cytochromes and Q_A^- in reaction centers from *Rhodopseudomonas viridis*. Biochim. Biophys. Acta 1015:96-108.

Georgescu RE, Alexov EG, Gunner MR. 2002. Combining conformational flexibility and continuum electrostatics for calculating pK_a's in proteins. Biophys J. 83:1731-1748.

Ginet N, Lavergne J. 2001. Absorption changes induced by the binding of triazines to the Qb pocket in reaction centers of Rhodobacter capsulatus. Biochemistry 40:2995-3001.

Goldsmith JO, Boxer SG. 1996. Rapid isolation of bacteria photosynthetic reaction centers with an engineered poly-histidine tag. Biochim Biophys Acta 1276:171-175.

Gordon DB, Marshall SA, Mayo SL. 1999. Energy functions for protein design. Curr Opin Struct Biol 9(4):509-13.

Govidnjee. 1982. Photosynthesis: Energy conversion by Plants and Bacteria. New York: Academic Press.

Graige MS, Paddock ML, Bruce JM, Feher G, Okamura MY. 1996. Mechanism of proton-coupled electron transfer for quinone (Q_B) reduction in reaction centers of *Rb. Sphaeroides*. J. Am. Chem. Soc. 118:9005-9016.

Gratzel M. 2001. Photoelectrochemical cells. Nature 414:338-344.

Guergova-Kuras M, Boudreaux B, Joliot A, Joliot P, Redding K. 2001. Evidence for two active branches for electron transfer in photosystem I. Proc. Natl. Acad. Sci. USA 98:4437-4442.

Gunner MR. 1991. The reaction center protein from purple bacteria: Structure and function. Current Topics in Bioenergetics 16:319-367.

Gunner MR, Saleh MA, Cross E, ud-Doula A, Wise M. 2000. Backbone dipoles generate positive potentials in all proteins: origins and implications of the effect. Biophys J 78(3):1126-44.

Hagfeldt A, Gratzel M. 2000. Molecular photovoltaics. Acc. Chem. Res 33:269-277.

Hansch C, Leo A, Taft RW. 1991. A servey of hammett substituent onstants and resonance and field parameters. Chem. Rev. 91:165-195.

Hastings G, Sivakumar V. 2001. A fourier transform infared absorption difference spectrum associated with the reduction of A1 in photosystem I: Are both phylloquinones involved in electron transfer? Biochemistry 40:3681-3689.

Ishikita H, Knapp EW. 2003. Redox potential of quinones in both electron transfer branches of photosystem I. J. Biol. Chem. 278:2002-11.

Ishikita H, Morra G, Knapp EW. 2003. Redox potential of quinones in photosynthetic reaction centers from *Rhodobacter sphaeroides*: dependence on protonation of Glu-L212 and Asp-L213. Biochemistry 42(13):3882-92.

Janouskova M, Pavlikova D, Macek T, Vosatka M. 2005. Influence of arbuscular mycorrhiza on the growth and cadium uptake of tabacco with inserted metallothionein gene. Applied Soil Ecology 29(3):209-214.

Jeuken LJ. 2003. Conformational reorganisation in interfacial protein electron transfer. Biochim Biophys Acta 1604(2):67-76.

Jiang YL, Ichikawa Y, Striver JT. 2002. Inhibition of uracil DNA glycosylase by an Oxacarbenium Ion mimc. Biochemistry 41:7116-7124.

Johnson GN, Rutherford AW, Krieger A. 1995. A change in the midpoint potential of the quinone QA in photosystem II associated with photoactivation of oxygen evolution. Biochim Biophys Acta 1229:202-207.

Joliot P, Joliot A. 1999. In vivo analysis of the electron transfer within photosystem I: Are the two phylloquinones involved? Biochemistry 38:11130-11136.

Jordan P, Fromme P, Witt HT, Klukas O, Saenger W, Krauß N. 2001. Three-dimensional structure of cyanobacterial photosystem I at 2.5Å resolution. Nature 411:909-917.

Kalman L, Maroti P. 1994. Stabilization of reduced primary quinone by proton uptake in reaction centers of Rhodobacter spaeroides. Biochemistry 33:9237-9244.

Kalman L, Sebban P, Hanson DK, Schiffer M, Maroti P. 1998. Flash-induced changes in buffering capacity of reaction centers from photosynthetic bacteria reveal complex interaction between quinone pockets. Biochim Biophys Acta 1365:513-521.

Kass H, Fromme P, Witt H, Lubitz W. 2001. Orientation and electronic structure of the primary donor radical cation P700+ in photosystem I: A single crystal EPR and ENDOR study. J. Phys. Chem. B 105:1225-1239.

Kaupp M. 2002. The function of photosystem I. Quantum chemical insight into the role of tryptophan-quinone interactions. Biochemistry 41(9):2895-900.

Kim J, Mao J, Gunner MR. 2005. Distribution and ionization states of acidic and basic residues buried in proteins. J. Mol. Biol. submitted.

Kirmaier C, Holten D. 1993. Electron transfer and charge recombination reactions in wild-type and mutant bacterial reaction centers. In: Deisenhofer J, Norris JR, editors. The Photosynthetic Reaction Center. San Diego: Academic Press. p 49-70.

Kirmaier C, Holten D, Parson WW. 1985. Temperature and detection-wavelenth dependence of the picosecond electron transfer kinetics measured in *Rhodopseudomonas sphaeroides* reaction centers. Resolution of new spectral and kinetic compontents in the primary charge separation process. Biochim. Biophys. Acta 810:33-48.

Krabben L, Schlodder E, Jordan R, Carbonera D, Giacometti G, Lee H, Webber AN, Lubitz W. 2000. Influence of the axial ligands on the spectral properties of P700 of photosystem I: A study of site-directed mutants. Biochemistry 39(13012-13025).

Kramers HA. 1940. Brownian motion in a field of force and the diffusion model of chemical reactions. Physica 7:284-304.

Krieger A, Rutherford AW, Johnson G. 1995. On the determination of redox midpoint potential of the primary quinone electron acceptor, QA, in photosystem II. Biochim Biophys Acta 1229:193-201.

Kurz LC, Weitkamp E, Frieden C. 1987. Adenosine Deaminase: Viscosity studies and the mechanism of binding of substrate and of ground- and transition-state analog inhibitors. Biochemistry 26(11):3027-3032.

Lewis SN, Crabtree G. 2005. Basic Research Needs for Solar Energy Utilization. 1-13 p.

Li J, Gilroy D, Tiede DM, Gunner MR. 1998. Kinetic phases in the electron transfer from $P^+Q_A^-Q_B$ to $P^+Q_AQ_B^-$ and the associated processes in *Rhodobacter sphaeroides* R-26 reaction centers. Biochemistry 37(9):2818-2829.

Li J, Takahashi E, Gunner MR. 2000. $-\Delta G°_{AB}$ and pH dependence on the electron transfer from $P^+Q_A^-Q_B$ to $P^+Q_AQ_B^-$ in *Rhodobacter sphaeroides* reaction centers. Biochemistry 39:7445-7454.

Li Y, Lucas MG, Konovalova T, Abbott B, MacMillian F, Petrenko A, Sivakumar V, Wang R, Hastings G, Gu F and others. 2004. Mutation of the Putative hydrogen-bond donor to P700 of photosystem I. Biochemistry 43:12634-12647.

Lidell PA, Kodis, G., de la Garza, L., Moore, A.L., Moore, T.A.,. 2004. Benzene templated model systems for photosynthetic antenna reaction center function. J. Phys. Chem. B 108:10256.

Lohse A, Hardlei T, Jensen A, Plesner I, Bols M. 2000. Investigation of the slow inhibition of almond B-Glucosidase and yeast isomaltase by 1-azasugar inhibitors: Evidence for the 'direct binding' model. Biochemical J 349:211-215.

Mao J, Hauser K, Gunner MR. 2003. How cytochromes with different folds control heme redox potentials. Biochemistry 42(33):9829-40.

Mao JJ, Song YF, Gunner M. 2004. Multi-Conformation Continuum Electrostatics (MCCE): An efficient, accurate program for calculation of pKas and Ems in proteins. Biophysical Journal 86(1):633a-633a.

McPherson PH, Okamura MY, Feher G. 1988. Light-induced proton uptake by photosynthetic reaction centers from *Rhodobacter sphaeroides* R-26. I. Protonation of the one-electron states $D^+Q_A^-$, DQ_A^-, $D_AQ_AQ_B^-$, and $DQ_AQ_B^-$. Biochim. Biophys. Acta 934:348-368.

McPherson PH, Okamura MY, Feher G. 1990. Electron transfer from the reaction center of *Rb. sphaeroides* to the quinone pool: doubly reduced Q_B leaves the reaction center. Biochim. Biophys. Acta 1016:289-292.

Merkler DJ, Brenowitz MS, Schramm VL. 1990. The rate constant describing slow-onset inhibition of Yeast AMP Deaminase by coformycin analogues is independent of inhibitor structure. Biochemistry 29:8358-8364.

Miksovska J, Maroti P, Tandori J, Schiffer M, Hanson DK, Sebban P. 1996. Distant electrostatic interactions modulate the free energy level of Q_A^- in the photosynthetic reaction center. Biochemistry 35:15411-15417.

Moller IM. 2001. PLANT MITOCHONDRIA AND OXIDATIVE STRESS: Electron Transport, NADPH Turnover, and Metabolism of Reactive Oxygen Species. Annu Rev Plant Physiol Plant Mol Biol 52:561-591.

Morrison JF, Walsh CT. 1988. The behavior and significance of slow-binding enzyme inhibitors. Adv. Enzymol. Relat. Areas Mol. Biol. 61:201-301.

Mulkidjanian AY. 1999. Photosystem II of green plants: on the possible role of retarded protonic relaxation in water oxidation. Biochim Biophys Acta. 1410:1-6.

Murphy RB, Philipp, D. M., Friesner, R. A. 2000. A mixed quantum mechanics/molecular mechanics (QM/MM) method for large-scale modeling of chemistry in protein environments. Journal of Computational Chemistry 21(16):1442-1457.

Nabedryk E, Bagley KA, Thibodeau DL. 1990. A protein conformational change associated with the photoreduction of the primary and secondary quinones in the bacterial reaction center. FEBS Letter 266:59-62.

Nelson J. 1999. Continuous time random walk model of electron transport in nanocrystalline TiO2 eletrodes. Phys Rev B 59:15374-15380.

Nelson N, Ben-Shem A. 2004. The complex architecture of oxygenic photosynthesis. Nature Reviews 5:1-12.

Nicholls A, Honig B. 1991. A rapid finite difference algorithm utilizing successive over-relaxation to solve the Poisson-Boltzmann equation. J. Comp. Chem. 12:435-445.

Noguchi T, Inoue,Y., Tang, X.S.,. 1999. Hydrogen bonding interactions between the primary quinone acceptor and a histidine side chain in photosystem II as revealed by Fourier transform infrared spectroscopy. Biochemistry 38:399.

Nonella M, Schulten K. 1991. Molecular Dynamics Simulation of Electron Transfer in Proteins. Theory and Application to Q_A --> Q_B Transfer in the Photosynthetic Reaction Center. J. Phys. Chem. 95:2059-2067.

Nozik AJ. 2002. Quantum Dot solar cells. Physica 14:115.

Nugent JH. 1996. Oxygenic photosynthesis. Electron transfer in photosystem I and photosystem II. Eur J Biochem 237(3):519-531.

O'Malley PJ. 1999. Density functional calculated spin densities and hyperfine couplings for hydrogen bonded 1,4-naphthosemiquinone and phyllosemiquinone anion radicals: a model for the A1 free radical formed in photosystem I. Biochim Biophys Acta 1411(1):101-113.

O'Regan B, Gratzel, M.,. 1991. A low cost high efficiency solar cell based on dye-sensitized colloidal TiO2 films. Nature 353:737-740.

Ohno K, Kamiya N, Asakawa N, Inoue Y, Sakurai M. 2001. Application of an integrated MOZYME plus DFT method to pKa calculations for proteins. Chemical Physics Letters 341(3-4):387-392.

Okamura MY, Feher G. 1992. Proton transfer in reaction centers from photosynthetic bacteria. Annu. Rev. Biochem. 61:861-896.

Okamura MY, Feher G. 1995. Proton-coupled electron transfer reactions of Q_B in reaction centers from photosynthetic bacteria. In: Blankenship R, Madigan M, Bauer C, editors. Anoxygenic Photosynthetic Bacteria. Dordrecht: Kluwer Academic Publishers. p 577-593.

Okamura MY, Feher G, Nelson N. 1982. Reaction centers. In: Govindjee, editor. Photosynthesis: Energy conversion by Plants and Bacteria. New York: Academic Press. p 195-272.

Okamura MY, Isaacson RA, Feher G. 1975. The primary acceptor in bacterial photosynthesis: Obligatory role of ubiquinone in photoactive reaction centers of *Rhodopseudomonas sphaeroides*. Proc. Natl. Acad. Sci. USA 72:3492-3496.

Okamura MY, Stiener LA, Feher G. 1974. Characterization of reaction centers from photosynthetic bacteria. I. Subunit structure of the protein mediating the primary photochemistry in *rhodopseudomonas spheroides* R-26. Biochemistry 13:1394-1402.

Pandhare J, Dash C, Rao M, Deshpande V. 2003. Slow tight binding inhibition of proteinase K by a proteinaceous inhibitor. journal of biochemical chemistry 278:48735-48744.

Parson WW, Chu Z-T, Warshel A. 1990. Electrostatic control of charge separation in bacterial photosynthesis. Biochim. Biophys. Acta 1017:251-272.

Peter Raven. RE, Susan Eichhorn. 1999. Biology of Plants: W.H. Freeman and Company.

Petrenko A, Maniero A, vanTol J, MacMillian F, Li Y, Brunel L-C, Redding K. 2004. A high field EPR study of P700+ in wild-typr and mutant photosystem I from Chlamydomonas reinhardtii. Biochemistry 43(7):1781-1786.

Prince RC, Dutton PL, Bruce JM. 1983. Electrochemistry of ubiquinones. FEBS Lett 160(1,2):273-276.

Pushkar Y, Golbeck J, Stehlik D, Zimmermann H. 2004. Asymmetric hydogen bonding of the quinone co-factor in Photosystem I probed by 13C labeled naphthoquinones. J.Phys.Chem. B 108:9439-9448.

Rabenstein B, Ullmann GM, Knapp EW. 2000. Electron transfer between the quinones in the photosynthetic reaction center and its coupling to conformational changes. Biochemistry 39(34):10487-96.

Radzicka A, Wolfenden R. 1988. Comparing the polarities of the amino acids: Side chain distribution coeffients between the vapor phase, cyclohexane, 1-octonal, and neutral aqueous solution. Biochemistry 27:1664-1670.

Rappaport F, Guergova-Kuras M, Nixon PJ, Diner B, Lavergne J. 2002. Kinetics and pathways of charge recombination in photosystem II. Biochemistry 41:8518-8527.

Rich PR. 2004. The quinone chemistry of bc complexes. Biochem. Biophys. Acta:in press.

Rich PR, Bendall DS. 1979. A mechanism for the reduction of cytochromes by quinols in solution and its relevance to biological electron transfer reactions. FEBS Lett. 105:189-194.

Rutherford AW, Evans MCW. 1980. Direct measurement of the redox potential of the primary and secondary quinone electron acceptors in *Rhodopseudomonas sphaeroides* (wild-type) by EPR spectrometry. FEBS Lett. 110:257-261.

Rutherford AW, Faller P. 2002. Photosystem II: evolutionary perspectives. Phil.Trans.R.Soc.Lond. B 358:245-253.

Rutherford AW, Nitschke W. 1996. Photosystem II and the quinone-iron containing reaction centers: comparisons and evolutionary perspectives. In: H.Baltscheffsky, editor. Origin and evolution of biological energy conversion. New York: VCH. p 143-175.

Saenger W, Jordan,P., Kraub,N.,. 2002. The assembly of protein subunits and co-factors in photosystem I. Cur. Opin. Struct. Biol. 12:244-254.

Santabarbara S, Kuprov I, Fairclough W, Purton S, Hore P, Heathcote P, Evans MC. 2005. Bidirectional electron transfer in photosystem I: determination of two distances between P700+ and A1- in spin-correlated radical pairs. Biochemistry 44(6):2119-2128.

Schaller RD, Klimov, V.I.,. 2004. High efficiency carrier mulitiplication in PbSe nanocrystals: Implications for solar energy conversion. Phys. Rev. Lett. 92:186601.

Schotte F, Soman J, Olson JS, Wulff M, Anfinrud P, A.,. 2004. Picosecond time-resolved X-ray crystallography: Probing protein function in real time. J. Struct. Biol. 147:235-238.

Schreiber G. 2002. Kinetic studies of protein-protein interactions. Curr. Opin. Struct. Biol. 12:41-47.

Seth J, Palaniappan, V., Wagner, R.W., Johnson, T.E., Lindsey, J.S., Bocian, D.F.,. 1996. Static Spectroscopic and Elelctrochemical Probes of Electronic Communications. J. Am. Chem. Soc. 118:11194-11207.

Sitkoff D, Sharp KA, Honig B. 1994. Accurate calculation of hydration free energies using macroscopic solvent models. J. Phys. Chem. 98:1978-1988.

Sivakumar V, Wang R, Hastings G. 2005. A1 reduction in intact cyanobacterial photosystem I particles studied by time-resolved step-scan fourier transform infared difference spectroscopy and isotope labeling. Biochemistry 44(1880-1893).

Song Y, Gunner MR. 2004. Comparison of bacteriorhodopsin and halorhodopsin by MCCE reveals a possible new chloride binding site in halorhodopsin. Biophysical Journal 86(1):611a-611a.

Steffen MA, Lao K, Boxer SG. 1994. Dielectric Asymmetry in the Photosynthetic Rection Center. Science 264:810-816.

Stein RR, Sastellvi AL, Bogaxz JP, Wraight CA. 1984. Herbicide-quinone competition in the acceptor complex of photosynthetic reaction centers from phodopseudomonas

sphaeroides: a bacterial model for PS-II-herbicide activity in plants. J. Cell. Biochem. 24:243-259.

Steinburg-Yfrach G, Rigaud, J.L., Durantini, E.N., Moore, A.L., Gust, D., Moore, T.A.,. 1998. Light driven production at ATP catalyzed by F0F1-ATP synthase in an artificial photosynthetic membrane. Nature (London) 392:479-482.

Steyaert J, Wyns L, Stanssens P. 1991. Subsite interactions of Ribonuclease T1: Viscosity effects indicate that the rate-limiting step of GpN transesterification depends on the nature of N. Biochemistry 30(8661-8665).

Stowell MHB, McPhillips TM, Rees DC, Soltis SM, Abresch E, Feher G. 1997. Light-induced structural changes in photosynthetic reaction center: implications for mechanism of electron-proton transfer. Science 276:812-816.

Sun L, Hammarstrom, L., Akermark, B., Styring, S.,. 2001. Towards artificial photosynthesis: ruthenium-maganese chemistry for energy production. Chem. Soc. Rev. 30:36-49.

Suponeva EP, Hotchandani S, Kisselev BA, Arbour C. 1995. Cyclic voltammetric and spectrophotometric study of microcrystalline chlorophyll a electrodeposited on the ITO optically transparent electrode. Journal of Electroanalytical Chemistry 387:123-126.

Swallow AJ. 1982a. midpoints of quinones. In: Trumpower BL, editor. Function of quinones in energy conserving systems. New York: Plenum Press. p 59-72.

Swallow AJ. 1982b. Physical chemistry of semiquinones. In: Trumpower BL, editor. Function of Quinones in Energy Conserving Systems. New York: Academic Press. p 59-72.

Takahashi E, Wells TA, Wraight CA. 2001. Protein control of the redox potential of the primary quinone acceptor in reaction centers from *Rhodobacter sphaeroides*. Biochemistry 40(4):1020-1028.

Tani FH, Barrington S. 2005. Zinc and Copper uptake by plants under two transpiration rates. Environmental Pollution 138(3):549-559.

Tiede DM, Hanson DK. 1992. Protein Relaxation Following Quinone Reduction In Rhodobacter Capsulatus: Detection of Likely Protonation Linked Optical Absorbance Changes of the Chromophores. In: Breton J, Vermeglio A, editors. The Photosynthetic Reaction Center II. New York: Plenum Press. p 341-350.

Tommos C, Babcock GT. 1998. Oxygen production in nature: a lightdriven metalloradical enzyme process. Acc. Chem. Res 31:18-25.

Trommer D, Neoembrini F, Fasciana M, Steinfeld A. 2005. Hydrogen Production by steam-gasification of petroleum coke using concentrated solar power-I. Thermodynamic and kinetic analyses. International Journal of Hydrogen Energy 30(6):605-618.

van der Boom T, Hayes, R.T., Zhao, Y., Bushard, P.J., Weiss, E.A.,Wasielewski, M.R.,. 2002. Charge transport in photofunctional nanoparticles self-assembled from Zinc. J. Am. Chem. Soc. 124:9582-9590.

van Holde KE. 2002. A hypothesis concerning diffusion-limited protein-ligand interactions. Biophys Chem 101-102:249-254.

van Mourik F, Reus M, Holzwarth AR. 2001. Long-lived charge-separated states in bacterial reaction centers isolated from Rhodobacter sphaeroides. Biochim Biophys Acta 1504(2-3):311-8.

Wang R, Sivakumar V, Johnson TW, Hastings G. 2004. FTIR difference spectroscopy in combination with isotope labeling for identification of the carbonyl modes of P700 and P700+ in photosystem I. Biophysical Journal 86:1061-1073.

Wang R, Sivakumar V, Li Y, Redding K, Hastings G. 2003. Mutation induced modulation of hydrogen bonding to P700 studied using FTIR difference spectroscopy. Biochemistry 42(33):9889-97.

Warncke K, Dutton PL. 1993a. Experimental resolution of the free energies of aqueous solvation contributions to ligand-protein binding: quinone-Q_A site interactions in the photosynthetic reaction center protein. Proc. Natl. Acad. Sci. USA 90:2920-2924.

Warncke K, Dutton PL. 1993b. Influence of QA site redox cofactor structure on equilibrium binding, in situ electrochemistry, and electron-transfer performance in the photosynthetic reaction center protein. Biochemistry 32(18):4769-79.

Webber AN, Lubitz W. 2001. P700: the primary electron donor of photosystem I. Biochim Biophys Acta 1507:61-79.

Webber AN, Su H, Bingham SE, Kass H, Krabben L, Kuhn M, Jordan R, Schlodder E, Lubitz W. 1996. Site-directed mutations affecting the spectroscopic characteristics and midpoint potential of the primary donor in photosystem I. Biochemistry 35:12857-12863.

Wells T, Takahashi E, Wraight CA. 2003. Primary Quinone (Q_A) Binding Site of Bacterial Photosynthetic Reaction Centers: Mutation at Residue M265 Probed by FTIR Spectroscopy. Biochemistry 42:4064-4074.

Woodbury NW, Parson WW, Gunner MR, Prince RC, Dutton PL. 1986. Radical-pair energetics and decay mechanisms in reaction center containing anthraquinones or benzoquinones in place of ubiquinone. Biochim. Biophys. Acta. 851:6-22.

Wraight CA. 1998. Functional linkage between the Q_A and Q_B sites of photosynthetic reaction centers. In: Garab G, editor. Proceedings of the XIth International Photosynthesis Congress. Dordrecht: Kluwer. p 693-698.

Wraight CA. 2004. Proton and electron transfer in the acceptor quinone complex of photosynthetic reaction centers from Rhodobacter sphaeroides. Front Biosci 9:309-37.

Xavier AV, Willson RC. 1998. Association and dissociation kinetics of Anti-Hen Egg Lysozyme monoclonal antibodies HyHel-5 and HyHel-10. Biophysical Journal 74:2036-2045.

Xiong J, Bauer CE. 2002. Complex evolution of photosynthesis. Annu Rev Plant Biol 53:503-21.

Xu Q, Baciou L, Sebban P, Gunner MR. 2002. Exploring the energy landscape for Q_A^- to Q_B electron transfer in bacterial photosynthetic reaction centers: Effect of substrate position and tail length on the conformational gating step. Biochemistry 41:10021-10025.

Xu Q, Gunner MR. 2000. Temperature dependence of the free energy, enthalpy and entropy of $P^+Q_A^-$ charge recombination in photosynthetic reaction centers. J.Phys.Chem. B 104:8035-8043.

Xu Q, Gunner MR. 2001. Trapping conformational intermediate states in the reaction center protein from photosynthetic bacteria. Biochemistry 40:3232-3241.

Xu Q, Gunner MR. 2002. Exploring the energy profile of the Q(A)(-) to Q(B) electron transfer reaction in bacterial photosynthetic reaction centers: pH dependence of the conformational gating step. Biochemistry 41(8):2694-2701.

Yang F, Shen G, Schlunchter WM, Zybailov B, Ganago AO, Vassiliev IR, Bryant DA, Golbeck J. 1998. Deletion of the PsaF polypeptide modifies the environment of the redox-active phylloquinone (A1). Evidence for unidirectionality of electron transfer in photosystem I. J Phys. Chem. B 102:8288-8299.

Yiallouros I, Vassiliou S, Yiotakis A, Zwilling R, Stoker W, Dive V. 1998. Phosphinic peptides, the first potent inhibitors of astacin, behave as extremely slow-binding inhibitors. Biochemical J 331:375-379.

Youvan DC, Marrs BL. 1987. Molecular mechanisms of photosynthesis. Sci. Amer.:42-48.

Zachariae U, Lancaster CR. 2001. Proton uptake associated with the reduction of the primary quinone Q_A influences the binding site of the secondary quinone Q_B in *Rhodopseudomonas viridis* photosynthetic reaction centers. Biochim Biophys Acta 1505:280-90.

Zhu Z, Gunner MR. 2005. Energetics of quinone-dependent electron and proton transfers in *Rhodobacter sphaeroides* photosynthetic reaction centers. Biochemistry 44:82-96.